Search for pair production of up-type vector-like quarks and for four-top-quark events in final states with multiple b-jets with the ATLAS detector

The ATLAS collaboration

E-mail: atlas.publications@cern.ch

ABSTRACT: A search for pair production of up-type vector-like quarks (T) with a significant branching ratio into a top quark and either a Standard Model Higgs boson or a Z boson is presented. The same analysis is also used to search for four-top-quark production in several new physics scenarios. The search is based on a dataset of pp collisions at $\sqrt{s} = 13\,\text{TeV}$ recorded in 2015 and 2016 with the ATLAS detector at the CERN Large Hadron Collider and corresponds to an integrated luminosity of $36.1\,\text{fb}^{-1}$. Data are analysed in the lepton+jets final state, characterised by an isolated electron or muon with high transverse momentum, large missing transverse momentum and multiple jets, as well as the jets+$E_{\text{T}}^{\text{miss}}$ final state, characterised by multiple jets and large missing transverse momentum. The search exploits the high multiplicity of jets identified as originating from b-quarks, and the presence of boosted, hadronically decaying top quarks and Higgs bosons reconstructed as large-radius jets, characteristic of signal events. No significant excess above the Standard Model expectation is observed, and 95% CL upper limits are set on the production cross sections for the different signal processes considered. These cross-section limits are used to derive lower limits on the mass of a vector-like T quark under several branching ratio hypotheses assuming contributions from $T \to Wb$, Zt, Ht decays. The 95% CL observed lower limits on the T quark mass range between 0.99 TeV and 1.43 TeV for all possible values of the branching ratios into the three decay modes considered, significantly extending the reach beyond that of previous searches. Additionally, upper limits on anomalous four-top-quark production are set in the context of an effective field theory model, as well as in an universal extra dimensions model.

KEYWORDS: Beyond Standard Model, Hadron-Hadron scattering (experiments), vector-like quarks

Contents

1 Introduction

The discovery of a new particle consistent with the Standard Model (SM) Higgs boson by the ATLAS [1] and CMS [2] experiments at the Large Hadron Collider (LHC) represents a milestone in high-energy physics. A comprehensive programme of measurements of the Higgs boson properties to unravel its nature is underway at the LHC, so far yielding results compatible with the SM predictions. This makes it more urgent than ever before to provide an explanation for why the electroweak mass scale (and the Higgs boson mass along with it) is so small compared to the Planck scale, a situation known as the hierarchy problem. Naturalness arguments [3] require that quadratic divergences that arise from radiative

corrections to the Higgs boson mass are cancelled out by some new mechanism in order to avoid fine-tuning. To that effect, several explanations have been proposed in theories beyond the SM (BSM).

One such solution involves the existence of a new strongly interacting sector, in which the Higgs boson would be a pseudo-Nambu-Goldstone boson [4] of a spontaneously broken global symmetry. One particular realisation of this scenario, referred to as Composite Higgs [5, 6], addresses many open questions in the SM, such as the stability of the Higgs boson mass against quantum corrections, and the hierarchy in the mass spectrum of the SM particles, which would be explained by partial compositeness. In this scenario, the top quark would be a mostly composite particle, while all other SM fermions would be mostly elementary. A key prediction is the existence of new fermionic resonances referred to as vector-like quarks, which are also common in many other BSM scenarios. Vector-like quarks are defined as colour-triplet spin-1/2 fermions whose left- and right-handed chiral components have the same transformation properties under the weak-isospin SU(2) gauge group [7, 8]. Depending on the model, vector-like quarks are classified as SU(2) singlets, doublets or triplets of flavours T, B, X or Y, in which the first two have the same charge as the SM top and bottom quarks while the vector-like Y and X quarks have charge $-4/3e$ and $5/3e$. In addition, in these models, vector-like quarks are expected to couple preferentially to third-generation quarks [7, 9] and can have flavour-changing neutral-current decays in addition to the charged-current decays characteristic of chiral quarks. As a result, an up-type T quark can decay not only into a W boson and a b-quark, but also into a Z or Higgs boson and a top quark ($T \rightarrow Wb$, Zt, and Ht). Similarly, a down-type B quark can decay into a Z or Higgs boson and a b quark, in addition to decaying into a W boson and a top quark ($B \rightarrow Wt$, Zb and Hb). Vector-like Y quarks decay exclusively into Wb and vector-like X quarks decay exclusively into Wt. To be consistent with the results from precision electroweak measurements a small mass-splitting between vector-like quarks belonging to the same SU(2) multiplet is required, but no requirement is placed on which member of the multiplet is heavier [10]. At the LHC, vector-like quarks with masses below ∼1 TeV would be predominantly produced in pairs via the strong interaction. For higher masses, single production, mediated by the electroweak interaction, may dominate depending on the coupling strength of the interaction between the vector-like quark and the SM quarks.

Another prediction of the Composite Higgs paradigm, as well as other BSM scenarios, such as Randall-Sundrum extra dimensions, is the existence of new heavy vector resonances, which would predominantly couple to the third-generation quarks and thus lead to enhanced four-top-quark production at high energies [11–15]. In particular, the class of models where such vector particles are strongly coupled to the right-handed top quark are much less constrained by precision electroweak measurements than in the case of couplings to the left-handed top quark [16]. In the limit of sufficiently heavy particles, these models can be described via an effective field theory (EFT) involving a four-fermion contact interaction [17]. The corresponding Lagrangian is

$$\mathcal{L}_{4t} = \frac{|C_{4t}|}{\Lambda^2}(\bar{t}_{\mathrm{R}}\gamma^{\mu}t_{\mathrm{R}})(\bar{t}_{\mathrm{R}}\gamma_{\mu}t_{\mathrm{R}}),$$

where t_R is the right-handed top quark spinor, γ_μ are the Dirac matrices, C_{4t} is the coupling constant, and Λ is the energy scale above which the effects of direct production of new vector particles must be considered. Anomalous four-top-quark production also arises in Universal Extra Dimensions (UED) models, which involve new heavy particles. For instance, in an UED model with two extra dimensions that are compactified using the geometry of the real projective plane (2UED/RPP) [18], the momenta of particles are discretised along the directions of the extra dimensions. A tier of Kaluza-Klein (KK) towers is labelled by two integers, k and ℓ, referred to as "tier (k, ℓ)". Within a given tier, the squared masses of the particles are given at leading order by $m^2 = k^2/R_4^2 + \ell^2/R_5^2$, where πR_4 and πR_5 are the sizes of the two extra dimensions. The model is parameterised by R_4 and R_5 or, alternatively, by $m_{\mathrm{KK}} = 1/R_4$ and $\xi = R_4/R_5$. Four-top-quark production can arise from tier $(1,1)$, where particles from this tier have to be pair produced because of symmetries of the model. Then they chain-decay into the lightest particle of this tier, the heavy photon $A^{(1,1)}$, by emitting SM particles. The branching ratios of $A^{(1,1)}$ into SM particles are not predicted by the model, although the decay into $t\bar{t}$ is expected to be dominant [19].

This paper presents a search for $T\bar{T}$ production with at least one T quark decaying into Ht with $H \to b\bar{b}$, or into Zt with $Z \to \nu\bar{\nu}$, as well as for anomalous four-top-quark production within an EFT model and within the 2UED/RPP model (see figure 1). Recent searches for $T\bar{T}$ production have been performed by the ATLAS [20, 21] and CMS [22, 23] collaborations using up to 36.1 fb^{-1} of pp collisions at $\sqrt{s} = 13$ TeV. The most restrictive 95% CL lower limits on the T quark mass obtained are 1.35 TeV and 1.16 TeV, corresponding to branching ratio assumptions of $\mathcal{B}(T \to Wb) = 1$ and $\mathcal{B}(T \to Zt) = 1$, respectively. Previous searches for anomalous $t\bar{t}t\bar{t}$ production have been performed by the ATLAS Collaboration using the full Run-1 dataset [24, 25], where 95% CL limits of $|C_{4t}|/\Lambda^2 < 6.6$ TeV^{-2} and $m_{KK} > 1.1$ TeV were obtained in the case of the EFT and the 2UED/RPP models, respectively. A recent search by the CMS Collaboration [26] using 35.9 fb^{-1} of pp collisions at $\sqrt{s} = 13$ TeV has set an upper limit of 41.7 fb on the SM $t\bar{t}t\bar{t}$ production cross section, about 4.5 times the SM prediction, thus placing some constraints on anomalous production with kinematics like in the SM.

This search uses 36.1 fb^{-1} of data at $\sqrt{s} = 13$ TeV recorded in 2015 and 2016 by the ATLAS Collaboration, and it closely follows the strategy developed in Run 1 [25], although it incorporates new ingredients, such as the identification of boosted objects, to substantially enhance sensitivity for heavy resonances. Data are analysed in the lepton+jets final state, characterised by an isolated electron or muon with high transverse momentum, large missing transverse momentum and multiple jets and, for the first time in searches for vector-like quarks, also in the jets+E_T^{miss} final state, characterised by multiple jets and large missing transverse momentum.
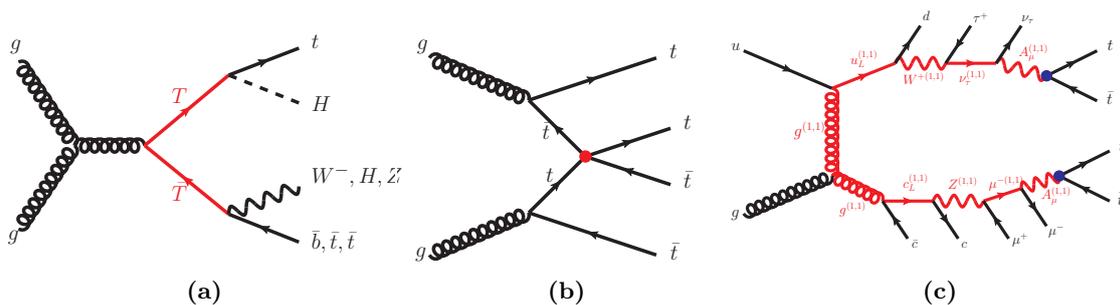
Figure 1. Representative leading-order Feynman diagrams for the signals probed by this search: (a) $T\bar{T}$ production, and (b) four-top-quark production via an effective four-top-quark interaction in an effective field theory model, and (c) four-top-quark production via cascade decays from Kaluza-Klein excitations in a universal extra dimensions model with two extra dimensions compactified using the geometry of the real projective plane.

2 ATLAS detector

The ATLAS detector [27] at the LHC covers almost the entire solid angle around the collision point,[1] and consists of an inner tracking detector surrounded by a thin super-conducting solenoid producing a 2 T axial magnetic field, electromagnetic and hadronic calorimeters, and a muon spectrometer incorporating three large toroid magnet assemblies. The inner detector consists of a high-granularity silicon pixel detector, including the insertable B-layer [28], installed in 2014, and a silicon microstrip tracker, together providing a precise reconstruction of tracks of charged particles in the pseudorapidity range $|\eta| < 2.5$, complemented by a transition radiation tracker providing tracking and electron identification information for $|\eta| < 2.0$. The calorimeter system covers the pseudorapidity range $|\eta| < 4.9$. Within the region $|\eta| < 3.2$, electromagnetic (EM) calorimetry is provided by barrel and endcap high-granularity lead/liquid-argon (LAr) electromagnetic calorimeters, with an additional thin LAr presampler covering $|\eta| < 1.8$, to correct for energy loss in material upstream of the calorimeters. Hadronic calorimetry is provided by a steel/scintillator-tile calorimeter, segmented into three barrel structures within $|\eta| < 1.7$, and two copper/LAr hadronic endcap calorimeters. The solid angle coverage is completed with forward copper/LAr and tungsten/LAr calorimeter modules optimised for electromagnetic and hadronic measurements, respectively. The muon spectrometer measures the trajectories of muons with $|\eta| < 2.7$ using multiple layers of high-precision tracking chambers located in a toroidal field of approximately 0.5 T and 1 T in the central and endcap regions of ATLAS, respectively. The muon spectrometer is also instrumented with separate trigger chambers covering $|\eta| < 2.4$. A two-level trigger system [29], consisting of a

---

[1]ATLAS uses a right-handed coordinate system with its origin at the nominal interaction point (IP) in the centre of the detector. The x-axis points from the IP to the centre of the LHC ring, the y-axis points upward, and the z-axis coincides with the axis of the beam pipe. Cylindrical coordinates (r,ϕ) are used in the transverse plane, ϕ being the azimuthal angle around the beam pipe. The pseudorapidity is defined in terms of the polar angle θ as $\eta = -\ln\tan(\theta/2)$. Angular distance is measured in units of $\Delta R \equiv \sqrt{(\Delta\eta)^2 + (\Delta\phi)^2}$.

hardware-based Level-1 trigger followed by a software-based High-Level Trigger (HLT), is used to reduce the event rate to a maximum of around 1 kHz for offline storage.

3 Object reconstruction

Interaction vertices from the proton-proton collisions are reconstructed from at least two tracks with transverse momentum (p_T) larger than 400 MeV that are consistent with originating from the beam collision region in the x-y plane. If more than one primary vertex candidate is found, the candidate whose associated tracks form the largest sum of squared p_T [30] is selected as the hard-scatter primary vertex.

Electron candidates [31, 32] are reconstructed from energy clusters in the EM calorimeter that are matched to reconstructed tracks in the inner detector and have $p_T > 30$ GeV and $|\eta_{\mathrm{cluster}}| < 2.47$; candidates in the transition region between the EM barrel and endcap calorimeter ($1.37 < |\eta_{\mathrm{cluster}}| < 1.52$) are excluded. They are also required to satisfy the "tight" likelihood-based identification criteria [31] based on calorimeter, tracking and combined variables that provide separation between electrons and jets. Muon candidates [33] are reconstructed by matching track segments in different layers of the muon spectrometer to tracks found in the inner detector. The resulting muon candidates are refitted using the complete track information from both detector systems and are required to have $p_T > 30$ GeV and $|\eta| < 2.5$. Electron (muon) candidates are matched to the primary vertex by requiring that the significance of their transverse impact parameter, d_0, satisfies $|d_0/\sigma(d_0)| < 5(3)$, where $\sigma(d_0)$ is the measured uncertainty in d_0, and by requiring that their longitudinal impact parameter, z_0, satisfies $|z_0 \sin \theta| < 0.5$ mm. To further reduce the background from non-prompt leptons, photon conversions and hadrons, lepton candidates are also required to be isolated. A lepton isolation criterion is defined by calculating the quantity $I_R = \sum p_T^{\mathrm{trk}}$, where the sum includes all tracks (excluding the lepton candidate itself) within the cone defined by $\Delta R < R_{\mathrm{cut}}$ about the direction of the lepton. The value of R_{cut} is the smaller of r_{min} and $10\,\mathrm{GeV}/p_T^{\ell}$, where r_{min} is set to 0.2 (0.3) for electron (muon) candidates, and p_T^{ℓ} is the lepton p_T. All lepton candidates must satisfy $I_R/p_T^{\ell} < 0.06$.

Candidate jets are reconstructed with the anti-k_t algorithm [34–36] with a radius parameter $R = 0.4$ (referred to as "small-R jets"), using topological clusters [37] built from energy deposits in the calorimeters calibrated to the electromagnetic scale. The reconstructed jets are then calibrated to the particle level by the application of a jet energy scale derived from simulation and *in situ* corrections based on $\sqrt{s} = 13$ TeV data [38]. Calibrated jets are required to have $p_T > 25$ GeV and $|\eta| < 2.5$. Quality criteria are imposed to reject events that contain any jets arising from non-collision sources or detector noise [39]. To reduce the contamination due to jets originating from pile-up interactions, an additional requirement on the Jet Vertex Tagger (JVT) [40] output is made for jets with $p_T < 60$ GeV and $|\eta| < 2.4$.

Jets containing b-hadrons are identified (b-tagged) via an algorithm [41, 42] that uses multivariate techniques to combine information about the impact parameters of displaced tracks and the topological properties of secondary and tertiary decay vertices reconstructed within the jet. For each jet, a value for the multivariate b-tagging discriminant is calculated. In this analysis, a jet is considered b-tagged if this value is above the threshold

corresponding to an average 77% efficiency to tag a b-quark jet, with a light-jet[2] rejection factor of $\sim$134 and a charm-jet rejection factor of $\sim$6.2, as determined for jets with $p_T > 20$ GeV and $|\eta| < 2.5$ in simulated $t\bar{t}$ events.

Overlaps between candidate objects are removed sequentially. Firstly, electron candidates that lie within $\Delta R = 0.01$ of a muon candidate are removed to suppress contributions from muon bremsstrahlung. Overlaps between electron and jet candidates are resolved next, and finally, overlaps between remaining jet candidates and muon candidates are removed. Clusters from identified electrons are not excluded during jet reconstruction. In order to avoid double-counting of electrons as jets, the closest jet whose axis is within $\Delta R = 0.2$ of an electron is discarded. If the electron is within $\Delta R = 0.4$ of the axis of any jet after this initial removal, the jet is retained and the electron is removed. The overlap removal procedure between the remaining jet candidates and muon candidates is designed to remove those muons that are likely to have arisen in the decay chain of hadrons and to retain the overlapping jet instead. Jets and muons may also appear in close proximity when the jet results from high-p_T muon bremsstrahlung, and in such cases the jet should be removed and the muon retained. Such jets are characterised by having very few matching inner-detector tracks. Selected muons that satisfy $\Delta R(\mu, \text{jet}) < 0.04 + 10 \text{ GeV}/p_T^\mu$ are rejected if the jet has at least three tracks originating from the primary vertex; otherwise the jet is removed and the muon is kept.

The candidate small-R jets surviving the overlap removal procedure discussed above are used as inputs for further jet reclustering [43] using the anti-k_t algorithm with a radius parameter $R = 1.0$. In this way it is possible to evaluate the uncertainty in the mass of the large-R jets that arises from the uncertainties in the energy scale and resolution of its constituent small-R jets. In order to suppress contributions from pile-up and soft radiation, the reclustered large-R (RCLR) jets are trimmed [44] by removing all small-R (sub)jets within a RCLR jet that have p_T below 5% of the p_T of the reclustered jet. Due to the pile-up suppression and $p_T > 25$ GeV requirements made on the small-R jets, the average fraction of small-R jets removed by the trimming requirement is less than 1%. The resulting RCLR jets are required to have $|\eta| < 2.0$ and are used to identify high-p_T hadronically decaying top quark or Higgs boson candidates by making requirements on their transverse momentum, mass, and number of constituents. Hadronically decaying top quark candidates are reconstructed as RCLR jets with $p_T > 300$ GeV, mass larger than 140 GeV, and at least two subjets. Higgs boson candidates are reconstructed as RCLR jets with $p_T > 200$ GeV, a mass between 105 and 140 GeV, and a p_T-dependent requirement on the number of subjets (exactly two for $p_T < 500$ GeV, and one or two for $p_T > 500$ GeV). In the following, these are referred to as "top-tagged" and "Higgs-tagged" jets, respectively, while the term "jet" without further qualifiers is used to refer to small-R jets.

The missing transverse momentum $\vec{p}_T^{\text{miss}}$ (with magnitude E_T^{miss}) is defined as the negative vector sum of the p_T of all selected and calibrated objects in the event, including a term to account for energy from soft particles in the event which are not associated with any of the selected objects. This soft term is calculated from inner-detector tracks

---

[2]Light-jet refers to a jet originating from the hadronisation of a light quark (u, d, s) or a gluon.

matched to the selected primary vertex to make it more resilient to contamination from pile-up interactions [45, 46].

4 Data sample and event preselection

This search is based on a dataset of pp collisions at $\sqrt{s} = 13$ TeV with 25 ns bunch spacing collected by the ATLAS experiment in 2015 and 2016, corresponding to an integrated luminosity of 36.1 fb^{-1}. Only events recorded with a single-electron trigger, a single-muon trigger, or a E_T^{miss} trigger under stable beam conditions and for which all detector subsystems were operational are considered.

Single-lepton triggers with low p_T threshold and lepton isolation requirements are combined in a logical OR with higher-threshold triggers without isolation requirements to give maximum efficiency. For muon triggers, the lowest p_T threshold is 20 (26) GeV in 2015 (2016), while the higher p_T threshold is 50 GeV in both years. For electrons, triggers with a p_T threshold of 24 (26) GeV in 2015 (2016) and isolation requirements are used along with triggers with a 60 GeV threshold and no isolation requirement, and with a 120 (140) GeV threshold with looser identification criteria. The E_T^{miss} trigger [29] considered uses an E_T^{miss} threshold of 70 GeV in the HLT in 2015 and a run-period-dependent E_T^{miss} threshold varying between 90 GeV and 110 GeV in 2016.

Events satisfying the trigger selection are required to have at least one primary vertex candidate. They are then classified into the "1-lepton" or "0-lepton" channels depending on the multiplicity of selected leptons. Events in the 1-lepton channel are required to satisfy a single-lepton trigger and to have exactly one selected electron or muon that matches, with $\Delta R < 0.15$, the lepton reconstructed by the trigger. In the following, 1-lepton events satisfying either the electron or muon selections are combined and treated as a single analysis channel. Events in the 0-lepton channel are required to satisfy the E_T^{miss} trigger and to have no selected leptons. In addition, events in the 1-lepton (0-lepton) channel are required to have ≥ 5 (≥ 6) small-R jets. In the following, all selected small-R jets are considered, including those used to build large-R jets. For both channels, backgrounds that do not include b-quark jets are suppressed by requiring at least two b-tagged jets.

Additional requirements are made to suppress the background from multijet production. In the case of the 1-lepton channel, requirements are made on E_T^{miss} as well as on the transverse mass of the lepton and E_T^{miss} system (m_T^W):[3] $E_T^{miss} > 20$ GeV and $E_T^{miss} + m_T^W > 60$ GeV. In the case of the 0-lepton channel, the requirements are $E_T^{miss} > 200$ GeV (for which the E_T^{miss} trigger is fully efficient) and $\Delta\phi_{min}^{4j} > 0.4$, where $\Delta\phi_{min}^{4j}$ is the minimum azimuthal separation between $\vec{p}_T^{miss}$ and each of the four highest-p_T jets. The latter requirement in the 0-lepton channel is very effective in suppressing multi-jet events, where the large E_T^{miss} results from the mismeasurement of a high-p_T jet or the presence of neutrinos emitted close to a jet axis.

---

[3]$m_T^W = \sqrt{2p_T^\ell E_T^{miss}(1 - \cos\Delta\phi)}$, where p_T^ℓ is the transverse momentum (energy) of the muon (electron) and $\Delta\phi$ is the azimuthal angle separation between the lepton and the direction of the missing transverse momentum.

Preselection requirements		
Requirement	1-lepton channel	0-lepton channel
Trigger	Single-lepton trigger	$E_{\mathrm{T}}^{\mathrm{miss}}$ trigger
Leptons	$=1$ isolated e or μ	$=0$ isolated e or μ
Jets	≥ 5 jets	≥ 6 jets
b-tagging	≥ 2 b-tagged jets	≥ 2 b-tagged jets
$E_{\mathrm{T}}^{\mathrm{miss}}$	$E_{\mathrm{T}}^{\mathrm{miss}} > 20$ GeV	$E_{\mathrm{T}}^{\mathrm{miss}} > 200$ GeV
Other $E_{\mathrm{T}}^{\mathrm{miss}}$-related	$E_{\mathrm{T}}^{\mathrm{miss}} + m_{\mathrm{T}}^{W} > 60$ GeV	$\Delta\phi_{\mathrm{min}}^{4\mathrm{j}} > 0.4$

Table 1. Summary of preselection requirements for the 1-lepton and 0-lepton channels. Here m_{T}^{W} is the transverse mass of the lepton and the $E_{\mathrm{T}}^{\mathrm{miss}}$ vector, and $\Delta\phi_{\mathrm{min}}^{4\mathrm{j}}$ is the minimum azimuthal separation between the $E_{\mathrm{T}}^{\mathrm{miss}}$ vector and each of the four highest-p_{T} jets.

The above requirements are referred to as the "preselection" and are summarised in table 1.

5 Signal and background modelling

Signal and most background processes were modelled using Monte Carlo (MC) simulations. In the simulation, the top quark and SM Higgs boson masses were set to 172.5 GeV and 125 GeV, respectively. All simulated samples, except those produced with the SHERPA [47] event generator, utilised EVTGEN v1.2.0 [48] to model the decays of heavy-flavour hadrons. To model the effects of pile-up, events from minimum-bias interactions were generated using the PYTHIA 8.186 [49] event generator and overlaid onto the simulated hard-scatter events according to the luminosity profile of the recorded data. The generated events were processed through a simulation [50] of the ATLAS detector geometry and response using GEANT4 [51]. A faster simulation, where the full GEANT4 simulation of the calorimeter response is replaced by a detailed parameterisation of the shower shapes [52], was adopted for some of the samples used to estimate systematic uncertainties. Simulated events are processed through the same reconstruction software as the data, and corrections are applied so that the object identification efficiencies, energy scales and energy resolutions match those determined from data control samples.

5.1 Signal modelling

Samples of simulated $T\bar{T}$ events were generated with the leading-order (LO) generator[4] PROTOS 2.2 [8, 53] using the NNPDF2.3 LO [54] parton distribution function (PDF) set and passed to PYTHIA 8.186 [49] for parton showering and fragmentation. The A14 [55] set of optimised parameters for the underlying event (UE) description using the NNPDF2.3 LO PDF set, referred to as the "A14 UE tune", was used. The samples were generated

---

[4]In the following, the order of a generator should be understood as referring to the order in the strong coupling constant at which the matrix element calculation is performed.

assuming singlet couplings and for heavy-quark masses between 350 GeV and 1.5 TeV in steps of 50 GeV. Additional samples were produced at three mass points (700 GeV, 950 GeV and 1.2 TeV) assuming doublet couplings in order to confirm that, at fixed branching fraction, kinematic differences arising from the different chirality of singlet and doublet couplings have negligible impact on this search. The vector-like quarks were forced to decay with a branching ratio of $1/3$ into each of the three modes (W, Z, H). These samples were reweighted using generator-level information to allow results to be interpreted for arbitrary sets of branching ratios that are consistent with the three decay modes summing to unity. The generated samples were normalised to the theoretical cross sections computed using TOP++ v2.0 [56] at next-to-next-to-leading order (NNLO) in quantum chromodynamics (QCD), including resummation of next-to-next-to-leading logarithmic (NNLL) soft gluon terms [57–61], and using the MSTW 2008 NNLO [62, 63] set of PDFs. The predicted pair-production cross section at $\sqrt{s} = 13$ TeV ranges from 24 pb for a vector-like quark mass of 350 GeV to 2.0 fb for a mass of 1.5 TeV, with an uncertainty that increases from 8% to 18% over this mass range. The theoretical uncertainties result from variations of the factorisation and renormalisation scales, as well as from uncertainties in the PDF and α_S. The latter two represent the largest contribution to the overall theoretical uncertainty in the cross section and were calculated using the PDF4LHC prescription [64] with the MSTW 2008 68% CL NNLO, CT10 NNLO [65, 66] and NNPDF2.3 5f FFN [54] PDF sets.

Samples of simulated four-top-quark events produced via an EFT and within the 2UED/RPP model were generated at LO with the MADGRAPH5_aMC@NLO [67] generator (referred to in the following as MG5_aMC; the versions used are 2.2.3 and 1.5.14 for EFT and 2UED/RPP, respectively) and the NNPDF2.3 LO PDF set, interfaced to PYTHIA 8 (the versions used are 8.205 and 8.186 for EFT and 2UED/RPP, respectively) and the A14 UE tune. The EFT $t\bar{t}t\bar{t}$ sample was normalised assuming $|C_{4t}|/\Lambda^2 = 4\pi$ TeV^{-2}, where C_{4t} denotes the coupling constant and Λ the energy scale of new physics, which yields a cross section of 928 fb computed using MG5_aMC. In the case of the 2UED/RPP model, samples were generated for four different values of m_{KK} (from 1 TeV to 1.8 TeV in steps of 200 GeV) and the BRIDGE [68] generator was used to decay the pair-produced excitations from tier (1,1) generated by MADGRAPH5. The corresponding predicted cross section ranges from 343 fb for $m_{KK} = 1$ TeV to 1.1 fb for $m_{KK} = 1.8$ TeV.

5.2 Background modelling

After the event preselection, the main background is $t\bar{t}$ production, often in association with jets, denoted by $t\bar{t}$+jets in the following. Small contributions arise from single-top-quark, W/Z+jets, multijet and diboson (WW, WZ, ZZ) production, as well as from the associated production of a vector boson V ($V = W, Z$) or a Higgs boson and a $t\bar{t}$ pair ($t\bar{t}V$ and $t\bar{t}H$). All backgrounds are estimated using samples of simulated events and initially normalised to their theoretical cross sections, with the exception of the multijet background, which is estimated using data-driven methods. The background prediction is further improved during the statistical analysis by performing a likelihood fit to data using multiple signal-depleted search regions, as discussed in section 6.

The nominal sample used to model the $t\bar{t}$ background was generated with the NLO generator POWHEG-BOX v2 [69–72] using the CT10 PDF set [65]. The POWHEG-BOX model parameter h_{damp}, which controls matrix element to parton shower matching and effectively regulates the high-p_T radiation, was set to the top quark mass, a setting that was found to describe the $t\bar{t}$ system's p_T at $\sqrt{s} = 7$ TeV [73]. The nominal $t\bar{t}$ sample was interfaced to PYTHIA 6.428 [74] with the CTEQ6L PDF set and the Perugia 2012 (P2012) UE tune [75]. Alternative $t\bar{t}$ simulation samples used to derive systematic uncertainties are described in section 7.3.

All $t\bar{t}$ samples were generated inclusively, but events are categorised depending on the flavour content of additional particle jets not originating from the decay of the $t\bar{t}$ system (see ref. [76] for details). Events labelled as either $t\bar{t}+\geq 1b$ or $t\bar{t}+\geq 1c$ are generically referred in the following as $t\bar{t}+$HF events, where HF stands for "heavy flavour". A finer categorisation of $t\bar{t}+\geq 1b$ events is considered for the purpose of applying further corrections and assigning systematic uncertainties associated with the modelling of heavy-flavour production in different topologies [76]. The remaining events are labelled as $t\bar{t}+$light-jets events, including those with no additional jets. In previous studies, better agreement between data and prediction was observed, particularly for the top quark p_T distribution, when comparing to NNLO calculations [77]. These small improvements to the modelling are incorporated by reweighting all $t\bar{t}$ samples to match their top quark p_T distribution to that predicted at NNLO accuracy in QCD [78, 79]. This correction is not applied to $t\bar{t}+\geq 1b$ events, which instead are reweighted to an NLO prediction in the four-flavour (4F) scheme of $t\bar{t}+\geq 1b$ including parton showering [80], based on SHERPA+OPENLOOPS [47, 81] (referred to as SHERPAOL in the following) using the CT10 PDF set. This reweighting is performed separately for each of the $t\bar{t}+\geq 1b$ categories in such a way that their inter-normalisation and the shape of the relevant kinematic distributions are at NLO accuracy, while preserving the nominal $t\bar{t}+\geq 1b$ cross section in POWHEG-BOX+PYTHIA. The corrections described in this paragraph are applied to the nominal as well as the alternative $t\bar{t}$ samples.

Samples of single-top-quark events corresponding to the t-channel production mechanism were generated with the POWHEG-BOX v1 [82] generator that uses the 4F scheme for the NLO matrix element calculations and the fixed 4F CT10f4 [65] PDF set. Samples corresponding to the Wt- and s-channel production mechanisms were generated with POWHEG-BOX v2 using the CT10 PDF set. Overlaps between the $t\bar{t}$ and Wt final states are avoided by using the "diagram removal" scheme [83]. The parton shower, hadronisation and the underlying event are modelled using PYTHIA 6.428 with the CTEQ6L1 PDF set in combination with the P2012 UE tune. The single-top-quark samples were normalised to the approximate NNLO theoretical cross sections [84–86].

Samples of W/Z+jets events were generated with the SHERPA 2.2 [47] generator. The matrix element was calculated for up to two partons at NLO and up to four partons at LO using COMIX [87] and OPENLOOPS [81]. The matrix element calculation was merged with the SHERPA parton shower [88] using the ME+PS@NLO prescription [89]. The PDF set used for the matrix-element calculation is NNPDF3.0NNLO [90] with a dedicated parton shower tuning developed for SHERPA. Separate samples were generated for different W/Z+jets categories using filters for a b-jet ($W/Z+ \geq 1b$+jets), a c-jet and no b-jet

($W/Z+ \geq 1c$+jets), and with a veto on b- and c-jets (W/Z+light-jets), which were combined into the inclusive W/Z+jets samples. Both the W+jets and Z+jets samples were normalised to their respective inclusive NNLO theoretical cross sections in QCD calculated with FEWZ [91].

Samples of $WW/WZ/ZZ$+jets events were generated with Sherpa 2.1.1 using the CT10 PDF set and include processes containing up to four electroweak vertices. The matrix element includes zero additional partons at NLO and up to three partons at LO using the same procedure as for the W/Z+jets samples. The final states simulated require one of the bosons to decay leptonically and the other hadronically. All diboson samples were normalised to their NLO theoretical cross sections provided by Sherpa.

Samples of $t\bar{t}V$ and $t\bar{t}H$ events were generated with MG5_aMC 2.3.2, using NLO matrix elements and the NNPDF3.0NLO [90] PDF set. Showering was performed using Pythia 8.210 and the A14 UE tune. The $t\bar{t}V$ samples were normalised to the NLO cross section computed with MG5_aMC. The $t\bar{t}H$ sample was normalised using the NLO cross section [92–96] and the Higgs boson decay branching ratios calculated using Hdecay [97].

The production of four-top-quark events in the SM was simulated by samples generated at LO using MG5_aMC 2.2.2 and the NNPDF2.3 LO PDF set, interfaced to Pythia 8.186 in combination with the A14 UE tune. The sample was normalised to a cross section of 9.2 fb, computed at NLO [67].

The background from multijet production ("multijet background" in the following) in the 1-lepton channel contributes to the selected data sample via several production and misreconstruction mechanisms. In the electron channel, it consists of non-prompt electrons (from semileptonic b- or c-hadron decays) as well as misidentified photons (e.g. from a conversion of a photon into an e^+e^- pair) or jets with a high fraction of their energy deposited in the EM calorimeter. In the muon channel, the multijet background is predominantly from non-prompt muons. The multijet background normalisation and shape are estimated directly from data by using the "matrix method" technique [98], which exploits differences in lepton identification and isolation properties between prompt leptons and leptons that are either non-prompt or result from the misidentification of photons or jets. Further details can be found in ref. [25]. The main type of multijet background that contributes to the 0-lepton channel are events in which the energy of a high-$p_{\rm T}$ jet is mismeasured, consequently leading to a large missing transverse momentum in the final state. Most of this background is suppressed by selecting events satisfying $\Delta\phi_{\rm min}^{4j} > 0.4$. The remaining multijet background in each search region is estimated from a control region defined with the same selection as the search region, but with the selection on $\Delta\phi_{\rm min}^{4j}$ changed to $\Delta\phi_{\rm min}^{4j} < 0.1$. The normalisation of the multijet background is extrapolated from the control region to its corresponding search region by performing an exponential fit to the $\Delta\phi_{\rm min}^{4j}$ distribution in the range $0 < \Delta\phi_{\rm min}^{4j} < 0.4$. The background prediction is validated by comparing the data and total prediction in multijet-rich samples selected by choosing ranges of $\Delta\phi_{\rm min}^{4j}$ (e.g. $0.3 < \Delta\phi_{\rm min}^{4j} < 0.4$).
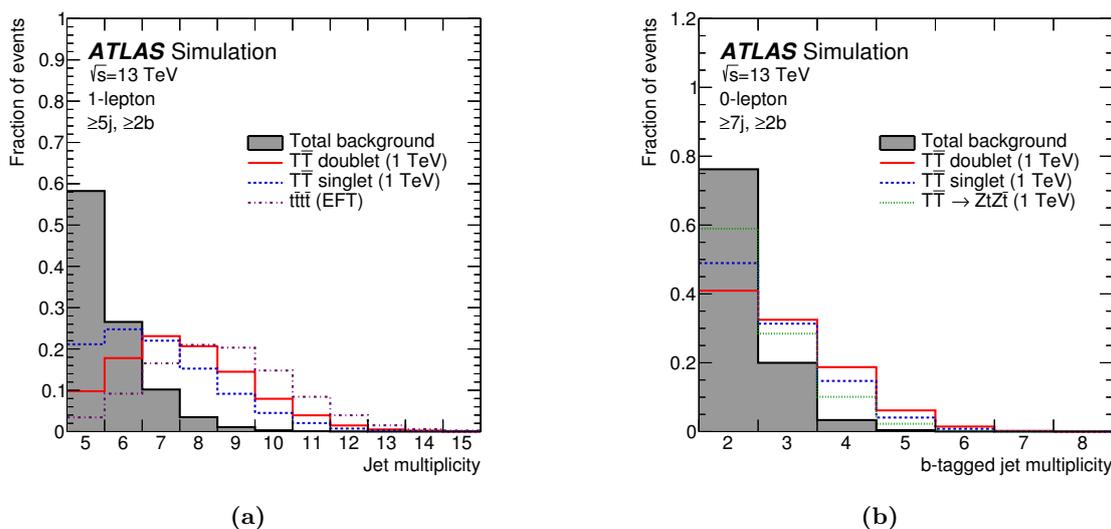
Figure 2. Comparison of the distribution of (a) the jet multiplicity, and (b) the b-tagged jet multiplicity, between the total background (shaded histogram) and several signal scenarios considered in this search. The selection used in (a) corresponds to events in the 1-lepton channel satisfying the preselection requirements, whereas the selection used in (b) corresponds to events in the 0-lepton channel satisfying the preselection requirements and ≥ 7 jets. The signals shown correspond to: $T\bar{T}$ production in the weak-isospin doublet and singlet scenarios, and in the $\mathcal{B}(T \to Zt) = 1$ case, assuming $m_T = 1$ TeV; and $t\bar{t}t\bar{t}$ production within an EFT model.

6 Search strategy

The searches discussed in this paper primarily target $T\bar{T}$ production where at least one of the T quarks decays into a Higgs boson and a top quark resulting in the following processes: $T\bar{T} \to HtHt$, $HtZt$ and $HtWb$.[5] For the dominant $H \to b\bar{b}$ decay mode, the final-state signatures in both the 1-lepton and 0-lepton searches are characterised by high jet and b-tagged jet multiplicities, which provide a powerful experimental handle to suppress the background. The presence of high-momentum Z bosons decaying into $\nu\bar{\nu}$ or W bosons decaying leptonically, either to an electron or muon that is not reconstructed or to a hadronically decaying τ-lepton that is identified as a jet, yields high $E_{\mathrm{T}}^{\mathrm{miss}}$, which is exploited by the 0-lepton search. Both searches have some sensitivity to $T\bar{T} \to ZtZt$ and $ZtWb$, with $Z \to b\bar{b}$. Possible contributions from pair production of the B or X quarks that would be included, along with the T quark, in a weak-isospin doublet are ignored. Such particles are expected to decay primarily through $X, B \to Wt$ [8], and thus not lead to high b-tagged jet multiplicity, which is the primary focus of these searches. High jet and b-tagged jet multiplicities are also characteristic of $t\bar{t}t\bar{t}$ events (both within the SM and in BSM scenarios); this search is sensitive to these events. The four-top-quark production scenarios considered here do not feature large $E_{\mathrm{T}}^{\mathrm{miss}}$, so only the 1-lepton search is used to probe them. No dedicated re-optimisation for $t\bar{t}t\bar{t}$ events was performed.

---

[5]In the following, $HtZt$ is used to denote both $HtZ\bar{t}$ and its charge conjugate, $H\bar{t}Zt$. Similar notation is used for other processes, as appropriate.
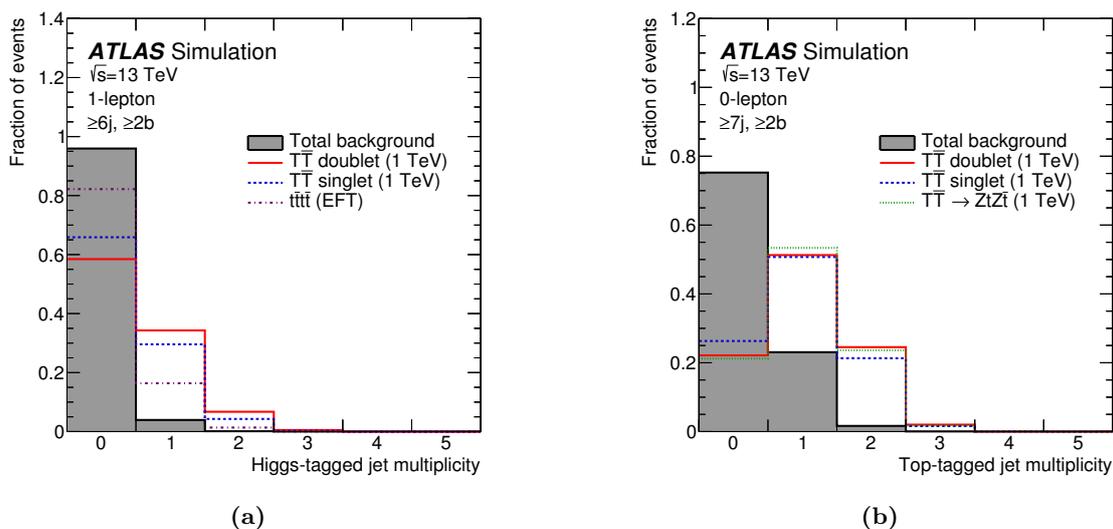
Figure 3. Comparison of the distribution of (a) the Higgs-tagged jet multiplicity and (b) the top-tagged jet multiplicity, between the total background (shaded histogram) and several signal scenarios considered in this search. The selection used in (a) corresponds to events in the 1-lepton channel satisfying the preselection requirements and ≥6 jets, whereas the selection used in (b) corresponds to events in the 0-lepton channel satisfying the preselection requirements and ≥7 jets. The signals shown correspond to: $T\bar{T}$ production in the weak-isospin doublet and singlet scenarios, and in the $\mathcal{B}(T \to Zt) = 1$ case, assuming $m_T = 1$ TeV; and $t\bar{t}t\bar{t}$ production within an EFT model.

In figure 2(a) the jet multiplicity distribution in the 1-lepton channel after preselection (described in section 4) is compared between the total background and several signal scenarios, chosen to illustrate differences among various types of signals the search is sensitive to. A similar comparison for the b-tagged jet multiplicity distribution is shown in figure 2(b) for events in the 0-lepton channel after preselection plus the requirement of ≥7 jets.

Compared to Run 1, the larger centre-of-mass energy in Run 2 provides sensitivity to higher-mass signals, which decay into boosted heavy SM particles (particularly Higgs bosons and top quarks). These potentially give rise to a high multiplicity of large-R jets that capture their decay products (see section 3). While $t\bar{t}$+jets events in the 1-lepton and 0-lepton channels are expected to typically contain one top-tagged jet, the signal events of interest are characterised by higher Higgs-tagged jet and top-tagged jet multiplicities, as illustrated in figures 3(a) and 3(b). The small fraction (about 5%) of background events with ≥2 top-tagged jets or ≥1 Higgs-tagged jets results from the misidentification of at least one large-R jet where initial- or final-state radiation was responsible for a large fraction of the constituents.

In order to optimise the sensitivity of the searches, the selected events are categorised into different regions depending on the jet multiplicity (5 and ≥6 jets in the 1-lepton channel; 6 and ≥7 jets in the 0-lepton channel), b-tagged jet multiplicity (3 and ≥4 in the 1-lepton channel; 2, 3 and ≥4 in the 0-lepton channel) and Higgs- and top-tagged jet
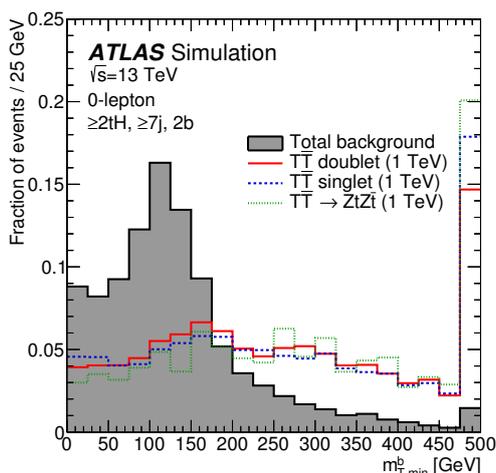
Figure 4. Comparison of the distribution of the minimum transverse mass of $E_{\mathrm{T}}^{\mathrm{miss}}$ and any of the three (or two, in events with exactly two b-tagged jets) leading b-tagged jets in the event ($m_{\mathrm{T,\,min}}^{\mathrm{b}}$), between the total background (shaded histogram) and several signal scenarios considered in this search. The selection used corresponds to events in the ($\geq$2tH, $\geq$7j, 2b) region of the 0-lepton channel. The signals shown correspond to $T\bar{T}$ production in the weak-isospin doublet and singlet scenarios, and in the $\mathcal{B}(T \to Zt) = 1$ case, assuming $m_T = 1$ TeV. The last bin in the figure contains the overflow.

multiplicity (0, 1 and $\geq$2). In the following, channels with N_{t} top-tagged jets, N_{H} Higgs-tagged jets, n jets, and m b-tagged jets are denoted by "N_{t}t, N_{H}H, nj, mb". Whenever the top/Higgs-tagging requirement is made on the sum $N_{\mathrm{t}} + N_{\mathrm{H}} \equiv N_{\mathrm{tH}}$, the channel is denoted by "N_{tH}tH, nj, mb". In addition, events in the 0-lepton channel are further categorised into two regions according to the value of $m_{\mathrm{T,\,min}}^{\mathrm{b}}$, the minimum transverse mass of $E_{\mathrm{T}}^{\mathrm{miss}}$ and any of the three (or two, in events with exactly two b-tagged jets) leading b-tagged jets in the event: $m_{\mathrm{T,\,min}}^{\mathrm{b}} < 160$ GeV (referred to as "LM", standing for "low mass") and $m_{\mathrm{T,\,min}}^{\mathrm{b}} > 160$ GeV (referred to as "HM", standing for "high mass"). This kinematic variable is bounded from above by the top quark mass for semileptonic $t\bar{t}$ background events, while the signal can have higher values of $m_{\mathrm{T,\,min}}^{\mathrm{b}}$ due to the presence of high-p_{T} neutrinos from $T \to Zt$, $Z \to \nu\nu$ or $T \to Wb$, $W \to \ell\nu$ decays. Although the requirements of a minimum top/Higgs-tagged jet multiplicity reduces the value of $m_{\mathrm{T,\,min}}^{\mathrm{b}}$ because of the resulting stronger collimation of the top quark decay products, this variable still provides useful discrimination between signal and $t\bar{t}$ background, as shown in figure 4. While the 1-lepton channel only considers regions with exactly 3 or $\geq$4 b-tagged jets, the 0-lepton channel also includes regions with exactly two b-jets and $m_{\mathrm{T,\,min}}^{\mathrm{b}} > 160$ GeV, to gain sensitivity to $T\bar{T} \to ZtZt$ decays with at least one $Z \to \nu\bar{\nu}$ decay.

To further improve the separation between the $T\bar{T}$ signal and background, the distinct kinematic features of the signal are exploited. In particular, the large T quark mass results in leptons and jets with large energy in the final state and the effective mass (m_{eff}), defined as the scalar sum of the transverse momenta of the lepton, the selected jets and the missing transverse momentum, provides a powerful discriminating variable between signal

and background. The m_{eff} distribution peaks at approximately $2m_T$ for signal events and at lower values for the $t\bar{t}$+jets background. For the same reasons, the various $t\bar{t}t\bar{t}$ signals from BSM scenarios also populate high values of m_{eff}. An additional selection requirement of $m_{\text{eff}} > 1$ TeV is made in order to minimise the effect of possible mismodelling of the m_{eff} distribution at low values originating from small backgrounds with large systematic uncertainties, such as multijet production. Such a requirement is applied for regions with $N_{\text{t}} + N_{\text{H}} \leq 1$ in the 1-lepton channel, and for all regions in the 0-lepton channel. Since the $T\bar{T}$ signal is characterised by having at least one top/Higgs-tagged jet and large values of m_{eff}, this minimum requirement on m_{eff} does not decrease the signal efficiency. In figure 5, the m_{eff} distribution is compared between signal and background for events in signal-rich regions of the 1-lepton and 0-lepton channels. The kinematic requirements in these regions result in a significantly harder m_{eff} spectrum for the background than in regions without top/Higgs-tagged jets, but this variable still shows good discrimination between signal and background. Thus, the m_{eff} distribution is used as the final discriminating variable in all regions considered in this search.

The regions with ≥ 6 jets (≥ 7 jets) are used to perform the search in the 1-lepton (0-lepton) channel (referred to as "search regions"), whereas the regions with exactly 5 jets (6 jets) are used to validate the background modelling in different regimes of event kinematics and heavy-flavour content (referred to as "validation regions"). A total of 12 search regions and 10 validation regions are considered in the 1-lepton channel, whereas 22 search regions and 16 validation regions are considered in the 0-lepton channel, defined in tables 2 and 3 respectively. In each channel, there are fewer validation regions than signal regions since some validation regions are merged to ensure a minimum of about 10 expected events. The level of possible signal contamination in the validation regions that have high event yields, and are therefore the regions that are most useful to validate the background prediction, depends on the signal scenario considered but is typically well below 10% for a 1 TeV T quark.

The overall rate and composition of the $t\bar{t}$+jets background strongly depends on the jet and b-tagged jet multiplicities, as illustrated in figure 6. The $t\bar{t}$+light-jets background is dominant in events with exactly two b-tagged jets, which typically correspond to the two b-quarks from the top quark decays. It also contributes significantly to events with exactly three b-tagged jets, in which typically a charm quark from the hadronic W boson decay is also b-tagged. Contributions from $t\bar{t}+\geq 1c$ and $t\bar{t}+\geq 1b$ become significant as the b-tagged jet multiplicity increases, with the $t\bar{t}+\geq 1b$ background being dominant for events with ≥ 4 b-tagged jets. The regions with different top/Higgs-tagged jet multiplicities probe different kinematic regimes, both soft (e.g. low-mass T quark) and hard (e.g. high-mass T quark or BSM $t\bar{t}t\bar{t}$ production). The search regions with the higher multiplicities of top-/Higgs-tagged jets and b-tagged jets in both the 1-lepton and 0-lepton channels, as well as the HM regions in the 0-lepton channel, have the largest signal-to-background ratio, and therefore drive the sensitivity of the search. The remaining search regions have significantly lower signal-to-background ratios, but are useful for checking and correcting the $t\bar{t}$+jets background prediction and constraining the related systematic uncertainties (see section 7) through a likelihood fit to data (see section 8). A summary of the signal-to-background ratio in the different search regions is displayed in figure 7 for the T quark signal with
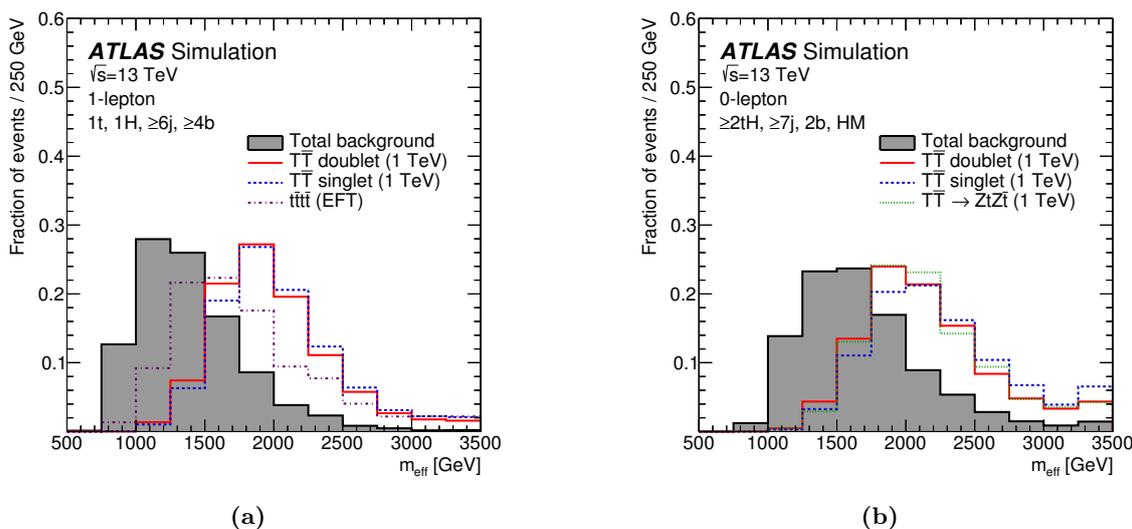
Figure 5. Comparison of the distribution of the effective mass (m_{eff}), between the total background (shaded histogram) and several signal scenarios considered in this search. The selection used in (a) corresponds to events in the (1t, 1H, $\geq$6j, $\geq$4b) region of the 1-lepton channel, whereas the selection used in (b) corresponds to events in the ($\geq$2tH, $\geq$7j, 2b, HM) region of the 0-lepton channel. The signals shown correspond to: $T\bar{T}$ production in the weak-isospin doublet and singlet scenarios, and in the $\mathcal{B}(T \rightarrow Zt) = 1$ case, assuming $m_T = 1$ TeV; and $t\bar{t}t\bar{t}$ production within an EFT model. The last bin in each distribution contains the overflow.

various decay configurations. A similar fitting strategy was followed in the Run-1 search in the 1-lepton channel [25].

A summary of the observed and expected yields before the fit to data in five of the most sensitive search regions in the 1-lepton and 0-lepton channels can be found in tables 4 and 5, respectively. The search regions shown in table 4 for the 1-lepton channel are a selection of some of the regions with the highest $S/\sqrt{B}$ ratio (where S and B are the expected signal and background yields, respectively) across several signal benchmark scenarios considered ($T\bar{T}$ in the $\mathcal{B}(T \rightarrow Ht) = 1$, T doublet, and T singlet scenarios, in all cases assuming $m_T = 1$ TeV, and $t\bar{t}t\bar{t}$ within an EFT and the 2UED/RPP models). Similarly, the search regions shown in table 5 for the 0-lepton channel are a superset of the regions with the highest $S/\sqrt{B}$ ratio for different $T\bar{T}$ signal benchmark scenarios (T doublet, T singlet and $\mathcal{B}(T \rightarrow Zt) = 1$, also assuming $m_T = 1$ TeV).

7 Systematic uncertainties

Several sources of systematic uncertainty are considered that affect the normalisation of signal and background and/or the shape of their m_{eff} distributions. Each source of systematic uncertainty is considered to be uncorrelated with the other sources. Correlations for a given systematic uncertainty are maintained across processes and channels, unless explicitly stated otherwise.

1-lepton channel				
Search regions ($\geq$6 jets)				
N_t	N_H	b-tag multiplicity	m_eff	Channel name
0	0	3	>1 TeV	0t, 0H, $\geq$6j, 3b
0	0	$\geq$4	>1 TeV	0t, 0H, $\geq$6j, $\geq$4b
1	0	3	>1 TeV	1t, 0H, $\geq$6j, 3b
1	0	$\geq$4	>1 TeV	1t, 0H, $\geq$6j, $\geq$4b
0	1	3	>1 TeV	0t, 1H, $\geq$6j, 3b
0	1	$\geq$4	>1 TeV	0t, 1H, $\geq$6j, $\geq$4b
1	1	3	—	1t, 1H, $\geq$6j, 3b
1	1	$\geq$4	—	1t, 1H, $\geq$6j, $\geq$4b
$\geq$2	0 or 1	3	—	$\geq$2t, 0–1H, $\geq$6j, 3b
$\geq$2	0 or 1	$\geq$4	—	$\geq$2t, 0–1H, $\geq$6j, $\geq$4b
$\geq$0	$\geq$2	3	—	$\geq$0t, $\geq$2H, $\geq$6j, 3b
$\geq$0	$\geq$2	$\geq$4	—	$\geq$0t, $\geq$2H, $\geq$6j, $\geq$4b
Validation regions (5 jets)				
N_t	N_H	b-tag multiplicity	m_eff	Channel name
0	0	3	>1 TeV	0t, 0H, 5j, 3b
0	0	$\geq$4	>1 TeV	0t, 0H, 5j, $\geq$4b
1	0	3	>1 TeV	1t, 0H, 5j, 3b
1	0	$\geq$4	>1 TeV	1t, 0H, 5j, $\geq$4b
0	1	3	>1 TeV	0t, 1H, 5j, 3b
0	1	$\geq$4	>1 TeV	0t, 1H, 5j, $\geq$4b
1	1	3	—	1t, 1H, 5j, 3b
$\geq$2	0 or 1	3	—	$\geq$2t, 0–1H, 5j, 3b
$\geq$0	$\geq$2	3	—	$\geq$0t, $\geq$2H, 5j, 3b
$N_\text{t} + N_\text{H} \geq 2$		$\geq$4	—	$\geq$2tH, 5j, $\geq$4b

Table 2. Definition of the search and validation regions (see text for details) in the 1-lepton channel.

0-lepton channel					
Search regions ($\geq$7 jets)					
N_{t}	N_{H}	b-tag multiplicity	$m_{\text{T, min}}^{\text{b}}$	m_{eff}	Channel name
0	0	2	>160 GeV	>1 TeV	0t, 0H, $\geq$7j, 2b, HM
0	0	3	<160 GeV	>1 TeV	0t, 0H, $\geq$7j, 3b, LM
0	0	3	>160 GeV	>1 TeV	0t, 0H, $\geq$7j, 3b, HM
0	0	$\geq$4	<160 GeV	>1 TeV	0t, 0H, $\geq$7j, $\geq$4b, LM
0	0	$\geq$4	>160 GeV	>1 TeV	0t, 0H, $\geq$7j, $\geq$4b, HM
1	0	2	>160 GeV	>1 TeV	1t, 0H, $\geq$7j, 2b, HM
1	0	3	<160 GeV	>1 TeV	1t, 0H, $\geq$7j, 3b, LM
1	0	3	>160 GeV	>1 TeV	1t, 0H, $\geq$7j, 3b, HM
1	0	$\geq$4	<160 GeV	>1 TeV	1t, 0H, $\geq$7j, $\geq$4b, LM
1	0	$\geq$4	>160 GeV	>1 TeV	1t, 0H, $\geq$7j, $\geq$4b, HM
0	1	2	>160 GeV	>1 TeV	0t, 1H, $\geq$7j, 2b, HM
0	1	3	<160 GeV	>1 TeV	0t, 1H, $\geq$7j, 3b, LM
0	1	3	>160 GeV	>1 TeV	0t, 1H, $\geq$7j, 3b, HM
0	1	$\geq$4	<160 GeV	>1 TeV	0t, 1H, $\geq$7j, $\geq$4b, LM
0	1	$\geq$4	>160 GeV	>1 TeV	0t, 1H, $\geq$7j, $\geq$4b, HM
1	1	3	<160 GeV	>1 TeV	1t, 1H, $\geq$7j, 3b, LM
1	1	3	>160 GeV	>1 TeV	1t, 1H, $\geq$7j, 3b, HM
$\geq$2	0 or 1	3	<160 GeV	>1 TeV	$\geq$2t, 0–1H, $\geq$7j, 3b, LM
$\geq$2	0 or 1	3	>160 GeV	>1 TeV	$\geq$2t, 0–1H, $\geq$7j, 3b, HM
$\geq$0	$\geq$2	3	—	>1 TeV	$\geq$0t, $\geq$2H, $\geq$7j, 3b
$N_{\text{t}} + N_{\text{H}} \geq 2$		2	>160 GeV	>1 TeV	$\geq$2tH, $\geq$7j, 2b, HM
$N_{\text{t}} + N_{\text{H}} \geq 2$		$\geq$4	—	>1 TeV	$\geq$2tH, $\geq$7j, $\geq$4b
Validation regions (6 jets)					
N_{t}	N_{H}	b-tag multiplicity	$m_{\text{T, min}}^{\text{b}}$	m_{eff}	Channel name
0	0	2	>160 GeV	>1 TeV	0t, 0H, 6j, 2b, HM
0	0	3	<160 GeV	>1 TeV	0t, 0H, 6j, 3b, LM
0	0	3	>160 GeV	>1 TeV	0t, 0H, 6j, 3b, HM
0	0	$\geq$4	<160 GeV	>1 TeV	0t, 0H, 6j, $\geq$4b, LM
0	0	$\geq$4	>160 GeV	>1 TeV	0t, 0H, 6j, $\geq$4b, HM
1	0	2	>160 GeV	>1 TeV	1t, 0H, 6j, 2b, HM
1	0	3	<160 GeV	>1 TeV	1t, 0H, 6j, 3b, LM
1	0	3	>160 GeV	>1 TeV	1t, 0H, 6j, 3b, HM
1	0	$\geq$4	—	>1 TeV	1t, 0H, 6j, $\geq$4b
0	1	2	>160 GeV	>1 TeV	0t, 1H, 6j, 2b, HM
0	1	3	<160 GeV	>1 TeV	0t, 1H, 6j, 3b, LM
0	1	3	>160 GeV	>1 TeV	0t, 1H, 6j, 3b, HM
0	1	$\geq$4	—	>1 TeV	0t, 1H, 6j, $\geq$4b
$N_{\text{t}} + N_{\text{H}} \geq 2$		2	>160 GeV	>1 TeV	$\geq$2tH, 6j, 2b, HM
$N_{\text{t}} + N_{\text{H}} \geq 2$		3	—	>1 TeV	$\geq$2tH, 6j, 3b
$N_{\text{t}} + N_{\text{H}} \geq 2$		$\geq$4	—	>1 TeV	$\geq$2tH, 6j, $\geq$4b

Table 3. Definition of the search and validation regions (see text for details) in the 0-lepton channel.
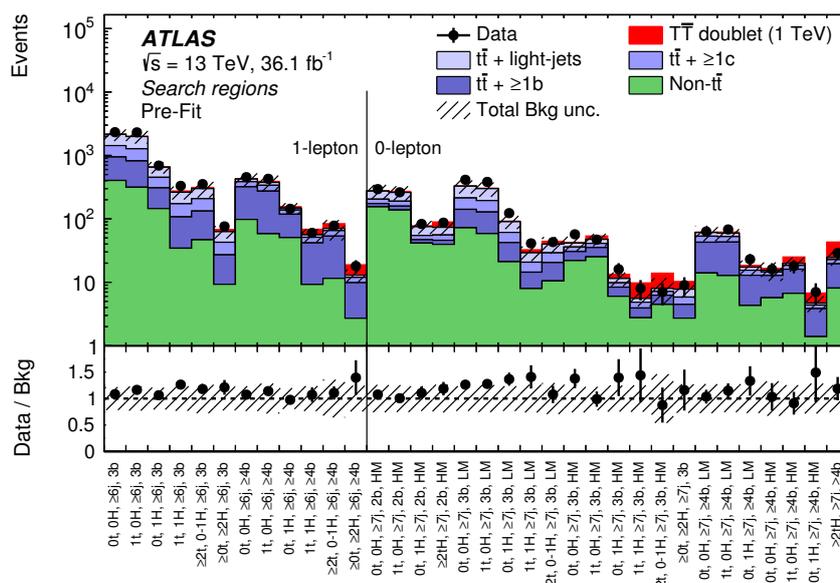
Figure 6. Comparison between the data and the background prediction for the yields in the search regions considered in the 1-lepton and 0-lepton channels, before the fit to data ("Pre-fit"). The small contributions from $t\bar{t}V$, $t\bar{t}H$, single-top, W/Z+jets, diboson, and multijet backgrounds are combined into a single background source referred to as "Non-$t\bar{t}$". The expected $T\bar{T}$ signal (solid red) corresponding to $m_T = 1$ TeV in the T doublet scenario is also shown, added on top of the background prediction. The bottom panel displays the ratio of data to the SM background ("Bkg") prediction. The hashed area represents the total uncertainty of the background, excluding the normalisation uncertainty of the $t\bar{t}+ \geq 1b$ background, which is determined via a likelihood fit to data.

The leading sources of systematic uncertainty vary depending on the analysis region considered. For example, the total systematic uncertainty of the background normalisation in the highest-sensitivity search region in the 1-lepton channel ($\geq 0t$, $\geq 2H$, $\geq 6j$, $\geq 4b$) is 25%, with the largest contributions originating from uncertainties in $t\bar{t}$+HF modelling and flavour tagging efficiencies (b, c, and light). The above uncertainty does not include the uncertainty in the $t\bar{t}+ \geq 1b$ normalisation, which is allowed to vary freely in the fit to data. However, as discussed previously, the joint fit to data across the 34 search regions considered in total in the 1-lepton and 0-lepton channels allows the overall background uncertainty to be reduced significantly, e.g., in the case of the search region specified above, down to 10% (including the uncertainty in the $t\bar{t}+ \geq 1b$ normalisation). Such a reduction results from the significant constraints that the data places on some systematic uncertainties, as well as the correlations among systematic uncertainties built into the likelihood model.

The following sections describe the systematic uncertainties considered in this analysis.

7.1 Luminosity

The uncertainty in the integrated luminosity is 2.1%, affecting the overall normalisation of all processes estimated from the simulation. It is derived, following a methodology
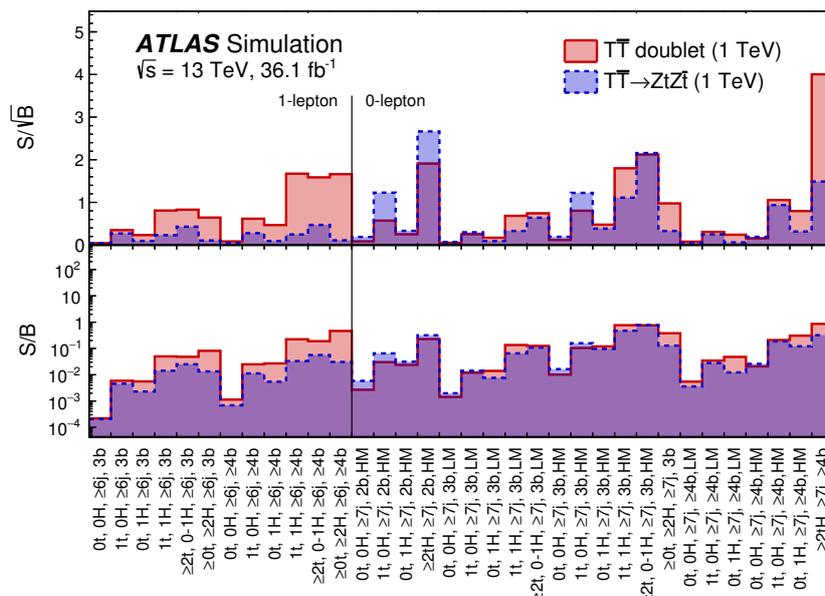
Figure 7. Signal-to-background ratio expressed as $S/\sqrt{B}$ (resp. S/B) in the top (resp. bottom) panel for each of the search regions. B and S stand for the total numbers of expected background and signal events in each region, respectively. For a 1 TeV T quark mass hypothesis, two branching ratio configurations are displayed: the doublet model (red filled area) and $\mathcal{B}(T \to Zt) = 1$ (blue filled area).

similar to that detailed in ref. [99], from a calibration of the luminosity scale using x-y beam-separation scans performed in August 2015 and May 2016.

7.2 Reconstructed objects

Uncertainties associated with leptons arise from the trigger, reconstruction, identification, and isolation efficiencies, as well as the lepton momentum scale and resolution. These are measured in data using $Z \to \ell^+\ell^-$ and $J/\psi \to \ell^+\ell^-$ events [31, 33]. The combined effect of all these uncertainties results in an overall normalisation uncertainty in signal and background of approximately 1%.

Uncertainties associated with jets arise from the jet energy scale and resolution, and the efficiency to pass the JVT requirement. The largest contribution results from the jet energy scale, whose uncertainty dependence on jet p_T and η, jet flavour, and pile-up treatment is split into 21 uncorrelated components that are treated independently in the analysis [38].

The leading uncertainties associated with reconstructed objects in this analysis originate from the modelling of the b-, c-, and light-jet-tagging efficiencies in the simulation, which is corrected to match the efficiencies measured in data control samples [41]. Uncertainties in these corrections include a total of six independent sources affecting b-jets and four independent sources affecting c-jets. Each of these uncertainties has a different dependence on jet p_T. Seventeen sources of uncertainty affecting light jets are considered, which depend on jet p_T and η. The sources of systematic uncertainty listed above are taken as uncorrelated between b-jets, c-jets, and light-jets. An additional uncertainty is included

1-lepton channel	≥2t, 0–1H, ≥6j, 3b	1t, 0H, ≥6j, ≥4b	1t, 1H, ≥6j, ≥4b	≥2t, 0–1H, ≥6j, ≥4b	≥0t, ≥2H, ≥6j, ≥4b
$T\bar{T}$ ($m_T = 1$ TeV)					
$\quad \mathcal{B}(T \to Ht) = 1$	19.6 ± 1.5	21.5 ± 2.6	24.3 ± 2.7	23.9 ± 2.8	14.6 ± 2.0
$\quad T$ doublet	14.2 ± 1.0	15.2 ± 1.6	12.5 ± 1.4	13.3 ± 1.5	5.96 ± 0.62
$\quad T$ singlet	7.88 ± 0.58	8.13 ± 0.94	5.47 ± 0.62	5.51 ± 0.69	2.18 ± 0.23
$t\bar{t}t\bar{t}$					
$\quad$ EFT ($|C_{4t}|/\Lambda^2 = 4\pi$ TeV^{-2})	535 ± 30	706 ± 80	171 ± 19	468 ± 55	34.3 ± 5.0
$\quad$ 2UED/RPP ($m_{\mathrm{KK}} = 1.6$ TeV)	9.77 ± 0.46	1.84 ± 0.35	1.00 ± 0.19	8.9 ± 1.4	0.39 ± 0.09
$t\bar{t}$+light-jets	91 ± 46	38 ± 17	4.8 ± 2.4	5.4 ± 3.3	0.99 ± 0.49
$t\bar{t}+\geq 1c$	75 ± 45	64 ± 38	9.5 ± 5.6	11.8 ± 7.5	2.1 ± 1.3
$t\bar{t}+\geq 1b$	86 ± 41	215 ± 83	32.4 ± 9.5	42 ± 22	7.1 ± 2.2
$t\bar{t}V$	9.7 ± 1.8	11.4 ± 2.4	1.73 ± 0.39	2.46 ± 0.53	0.41 ± 0.10
$t\bar{t}H$	4.90 ± 0.78	15.0 ± 2.8	3.79 ± 0.65	2.84 ± 0.62	1.19 ± 0.20
W+jets	9.4 ± 4.4	8.2 ± 4.2	0.69 ± 0.50	1.32 ± 0.71	0.54 ± 0.48
Z+jets	1.31 ± 0.64	0.95 ± 0.48	0.10 ± 0.07	0.13 ± 0.08	0.06 ± 0.05
Single top	13.1 ± 5.5	16.6 ± 7.0	1.69 ± 0.76	1.97 ± 0.95	0.26 ± 0.21
Diboson	1.8 ± 1.1	0.99 ± 0.55	0.11 ± 0.09	0.22 ± 0.14	0.01 ± 0.04
$t\bar{t}t\bar{t}$ (SM)	2.82 ± 0.86	4.9 ± 1.6	1.12 ± 0.36	2.55 ± 0.82	0.23 ± 0.07
Total background	299 ± 83	380 ± 110	56 ± 13	71 ± 25	12.9 ± 3.2
Data	353	428	60	78	18

Table 4. Predicted and observed yields in the 1-lepton channel in five of the most sensitive search regions (depending on the signal scenario) considered. The multijet background is estimated to be negligible in these regions and thus not shown. The background prediction is shown before the fit to data. Also shown are the signal predictions for different benchmark scenarios considered. The quoted uncertainties are the sum in quadrature of statistical and systematic uncertainties in the yields, excluding the normalisation uncertainty of the $t\bar{t}+ \geq 1b$ background, which is determined via a likelihood fit to data.

due to the extrapolation of these corrections to jets with p_{T} beyond the kinematic reach of the data calibration samples used ($p_{\mathrm{T}} > 300$ GeV for b- and c-jets, and $p_{\mathrm{T}} > 750$ GeV for light-jets); it is taken to be correlated among the three jet flavours. This uncertainty is evaluated in the simulation by comparing the tagging efficiencies while varying e.g. the fraction of tracks with shared hits in the silicon detectors or the fraction of fake tracks resulting from random combinations of hits, both of which typically increase at high p_{T} due to growing track multiplicity and density of hits within the jet. Finally, an uncertainty related to the application of c-jet scale factors to τ-jets is considered, but has a negligible impact in this analysis. The combined effect of these uncertainties results in an uncertainty in the $t\bar{t}$ background normalisation ranging from 4% to 12% depending on the analysis region. The corresponding uncertainty range for signal is 2–12%, assuming $T\bar{T}$ production in the weak-isospin doublet scenario and $m_T = 1$ TeV.

0-lepton channel	≥2tH, ≥7j, 2b, HM	1t, 1H, ≥7j, 3b, HM	≥2t, 0–1H, ≥7j, 3b, HM	1t, 0H, ≥7j, ≥4b, HM	≥2tH, ≥7j, ≥4b
$T\bar{T}$ ($m_T = 1$ TeV)					
$\mathcal{B}(T \to Zt) = 1$	22.3 ± 2.3	2.60 ± 0.57	6.02 ± 0.61	4.72 ± 0.66	6.94 ± 0.98
T doublet	16.0 ± 1.1	4.22 ± 0.34	5.92 ± 0.49	5.32 ± 0.61	18.7 ± 2.0
T singlet	8.52 ± 0.61	1.81 ± 0.16	2.63 ± 0.22	2.32 ± 0.29	6.91 ± 0.80
$t\bar{t}$+light-jets	17.8 ± 9.8	0.72 ± 0.40	0.80 ± 0.53	1.30 ± 0.72	1.71 ± 0.98
$t\bar{t}$+≥1c	9.7 ± 6.4	0.92 ± 0.65	0.95 ± 0.71	2.4 ± 1.6	3.2 ± 2.0
$t\bar{t}$+≥1b	6.3 ± 4.2	1.17 ± 0.59	1.78 ± 0.74	9.4 ± 3.2	11.4 ± 4.1
$t\bar{t}V$	5.5 ± 1.0	0.49 ± 0.12	0.88 ± 0.19	1.19 ± 0.27	1.01 ± 0.24
$t\bar{t}H$	0.61 ± 0.12	0.17 ± 0.05	0.13 ± 0.04	0.85 ± 0.17	1.08 ± 0.25
W+jets	9.6 ± 4.1	0.52 ± 0.27	0.80 ± 0.37	0.81 ± 0.40	0.56 ± 0.28
Z+jets	8.6 ± 4.5	0.59 ± 0.28	0.8 ± 2.1	0.80 ± 0.40	0.63 ± 0.42
Single top	8.3 ± 4.4	0.69 ± 0.43	0.97 ± 0.59	1.8 ± 1.0	1.10 ± 0.61
Diboson	2.9 ± 1.9	0.11 ± 0.20	0.55 ± 0.66	0.24 ± 0.25	0.14 ± 0.15
$t\bar{t}t\bar{t}$ (SM)	0.22 ± 0.07	0.06 ± 0.02	0.12 ± 0.04	0.31 ± 0.10	0.77 ± 0.25
Multijet	3.9 ± 3.9	0.13 ± 0.17	0.20 ± 0.24	0.64 ± 0.68	2.8 ± 2.8
Total background	73 ± 19	5.6 ± 1.4	8.0 ± 3.7	19.7 ± 5.0	24.4 ± 6.3
Data	87	8	7	18	29

Table 5. Predicted and observed yields in the 0-lepton channel in five of the most sensitive search regions (depending on the signal scenario) considered. The background prediction is shown before the fit to data. Also shown are the signal predictions for different benchmark scenarios considered. The quoted uncertainties are the sum in quadrature of statistical and systematic uncertainties in the yields, excluding the normalisation uncertainty of the $t\bar{t}+ \geq 1b$ background, which is determined via a likelihood fit to data.

7.3 Background modelling

A number of sources of systematic uncertainty affecting the modelling of $t\bar{t}$+jets are considered. An uncertainty of 6% is assigned to the inclusive $t\bar{t}$ production cross section [56], including contributions from varying the factorisation and renormalisation scales, and from uncertainties in the PDF, α_S, and the top quark mass, all added in quadrature. Since several search regions have a sufficiently large number of events of $t\bar{t}+\geq 1b$ background, its normalisation is completely determined by the data during the fit procedure. In the case of the $t\bar{t}+\geq 1c$ normalisation, since the fit to the data is unable to precisely determine it and the analysis has very limited sensitivity to its uncertainty, a normalisation uncertainty of 50% is assumed.

Alternative $t\bar{t}$ samples were generated using POWHEG-BOX interfaced to HERWIG++ 2.7.1 [100] and MG5_aMC 2.2.1 interfaced to HERWIG++ 2.7.1 in order to estimate systematic uncertainties related to the modelling of this background. The effects of initial- and final-state radiation (ISR/FSR) are explored using two alternative POWHEG-BOX+PYTHIA samples, one with h_damp set to $2m_t$, the renormalisation and factorisation

scales set to half the nominal value and using the P2012 radHi UE tune, giving more radiation (referred to as "radHi"), and one with the P2012 radLo UE tune, $h_{\mathrm{damp}} = m_t$ and the renormalisation and factorisation scales set to twice the nominal value, giving less radiation (referred to as "radLow") [101].

Uncertainties affecting the modelling of $t\bar{t}+{\geq}1b$ production include shape uncertainties (including inter-category migration effects) associated with the NLO prediction from SHERPAOL, which is used for reweighting the nominal POWHEG-BOX+PYTHIA 6 $t\bar{t}+{\geq}1b$ prediction. These uncertainties include different scale variations, a different shower-recoil model scheme, and two alternative PDF sets (see ref. [102] for details), and are significantly smaller than those estimated by comparing different event generators. An uncertainty due to the choice of generator is assessed by comparing the $t\bar{t}+{\geq}1b$ predictions obtained after reweighting POWHEG-BOX+PYTHIA 6 to the NLO calculation from SHERPAOL and to an equivalent NLO calculation from MG5_aMC+PYTHIA 8, which differs in the procedure used to match the NLO matrix element calculation and the parton shower (see section 1.6.8 of ref. [103]). The uncertainty from the parton shower and hadronisation model is taken from the difference between the MG5_aMC calculation showered with either PYTHIA8 or HERWIG++. Additional uncertainties are assessed for the contributions to the $t\bar{t}+{\geq}1b$ background originating from multiple parton interactions or final-state radiation from top quark decay products, which are not part of the NLO prediction. The latter are assessed via the alternative "radHi" and "radLow" samples, as discussed below. The nominal NLO corrections, as well as their variations used to propagate the theoretical uncertainties in the NLO prediction, are adjusted so that the particle-level cross section of the $t\bar{t}+{\geq}1b$ background (i.e. prior to reconstruction-level selection requirements) is fixed to the nominal prediction, i.e. effectively only migrations across categories and distortions to the shape of the kinematic distributions are considered.

In the following, uncertainties affecting all $t\bar{t}+$jets processes are discussed. Uncertainties associated with the modelling of ISR/FSR are obtained from the comparison of the POWHEG-BOX+PYTHIA 6 "radHi" and "radLow" samples (see section 5.2) with the nominal POWHEG-BOX+PYTHIA 6 sample. An uncertainty associated with the choice of NLO generator is derived by comparing two $t\bar{t}$ samples, one generated with POWHEG-BOX+HERWIG++ and another generated with MG5_aMC+HERWIG++, and propagating the resulting fractional difference to the nominal POWHEG-BOX+PYTHIA 6 prediction. An uncertainty due to the choice of parton shower and hadronisation model is derived by comparing events produced by POWHEG-BOX interfaced to PYTHIA 6 or HERWIG++. Finally, the uncertainty in the modelling of the top quark's p_{T}, affecting only the $t\bar{t}+$light-jets and $t\bar{t}+{\geq}1c$ processes, is evaluated by taking the full difference between applying and not applying the reweighting to match the NNLO prediction. The above uncertainties are taken as uncorrelated between the $t\bar{t}+$light-jets, $t\bar{t}+{\geq}1c$ and $t\bar{t}+{\geq}1b$ processes. In the case of $t\bar{t}+{\geq}1b$, in all instances the various HF categories and the corresponding partonic kinematics for the alternative MC samples are reweighted to match the NLO prediction of SHERPAOL so that only effects other than distortions to the inter-normalisation of the various $t\bar{t}+{\geq}1b$ topologies and their parton-level kinematics are propagated. In the case of $t\bar{t}+$light-jets and $t\bar{t}+{\geq}1c$ the full effect of these uncertainties is propagated. Similarly

to the treatment of the NLO corrections and uncertainties associated with $t\bar{t}+{\geq}1b$ discussed above, in the case of the additional uncertainties derived by comparing alternative $t\bar{t}$ samples, the overall normalisation of the $t\bar{t}+{\geq}1c$ and $t\bar{t}+{\geq}1b$ background at the particle level is fixed to the nominal prediction. In this way, only migrations across categories and distortions to the shape of the kinematic distributions are considered. In order to maintain the inclusive $t\bar{t}$ cross section, the $t\bar{t}+$light-jets background is adjusted accordingly.

Uncertainties affecting the modelling of the single-top-quark background include a $+5\%/-4\%$ uncertainty in the total cross section estimated as a weighted average of the theoretical uncertainties in t-, Wt- and s-channel production [84–86]. Additional uncertainties associated with the modelling of ISR/FSR are assessed by comparing the nominal samples with alternative samples where generator parameters were varied (i.e. "radHi" and "radLow"). For the t- and Wt-channel processes, an uncertainty due to the choice of parton shower and hadronisation model is derived by comparing events produced by POWHEG-BOX interfaced to PYTHIA 6 or HERWIG++. These uncertainties are treated as fully correlated among single-top production processes, but uncorrelated with the corresponding uncertainty in the $t\bar{t}+$jets background. The sum in quadrature of the above uncertainties on the single top normalisation at the preselection level is 20% in the 1-lepton channel and 20%(25%) in LM(HM) regions of the 0-lepton channel, respectively. An additional systematic uncertainty on Wt-channel production concerning the separation between $t\bar{t}$ and Wt at NLO [104] is assessed by comparing the nominal sample, which uses the so-called "diagram subtraction" scheme, with an alternative sample using the "diagram removal" scheme. This uncertainty, which is taken to be single-sided, has a strong shape dependence and affects the Wt normalisation by about -50% in the 1-lepton channel and LM regions of the 0-lepton channel, and by about -75% in HM regions of the 0-lepton channel. Due to the small size of the simulated samples, and hence limited statistical precision, these uncertainties cannot be reliably estimated in each analysis region and so their estimates at the preselection level are used instead. They are treated as uncorrelated across regions with different top-tagged jet and Higgs-tagged jet multiplicities and between the 1-lepton and 0-lepton channels.

Uncertainties affecting the normalisation of the $V+$jets background are estimated for the sum of $W+$jets and $Z+$jets, and separately for $V+$light-jets, $V+{\geq}1c+$jets, and $V+{\geq}1b+$jets subprocesses. The total normalisation uncertainty of $V+$jets processes is estimated by comparing the data and total background prediction in the different analysis regions considered, but requiring exactly 0 b-tagged jets. Agreement between data and predicted background in these modified regions, which are dominated by $V+$light-jets, is found to be within approximately 30%. This bound is taken to be the normalisation uncertainty, correlated across all $V+$jets subprocesses. Since SHERPA 2.2 has been found to underestimate $V+$heavy-flavour by about a factor of 1.3 [105], additional 30% normalisation uncertainties are assumed for $V+{\geq}1c+$jets and $V+{\geq}1b+$jets subprocesses, considered uncorrelated between them. These uncertainties are treated as uncorrelated across regions with different top-/Higgs-tagged jet multiplicities and between the 1-lepton and 0-lepton channels.

Uncertainties in the diboson background normalisation include 5% from the NLO theory cross sections [106], as well as an additional 24% normalisation uncertainty added in quadrature for each additional inclusive jet-multiplicity bin, based on a comparison among

different algorithms for merging LO matrix elements and parton showers [107]. Therefore, normalisation uncertainties of $5\% \oplus \sqrt{3} \times 24\% = 42\%$ and $5\% \oplus \sqrt{4} \times 24\% = 48\%$ are assigned for events with exactly 5 jets and ≥ 6 jets, respectively (this assumes that two jets come from the W/Z decay, as in $WW/WZ \to \ell\nu jj$). Recent comparisons between data and SHERPA 2.1.1 for $WZ(\to \ell\nu\ell\ell)+ \geq 4$ jets show agreement within the experimental uncertainty of approximately 40% [108], which further justifies the above uncertainty. This uncertainty is taken to be uncorrelated across regions with different top-/Higgs-tagged jet multiplicities and between the 1-lepton and 0-lepton channels

Uncertainties in the $t\bar{t}V$ and $t\bar{t}H$ cross sections are 15% and $+10\%/-13\%$, respectively, from the uncertainties in their respective NLO theoretical cross sections [109–111]. Finally, an uncertainty of 30% is estimated for the NLO prediction of the SM $t\bar{t}t\bar{t}$ cross section [67]. Since no additional modelling uncertainties are taken into account for these backgrounds, and the 1-lepton and 0-lepton channels cover different kinematic phase spaces, the above uncertainties in the $t\bar{t}V$, $t\bar{t}H$, and SM $t\bar{t}t\bar{t}$ cross sections are taken to be uncorrelated between the two channels.

Uncertainties in the data-driven multijet background estimate receive contributions from the limited sample size in data, particularly at high jet and b-tag multiplicities, as well as from the uncertainty in the misidentified-lepton rate, measured in different control regions (e.g. selected with a requirement on either the maximum $E_{\mathrm{T}}^{\mathrm{miss}}$ or m_{T}^{W}). Based on the comparisons between data and total prediction in multijet-rich selections, the normalisation uncertainties assumed for this background are 50% (100%) for electrons with $|\eta_{\mathrm{cluster}}| \leq 1$ ($|\eta_{\mathrm{cluster}}| > 1$), and 50% for muons, taken to be uncorrelated across regions with different top-/Higgs-tagged jet multiplicities and between events containing electrons and events containing muons. In the case of the 0-lepton channel, the normalisation uncertainty assigned to the multijet background is 100%. No explicit shape uncertainty is assigned since the large statistical uncertainties associated with the multijet background prediction, which are uncorrelated between bins in the final discriminant distribution, are assumed to effectively cover possible shape uncertainties.

8 Statistical analysis

For each search, the m_{eff} distributions across all regions considered are jointly analysed to test for the presence of a signal predicted by the benchmark scenarios. The statistical analysis uses a binned likelihood function $\mathcal{L}(\mu, \theta)$ constructed as a product of Poisson probability terms over all bins considered in the search. This function depends on the signal-strength parameter μ, which multiplies the predicted production cross section for signal, and θ, a set of nuisance parameters that encode the effect of systematic uncertainties in the signal and background expectations. Therefore, the expected total number of events in a given bin depends on μ and θ. With the exception of the parameter that controls the normalisation of the $t\bar{t}+\geq 1b$ background, all other nuisance parameters are implemented in the likelihood function as Gaussian or log-normal constraints. The above-mentioned $t\bar{t}+\geq 1b$ normalisation factor is a free parameter of the fit.

For a given value of μ, the nuisance parameters θ allow variations of the expectations for signal and background according to the corresponding systematic uncertainties, and their fitted values result in the deviations from the nominal expectations that globally provide the best fit to the data. This procedure allows a reduction of the impact of systematic uncertainties on the search sensitivity by taking advantage of the highly populated background-dominated regions included in the likelihood fit. To verify the improved background prediction, fits under the background-only hypothesis are performed, and differences between the data and the post-fit background prediction are checked using kinematic variables other than the ones used in the fit. The m_{eff} distributions in validation regions not used in the fit are also checked. Statistical uncertainties in each bin of the predicted m_{eff} distributions due to the limited size of the simulated samples are taken into account by dedicated parameters in the fit.

The test statistic q_μ is defined as the profile likelihood ratio: $q_\mu = -2\ln(\mathcal{L}(\mu, \hat{\hat{\theta}}_\mu)/\mathcal{L}(\hat{\mu}, \hat{\theta}))$, where $\hat{\mu}$ and $\hat{\theta}$ are the values of the parameters that maximise the likelihood function (subject to the constraint $0 \leq \hat{\mu} \leq \mu$), and $\hat{\hat{\theta}}_\mu$ are the values of the nuisance parameters that maximise the likelihood function for a given value of μ. The test statistic q_μ is evaluated with the RooFit package [112, 113]. A related statistic is used to determine the probability that the observed data are compatible with the background-only hypothesis (i.e. the discovery test) by setting $\mu = 0$ in the profile likelihood ratio and leaving $\hat{\mu}$ unconstrained: $q_0 = -2\ln(\mathcal{L}(0, \hat{\hat{\theta}}_0)/\mathcal{L}(\hat{\mu}, \hat{\theta}))$. The p-value (referred to as p_0) representing the probability of the data being compatible with the background-only hypothesis is estimated by integrating the distribution of q_0 from background-only pseudo-experiments, approximated using the asymptotic formulae given in refs. [114], above the observed value of q_0. Some model dependence exists in the estimation of the p_0, as a given signal scenario needs to be assumed in the calculation of the denominator of q_μ, even if the overall signal normalisation is left floating and fitted to data. The observed p_0 is checked for each explored signal scenario. Upper limits on the signal production cross section for each of the signal scenarios considered are derived by using q_μ in the CL_s method [115, 116]. For a given signal scenario, values of the production cross section (parameterised by μ) yielding $\text{CL}_s < 0.05$, where CL_s is computed using the asymptotic approximation [114], are excluded at $\geq 95\%$ CL.

9 Results

This section presents the results obtained from searches in the 1-lepton and 0-lepton channels, as well as their combination, following the statistical analysis discussed in section 8.

9.1 Likelihood fits to data

A binned likelihood fit under the background-only hypothesis is performed on the m_{eff} distributions in all search regions considered. In this section, the results of the simultaneous likelihood fit to the search regions in the 1-lepton and 0-lepton channels are discussed. This combined fit is used to obtain results on $T\bar{T}$ production. In this combination, all common
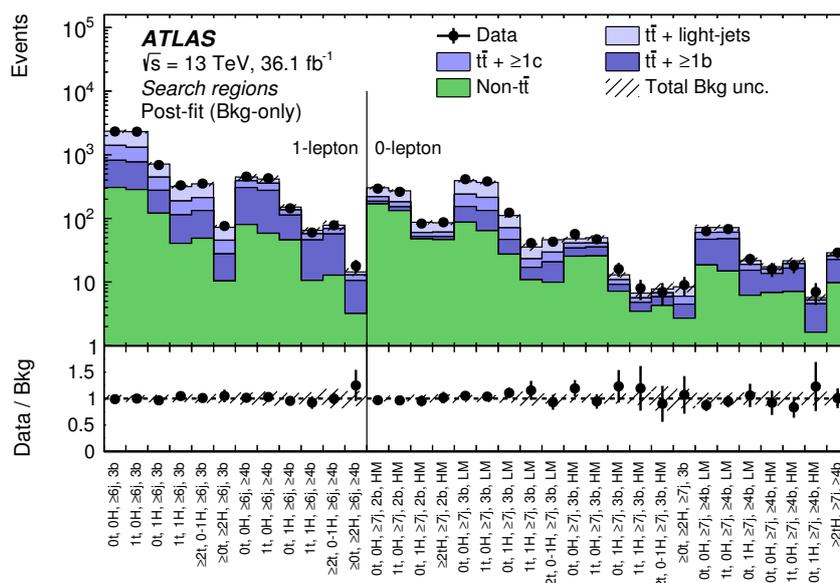
Figure 8. Comparison between the data and the background prediction for the yields in the search regions considered in the 1-lepton and 0-lepton channels, after the combined fit to data ("Post-fit") under the background-only hypothesis. The small contributions from $t\bar{t}V$, $t\bar{t}H$, single-top, W/Z+jets, diboson, and multijet backgrounds are combined into a single background source referred to as "Non-$t\bar{t}$". The bottom panel displays the ratio of data to the SM background ("Bkg") prediction. The hashed area represents the total uncertainty of the background.

systematic uncertainties are considered fully correlated between the 1-lepton and 0-lepton channels, with the exception of those affecting non-$t\bar{t}$ backgrounds. To obtain the results in the individual channels, separate fits are performed. In general, good agreement is found among the fitted nuisance parameters in the individual and combined fits.

A comparison of the distribution of observed and expected yields in the search regions in the 1-lepton and 0-lepton channels after the combined fit is shown in figure 8 (see figure 6 for the results before the combined fit). The post-fit yields in five of the most sensitive search regions in the 1-lepton and 0-lepton channels can be found in tables 6 and 7, respectively. For the same search regions, the corresponding m_{eff} distributions, both before and after the fit to data, are shown in figures 9–13. The binning used for the m_{eff} distributions in the different search regions represents a compromise between preserving enough discrimination between the background and the different signal hypotheses considered, and keeping the statistical uncertainty on the background prediction per bin well below 30%. While some of the systematic uncertainties from individual sources described in section 7 vary across the m_{eff} spectrum, the total pre-fit uncertainty is largely independent of m_{eff}. The large number of events in the signal-depleted regions, together with their different background compositions, and the assumptions of the fit model, constrain the combined effect of the sources of systematic uncertainty. As a result, an improved background prediction is obtained with significantly reduced uncertainty, not only in the signal-depleted channels, but also in the signal-rich channels such as ($\geq$0t, $\geq$2H, $\geq$6j, $\geq$4b) in the 1-lepton channel.

In the combined fit, the channels with three b-tagged jets are effectively used to constrain the leading uncertainties affecting the $t\bar{t}$+light-jets background prediction, while the channels with ≥ 4 b-tagged jets are sensitive to the uncertainties affecting the $t\bar{t}$+HF background prediction. In particular, one of the main corrections determined in the fit is a scale factor that multiplies the $t\bar{t}+\geq 1b$ normalisation by 0.90 ± 0.23 relative to the nominal prediction.[6] In addition, the nuisance parameter controlling the $t\bar{t}+\geq 1c$ normalisation is adjusted to scale this background by a factor of 1.3 ± 0.4 relative to its nominal prediction. The fit results in better agreement between data and prediction in the channels with ≥ 3 b-tagged jets, where the $t\bar{t}$+HF background dominates. Detailed studies were performed to verify the stability of the fit against variations in the treatment of the systematic uncertainties affecting the $t\bar{t}$+HF background (e.g. by decorrelating normalisation and shape uncertainties between different $t\bar{t}+\geq 1b$ categories, or by scaling the $t\bar{t}+\geq 1b$ and $t\bar{t}+\geq 1c$ backgrounds by a common factor), finding in all instances a robust post-fit background prediction. Furthermore, the impact on the background-only fit of injecting a $T\bar{T}$ signal (with $m_T = 1$ TeV) in the doublet configuration was confirmed to be negligible. Although there is no single nuisance parameter directly responsible for the normalisation of $t\bar{t}$+light-jets background, the yields for this contribution within each region are affected by systematic uncertainties in the $t\bar{t}$ modelling and the jet flavour tagging, and thus are changed after the fit.

A comparison of the distribution of observed and expected yields in all validation regions considered, before and after the combined fit in the search regions, is shown in figure 14. Agreement between data and prediction in normalisation and shape of the m_{eff} distribution for these regions, which are not used in the fit, is generally improved after the fit, giving confidence in the overall procedure. To increase the background yields and strengthen the validation of the fit strategy, comparisons between data and background prediction, before and after the fit, are performed for more-inclusive event selections. As an example, the distributions of two kinematic variables used to define the search strategy can be found in figures 15 and 16. They display respectively the Higgs-tagged jet multiplicity in the 1-lepton channel, after requiring at least 6 jets and 3 b-jets, and the distribution of the $m_{\mathrm{T, min}}^{\mathrm{b}}$ variable in the 0-lepton channel for events containing at least 7 jets and 2 b-jets, together with at least one top/Higgs-tagged jet. Although these variables are not directly used in the fit, a good description of the data by the post-fit background prediction is observed, which further validates the fitting procedure. The result of the background-only fit to data is used for the background prediction in the computation of the limits presented in the following subsections.

9.2 Limits on vector-like quark pair production

No significant excess above the SM expectation is found in any of the search regions. Upper limits at 95% CL on the $T\bar{T}$ production cross section are set in several benchmark scenarios as a function of the T quark mass m_T and are compared to the theoretical prediction from Top++. The resulting lower limits on m_T correspond to the central value of the

---

[6]Even though the $t\bar{t}+\geq 1b$ normalisation factor is assumed to be the same in all regions, the overall change in $t\bar{t}+\geq 1b$ normalisation can be different across channels due to the different impact of other nuisance parameters affecting the $t\bar{t}+\geq 1b$ background, such as those related to $t\bar{t}+\geq 1b$ modelling.
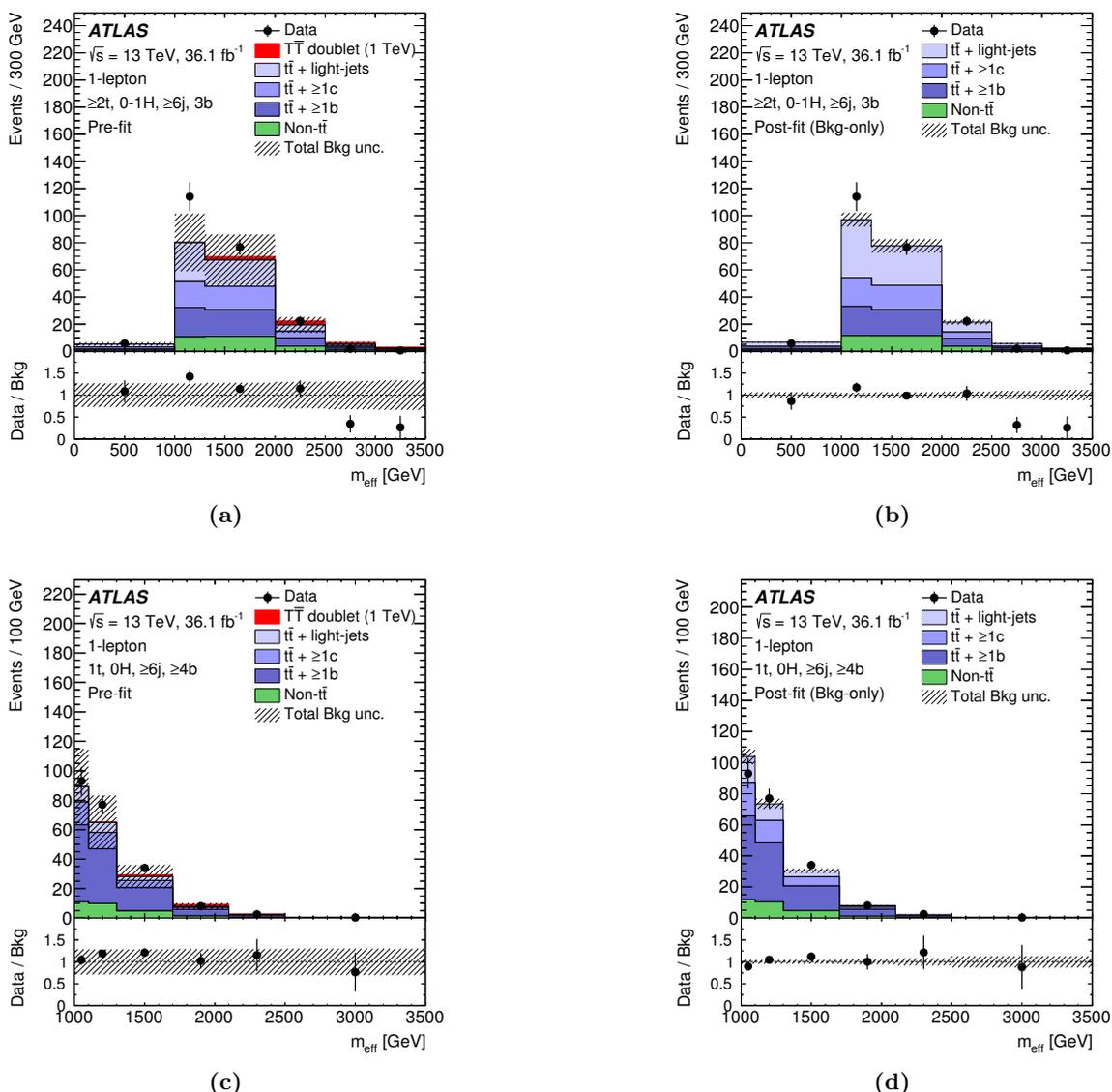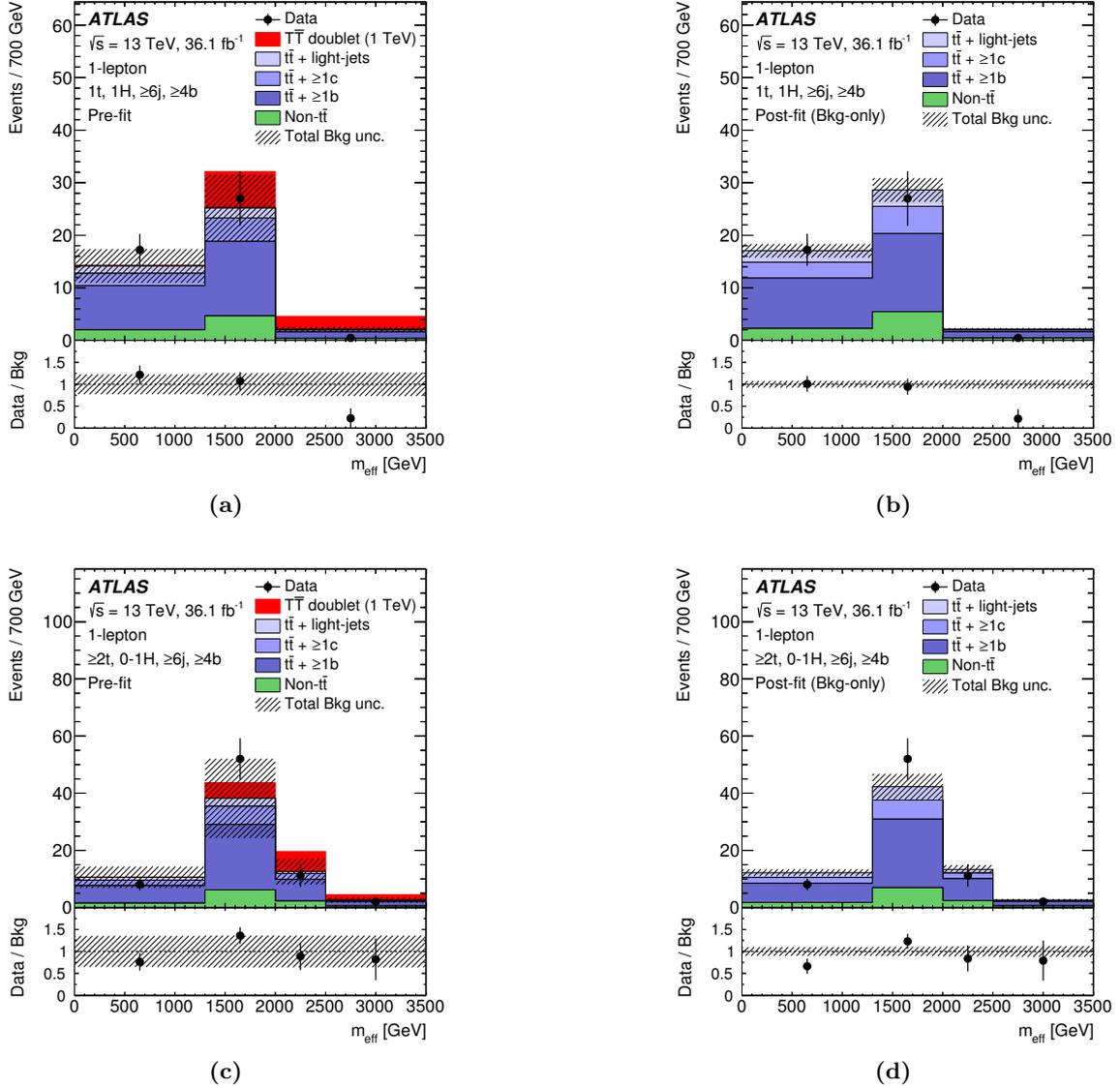
Figure 9. Comparison between the data and prediction for the m_{eff} distribution in some of the most sensitive search regions in the 1-lepton channel, before and after performing the combined fit to data in the 0-lepton and 1-lepton channels ("Pre-fit" and "Post-fit", respectively) under the background-only hypothesis. Shown are the ($\geq$2t, 0–1H, $\geq$6j, 3b) region (a) pre-fit and (b) post-fit, and the (1t, 0H, $\geq$6j, $\geq$4b) region (c) pre-fit and (d) post-fit. In the pre-fit figures the expected $T\bar{T}$ signal (solid red) corresponding to $m_T = 1$ TeV in the T doublet scenario is also shown, added on top of the background prediction. The small contributions from $t\bar{t}V$, $t\bar{t}H$, single-top, W/Z+jets, diboson, and multijet backgrounds are combined into a single background source referred to as "Non-$t\bar{t}$". The last bin in all figures contains the overflow. The bottom panels display the ratios of data to the total background prediction ("Bkg"). The hashed area represents the total uncertainty of the background. In the case of the pre-fit background uncertainty, the normalisation uncertainty of the $t\bar{t}+ \geq 1b$ background is not included.
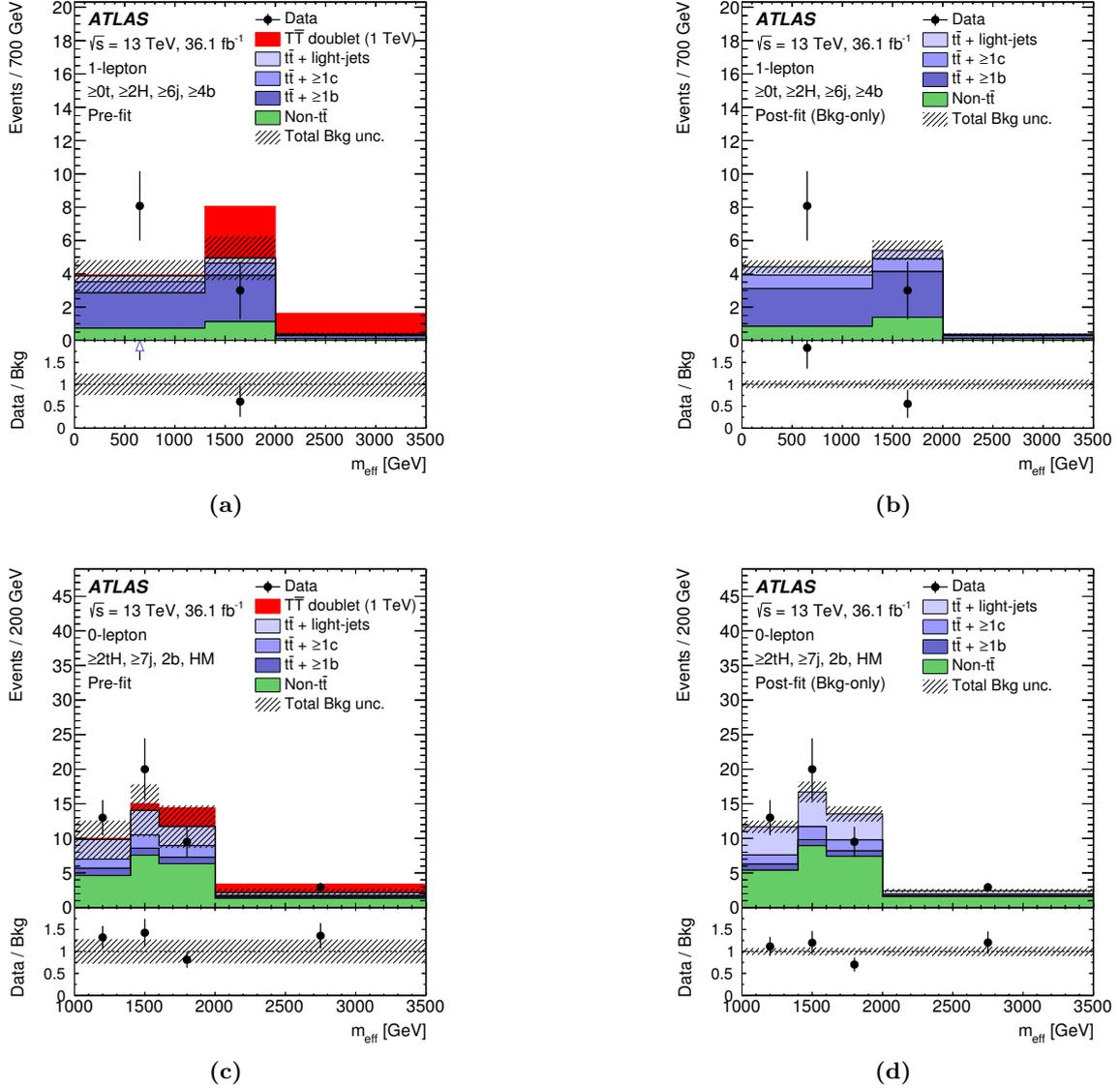
Figure 10. Comparison between the data and prediction for the m_{eff} distribution in some of the most sensitive search regions in the 1-lepton channel, before and after performing the combined fit to data in the 0-lepton and 1-lepton channels ("Pre-fit" and "Post-fit", respectively) under the background-only hypothesis. Shown are the (1t, 1H, $\geq$6j, $\geq$4b) region (a) pre-fit and (b) post-fit, and the ($\geq$2t, 0–1H, $\geq$6j, $\geq$4b) region (c) pre-fit and (d) post-fit. In the pre-fit figures the expected $T\bar{T}$ signal (solid red) corresponding to $m_T = 1$ TeV in the T doublet scenario is also shown, added on top of the background prediction. The small contributions from $t\bar{t}V$, $t\bar{t}H$, single-top, W/Z+jets, diboson, and multijet backgrounds are combined into a single background source referred to as "Non-$t\bar{t}$". The last bin in all figures contains the overflow. The bottom panels display the ratios of data to the total background prediction ("Bkg"). The blue triangles indicate points that are outside the vertical range of the figure. The hashed area represents the total uncertainty of the background. In the case of the pre-fit background uncertainty, the normalisation uncertainty of the $t\bar{t}+ \geq 1b$ background is not included.
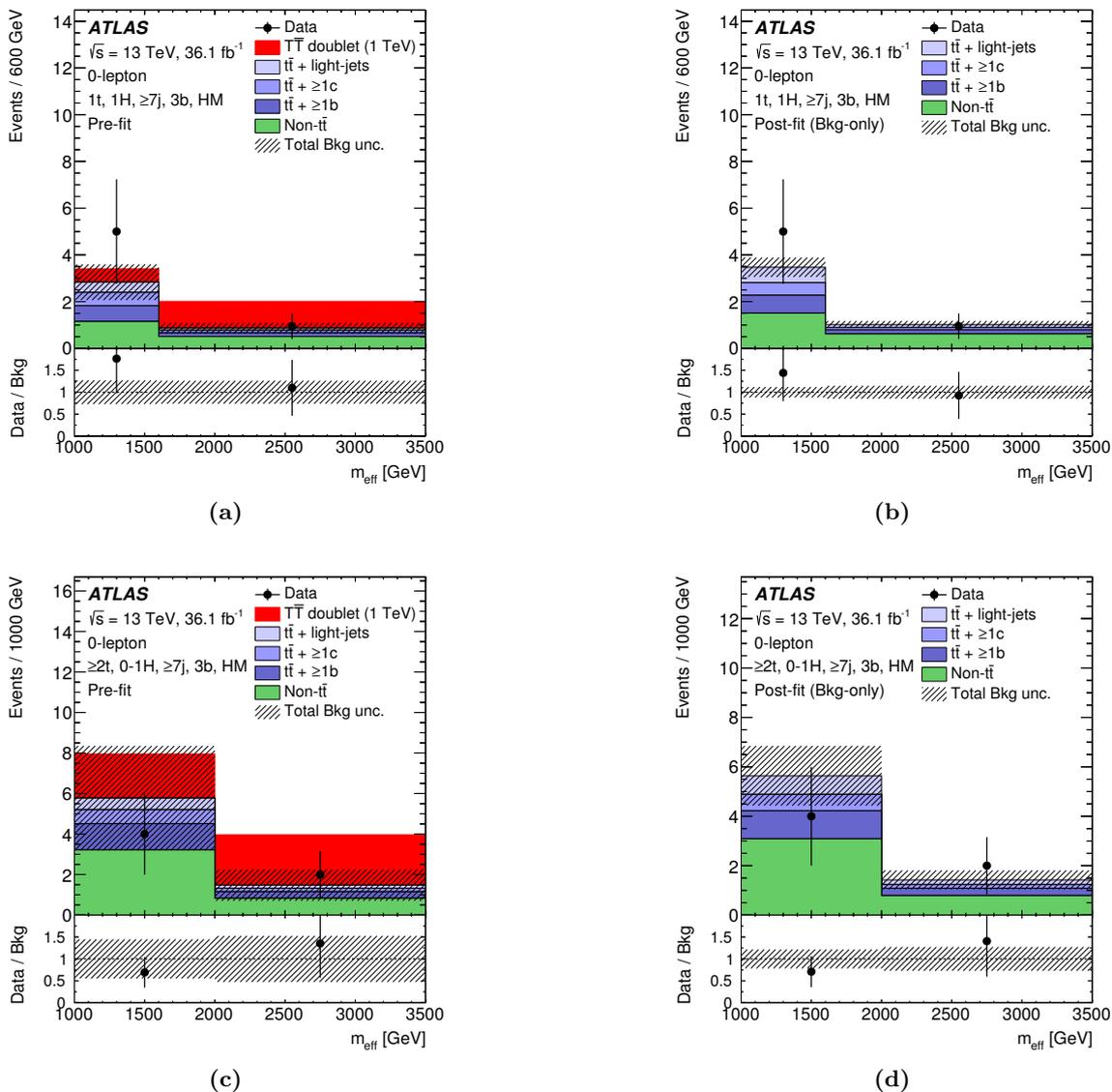
Figure 11. Comparison between the data and prediction for the m_{eff} distribution in some of the most sensitive search regions, before and after performing the combined fit to data in the 0-lepton and 1-lepton channels ("Pre-fit" and "Post-fit", respectively) under the background-only hypothesis. Shown are the ($\geq$2H, $\geq$6j, $\geq$4b) region in the 1-lepton channel (a) pre-fit and (b) post-fit, and the ($\geq$2tH, $\geq$7j, 2b, HM) region in the 0-lepton channel (c) pre-fit and (d) post-fit. In the pre-fit figures the expected $T\bar{T}$ signal (solid red) corresponding to $m_T = 1$ TeV in the T doublet scenario is also shown, added on top of the background prediction. The small contributions from $t\bar{t}V$, $t\bar{t}H$, single top, W/Z+jets, diboson, and multijet backgrounds are combined into a single background source referred to as "Non-$t\bar{t}$". The last bin in all figures contains the overflow. The bottom panels display the ratios of data to the total background prediction ("Bkg"). The blue triangles indicate points that are outside the vertical range of the figure. The hashed area represents the total uncertainty of the background. In the case of the pre-fit background uncertainty, the normalisation uncertainty of the $t\bar{t}+ \geq 1b$ background is not included.
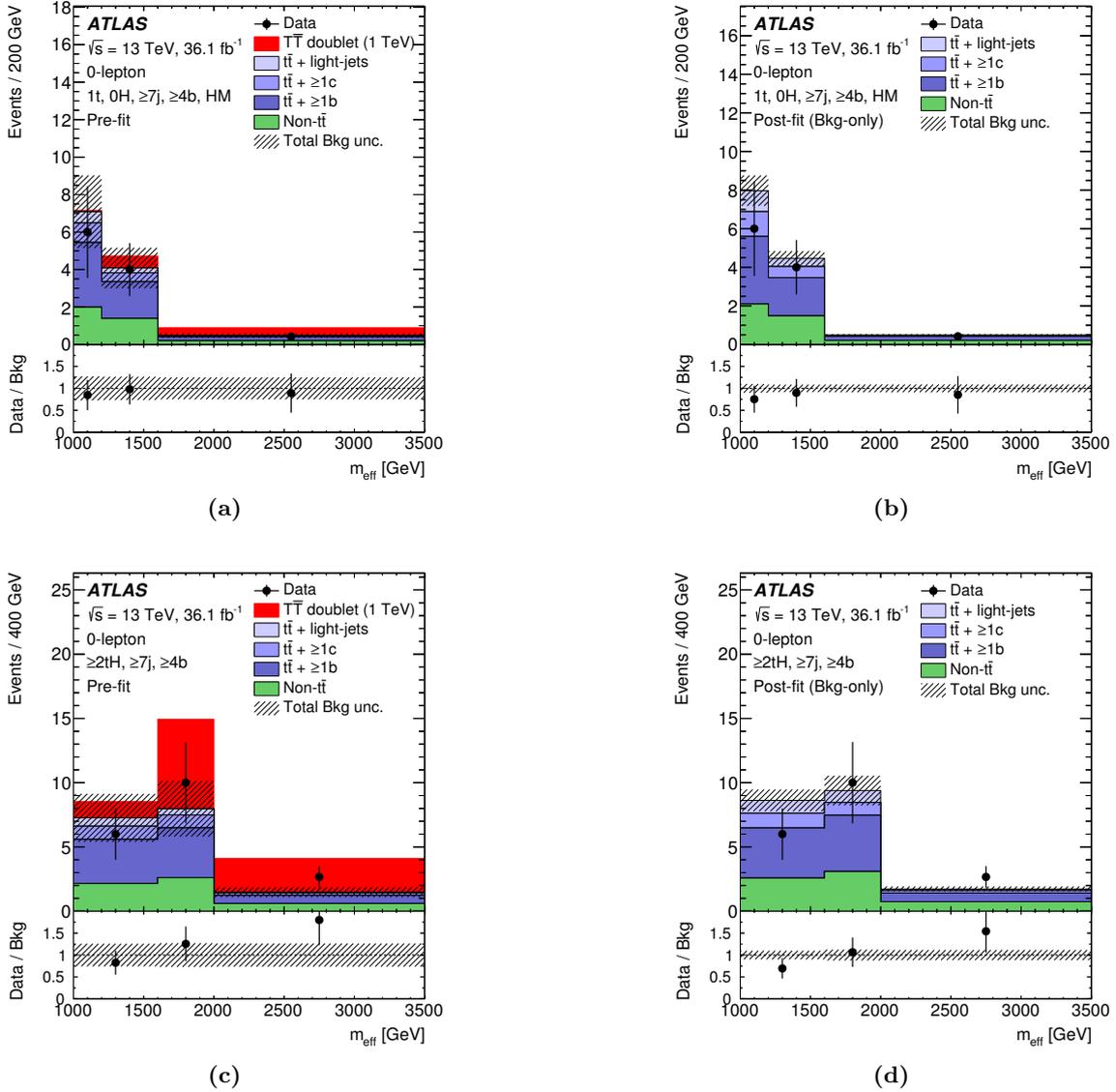
Figure 12. Comparison between the data and prediction for the m_{eff} distribution in some of the most sensitive search regions in the 0-lepton channel, before and after performing the combined fit to data in the 0-lepton and 1-lepton channels ("Pre-fit" and "Post-fit", respectively) under the background-only hypothesis. Shown are the (1t, 1H, ≥7j, 3b, HM) region (a) pre-fit and (b) post-fit, and the (≥2t, 0–1H, ≥7j, 3b, HM) region (c) pre-fit and (d) post-fit. In the pre-fit figures the expected $T\bar{T}$ signal (solid red) corresponding to $m_T = 1$ TeV in the T doublet scenario is also shown, added on top of the background prediction. The small contributions from $t\bar{t}V$, $t\bar{t}H$, single-top, $W/Z+$jets, diboson, and multijet backgrounds are combined into a single background source referred to as "Non-$t\bar{t}$". The last bin in all figures contains the overflow. The bottom panels display the ratios of data to the total background prediction ("Bkg"). The hashed area represents the total uncertainty of the background. In the case of the pre-fit background uncertainty, the normalisation uncertainty of the $t\bar{t}+ \geq 1b$ background is not included.

Figure 13. Comparison between the data and prediction for the m_{eff} distribution in some of the most sensitive search regions in the 0-lepton channel, before and after performing the combined fit to data in the 0-lepton and 1-lepton channels ("Pre-fit" and "Post-fit", respectively) under the background-only hypothesis. Shown are the (1t, 0H, $\geq$7j, $\geq$4b, HM) region (a) pre-fit and (b) post-fit, and the ($\geq$2tH, $\geq$7j, $\geq$4b) region (c) pre-fit and (d) post-fit. In the pre-fit figures the expected $T\bar{T}$ signal (solid red) corresponding to $m_T = 1$ TeV in the T doublet scenario is also shown, added on top of the background prediction. The small contributions from $t\bar{t}V$, $t\bar{t}H$, single-top, W/Z+jets, diboson, and multijet backgrounds are combined into a single background source referred to as "Non-$t\bar{t}$". The last bin in all figures contains the overflow. The bottom panels display the ratios of data to the total background prediction ("Bkg"). The hashed area represents the total uncertainty of the background. In the case of the pre-fit background uncertainty, the normalisation uncertainty of the $t\bar{t}+ \geq 1b$ background is not included.
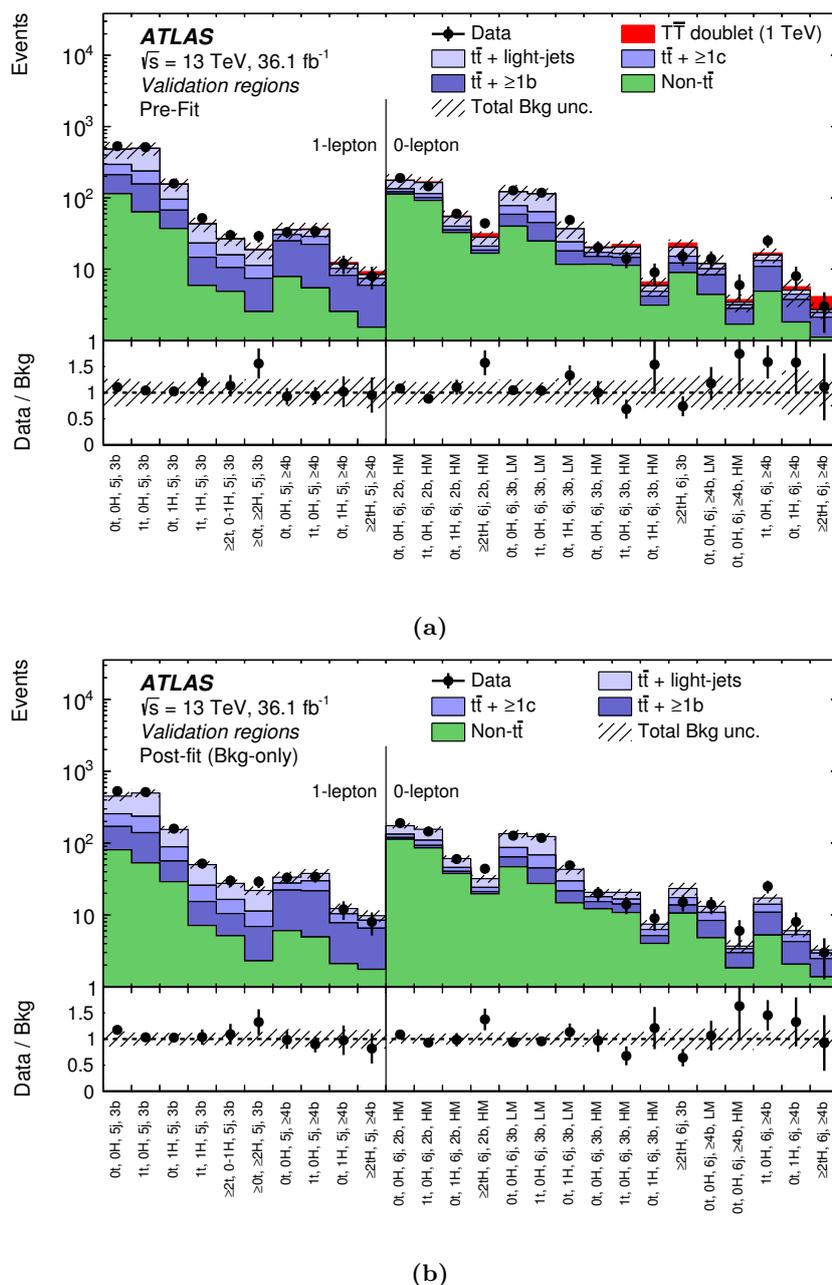
Figure 14. Comparison between the data and background prediction for the yields in each of the validation regions considered in the 1-lepton and 0-lepton channels (a) before the fit ("Pre-fit") and (b) after the fit ("Post-fit"). The fit is performed on the data in 1-lepton and 0-lepton channels under the background-only hypothesis considering only the search regions. In the pre-fit figure the expected $T\bar{T}$ signal (solid red) corresponding to $m_T = 1$ TeV in the T doublet scenario is also shown, added on top of the background prediction. The small contributions from $t\bar{t}V$, $t\bar{t}H$, single-top, W/Z+jets, diboson, and multijet backgrounds are combined into a single background source referred to as "Non-$t\bar{t}$". The bottom panels display the ratios of data to the total background prediction ("Bkg"). The hashed area represents the total uncertainty of the background. In the case of the pre-fit background uncertainty, the normalisation uncertainty of the $t\bar{t}+ \geq 1b$ background is not included.

1-lepton channel	≥2t, 0–1H, ≥6j, 3b	1t, 0H, ≥6j, ≥4b	1t, 1H, ≥6j, ≥4b	≥2t, 0–1H, ≥6j, ≥4b	≥0t, ≥2H, ≥6j, ≥4b
$t\bar{t}$+light-jets	137 ± 24	59 ± 11	7.6 ± 1.6	9.0 ± 2.0	1.50 ± 0.34
$t\bar{t}+{\geq}1c$	79 ± 34	81 ± 26	11.4 ± 3.8	12.4 ± 5.1	2.36 ± 0.84
$t\bar{t}+{\geq}1b$	84 ± 20	217 ± 27	35.3 ± 5.6	44.1 ± 9.1	7.4 ± 1.2
$t\bar{t}V$	10.7 ± 1.6	13.2 ± 2.1	2.12 ± 0.34	2.82 ± 0.46	0.50 ± 0.08
$t\bar{t}H$	5.26 ± 0.61	17.4 ± 2.3	4.28 ± 0.56	3.25 ± 0.46	1.33 ± 0.17
W+jets	11.4 ± 4.0	9.5 ± 3.4	0.71 ± 0.36	1.68 ± 0.59	0.78 ± 0.31
Z+jets	1.56 ± 0.55	1.11 ± 0.41	0.08 ± 0.06	0.16 ± 0.06	0.07 ± 0.04
Single top	11.3 ± 5.6	10.8 ± 6.2	2.01 ± 0.62	1.85 ± 0.90	0.24 ± 0.15
Diboson	2.20 ± 0.91	1.10 ± 0.50	0.20 ± 0.08	0.30 ± 0.12	0.03 ± 0.07
$t\bar{t}t\bar{t}$ (SM)	2.83 ± 0.84	5.3 ± 1.5	1.20 ± 0.35	2.74 ± 0.79	0.24 ± 0.07
Total background	349 ± 20	416 ± 18	64.9 ± 4.7	78.2 ± 8.0	14.4 ± 1.2
Data	353	428	60	78	18

Table 6. Predicted and observed yields in the 1-lepton channel in five of the most sensitive search regions (depending on the signal scenario) considered. The multijet background is considered negligible in these regions and thus not shown. The background prediction is shown after the combined fit to data in the 0-lepton and 1-lepton channels under the background-only hypothesis. The quoted uncertainties are the sum in quadrature of statistical and systematic uncertainties in the yields, computed taking into account correlations among nuisance parameters and among processes.

theoretical cross section. The scenarios considered involve different assumptions about the decay branching ratios. The search in the 1-lepton (0-lepton) channel is particularly sensitive to the benchmark scenario of $\mathcal{B}(T \to Ht) = 1$ ($\mathcal{B}(T \to Zt) = 1$). In contrast, both the 1-lepton and the 0-lepton searches have comparable sensitivity to the weak-isospin doublet and singlet scenarios, and thus their combination represents an improvement of 60–70 GeV on the expected T quark mass exclusion over the most sensitive individual search. The limits corresponding to the weak-isospin doublet and singlet scenarios obtained for the combination of the 1-lepton and 0-lepton searches are shown in figure 17. A summary of the observed and expected lower limits on the T quark mass in the different benchmark scenarios for the individual 1-lepton and 0-lepton searches, as well as their combination, is given in table 8. As can be seen, the observed mass limits for the 1-lepton search are above the expected limits in all benchmark scenarios. Detailed studies on the statistical model found no sources of systematic bias and showed that the results are consistent with downward statistical fluctuations in data in some of the highest m_{eff} bins in three search regions: (1t, 1H, ≥6j, ≥4b), (≥2t, 0–1H, ≥6j, 3b), and (≥0t, ≥2H, ≥6j, ≥4b). Several other regions with similar event kinematics and background composition to these three search regions show good agreement between data and expectations. In particular, additional

0-lepton channel	≥2tH, ≥7j, 2b, HM	1t, 1H, ≥7j, 3b, HM	≥2t, 0–1H, ≥7j, 3b, HM	1t, 0H, ≥7j, ≥4b, HM	≥2tH, ≥7j, ≥4b
$t\bar{t}$+light-jets	24.7 ± 5.0	1.08 ± 0.20	1.04 ± 0.25	2.20 ± 0.43	2.91 ± 0.57
$t\bar{t}$+≥1c	9.2 ± 4.9	0.85 ± 0.44	0.89 ± 0.48	2.9 ± 1.1	3.4 ± 1.4
$t\bar{t}$+≥1b	5.3 ± 1.9	1.31 ± 0.39	1.58 ± 0.55	9.4 ± 1.3	12.8 ± 2.4
$t\bar{t}V$	5.96 ± 0.88	0.59 ± 0.09	1.00 ± 0.15	1.46 ± 0.23	1.25 ± 0.19
$t\bar{t}H$	0.61 ± 0.08	0.19 ± 0.03	0.13 ± 0.02	1.02 ± 0.13	1.16 ± 0.17
W+jets	12.0 ± 3.2	0.63 ± 0.22	0.92 ± 0.34	0.71 ± 0.27	0.86 ± 0.22
Z+jets	10.6 ± 3.1	0.69 ± 0.26	0.4 ± 1.3	0.65 ± 0.29	0.94 ± 0.29
Single top	8.9 ± 3.2	0.77 ± 0.36	0.95 ± 0.48	1.84 ± 0.82	1.17 ± 0.47
Diboson	3.9 ± 1.6	0.41 ± 0.39	0.53 ± 0.44	0.37 ± 0.15	0.23 ± 0.10
$t\bar{t}t\bar{t}$ (SM)	0.20 ± 0.07	0.05 ± 0.02	0.12 ± 0.04	0.36 ± 0.10	0.87 ± 0.24
Multijet	4.1 ± 3.7	0.14 ± 0.13	0.18 ± 0.19	0.67 ± 0.62	3.3 ± 2.6
Total background	85.5 ± 6.8	6.70 ± 0.75	7.8 ± 1.7	21.6 ± 1.4	28.8 ± 3.1
Data	87	8	7	18	29

Table 7. Predicted and observed yields in the 0-lepton channel in five of the most sensitive search regions (depending on the signal scenario) considered. The background prediction is shown after the combined fit to data in the 0-lepton and 1-lepton channels under the background-only hypothesis. The quoted uncertainties are the sum in quadrature of statistical and systematic uncertainties in the yields, computed taking into account correlations among nuisance parameters and among processes.

regions with larger event yields were constructed to test this agreement by merging signal regions in certain categories, but retaining similar multiplicities of b-tagged jets or boosted objects as the original signal regions.

Table 8 also includes a comparison to the limits obtained by the ATLAS Run-1 $T\bar{T} \rightarrow Ht$+X search in the 1-lepton channel [25]: the current results extend the expected T quark mass exclusion by ∼390–490 GeV, depending on the assumed benchmark scenario.

The same analyses are used to derive exclusion limits on vector-like T quark production, for different values of m_T and as a function of $\mathcal{B}(T \rightarrow Wb)$ and $\mathcal{B}(T \rightarrow Ht)$, assuming that $\mathcal{B}(T \rightarrow Wb) + \mathcal{B}(T \rightarrow Zt) + \mathcal{B}(T \rightarrow Ht) = 1$. To probe this branching ratio plane, the signal samples are reweighted by the ratio of the desired branching ratio to the original branching ratio in PROTOS, and the complete analysis is repeated. Owing to the complementarity of the 1-lepton and 0-lepton searches in probing the branching ratio plane, their combination represents a significant improvement over the individual results, as illustrated in figure 18. In this case, the observed lower limits on the T quark mass range between 0.99 TeV and 1.43 TeV depending on the values of the branching ratios into the three decay modes. In particular, a vector-like T quark with mass below 0.99 TeV is excluded for any values of the branching ratios into the three decay modes. The corresponding range of expected lower limits is between 0.91 TeV and 1.34 TeV. Figure 19 presents the corresponding observed and expected T quark mass limits in the plane of $\mathcal{B}(T \rightarrow Ht)$ versus $\mathcal{B}(T \rightarrow Wb)$, obtained by linear interpolation of the calculated CL$_\text{s}$ versus m_T.
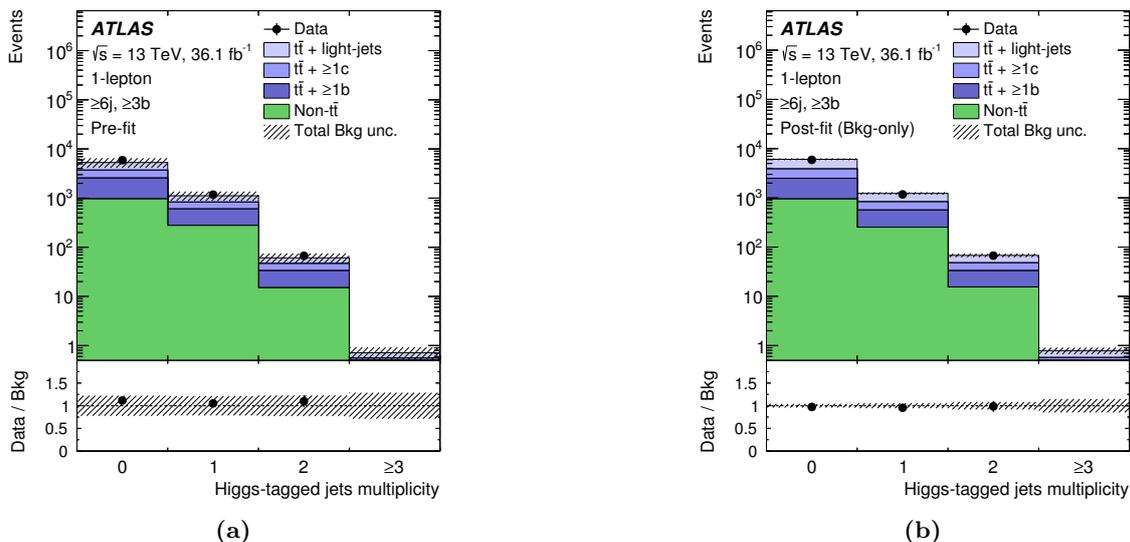
Figure 15. Comparison between the data and prediction for the Higgs-tagged jet multiplicity in the 1-lepton channel after preselection plus the requirement of ≥6 jets and ≥3 b-tagged jets, (a) before and (b) after performing the combined fit of the m_{eff} spectrum to data in the 0-lepton and 1-lepton channels search regions ("Pre-fit" and "Post-fit", respectively) under the background-only hypothesis. The small contributions from $t\bar{t}V$, $t\bar{t}H$, single-top, W/Z+jets, diboson, and multijet backgrounds are combined into a single background source referred to as "Non-$t\bar{t}$". The last bin in all figures contains the overflow. The bottom panels display the ratios of data to the total background prediction ("Bkg"). The hashed area represents the total uncertainty of the background. In the case of the pre-fit background uncertainty, the normalisation uncertainty of the $t\bar{t}+ \geq 1b$ background is not included.

95% CL lower limits on T quark mass [TeV]				
Search	$\mathcal{B}(T \to Ht) = 1$	$\mathcal{B}(T \to Zt) = 1$	Doublet	Singlet
1-lepton channel	1.47 (1.30)	1.12 (0.91)	1.36 (1.16)	1.23 (1.02)
0-lepton channel	1.11 (1.20)	1.12 (1.17)	1.12 (1.19)	0.99 (1.05)
Combination	1.43 (1.34)	1.17 (1.18)	1.31 (1.26)	1.19 (1.11)
Previous Run-1 ATLAS $T\bar{T} \to Ht$+X search [25]				
1-lepton channel	0.95 (0.88)	0.75 (0.69)	0.86 (0.82)	0.76 (0.72)

Table 8. Summary of observed (expected) 95% CL lower limits on T quark mass (in TeV) for the 1-lepton and 0-lepton channels, as well as their combination, with different assumptions about the decay branching ratios. The background estimate used in the computation of the limits is the result obtained from the background-only fit to data. Also shown are the corresponding limits obtained by the Run-1 ATLAS $T\bar{T} \to Ht$+X search in the 1-lepton channel [25].
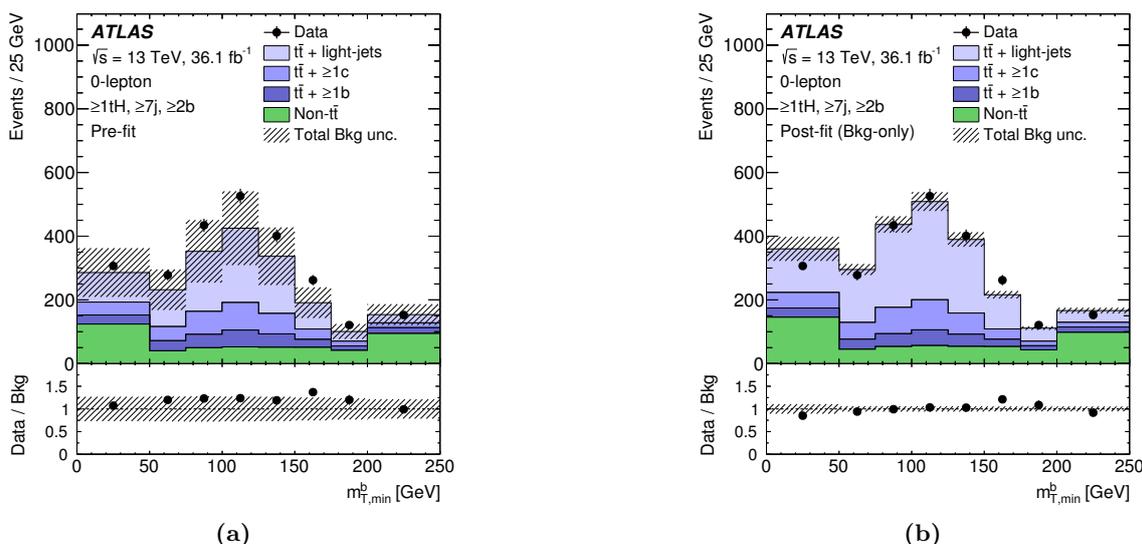
Figure 16. Comparison between the data and prediction for the distribution of the minimum transverse mass of E_T^{miss} and any of the three leading b-tagged jets in the event ($m_{T, min}^b$) in the ($\geq$1tH, $\geq$7j, $\geq$2b) region of the 0-lepton channel (a) before and (b) after performing the combined fit of the m_{eff} spectrum to data in the 0-lepton and 1-lepton channels search regions ("Pre-fit" and "Post-fit", respectively) under the background-only hypothesis. The small contributions from $t\bar{t}V$, $t\bar{t}H$, single-top, W/Z+jets, diboson, and multijet backgrounds are combined into a single background source referred to as "Non-$t\bar{t}$". The last bin in all figures contains the overflow. The bottom panels display the ratios of data to the total background prediction ("Bkg"). The hashed area represents the total uncertainty of the background. In the case of the pre-fit background uncertainty, the normalisation uncertainty of the $t\bar{t}+ \geq 1b$ background is not included.

9.3   Limits on four-top-quark production

The 1-lepton search is used to set limits on BSM four-top-quark production by considering different signal benchmark scenarios (see section 5.1 for details). In the case of $t\bar{t}t\bar{t}$ production via an EFT model with a four-top-quark contact interaction, the observed (expected) 95% CL upper limit on the production cross section is 16 fb (31^{+12}_{-9} fb). The upper limit on the production cross section can be translated into an observed (expected) limit on the free parameter of the model $|C_{4t}|/\Lambda^2 < 1.6$ TeV^{-2} (2.3 ± 0.4 TeV^{-2}). In the context of the 2UED/RPP model, the observed and expected upper limits on the production cross section times branching ratio are shown in figure 20 as a function of m_{KK} for the symmetric case ($\xi = R_4/R_5 = 1$), assuming production by tier (1,1) alone. The comparison to the LO theoretical cross section translates into an observed (expected) 95% CL limit on m_{KK} of 1.8 TeV (1.7 TeV).
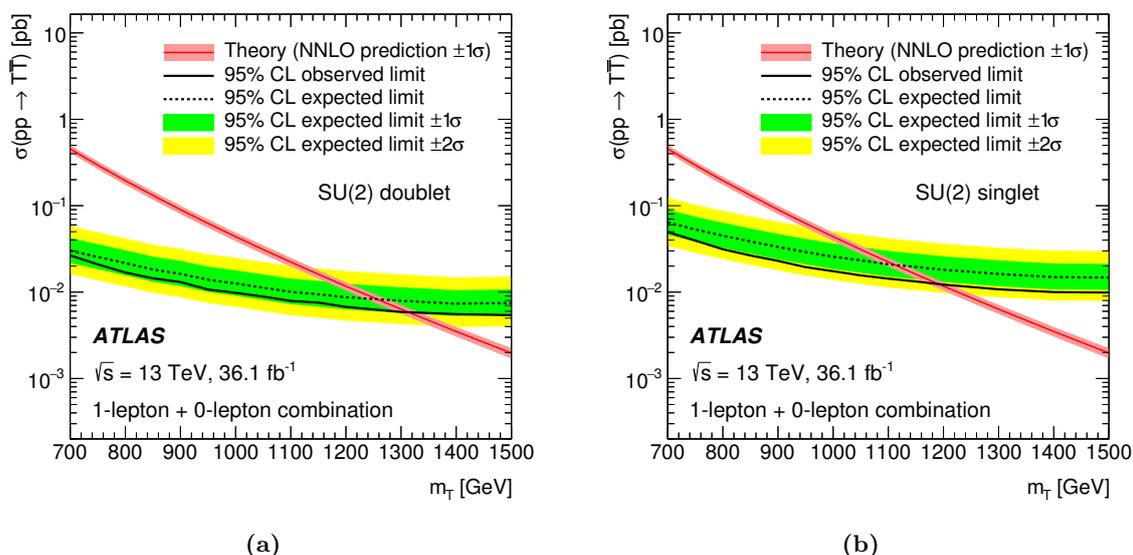
Figure 17. Observed (solid line) and expected (dashed line) 95% CL upper limits on the $T\bar{T}$ cross section as a function of the T quark mass for the combination of the 1-lepton and 0-lepton searches (a) for a T quark doublet, and (b) for a T quark singlet. The background estimate used in the computation of the limits is the result obtained from the background-only fit to data. The surrounding shaded bands correspond to ± 1 and ± 2 standard deviations around the expected limit. The thin red line and band show the theoretical prediction and its ± 1 standard deviation uncertainty.
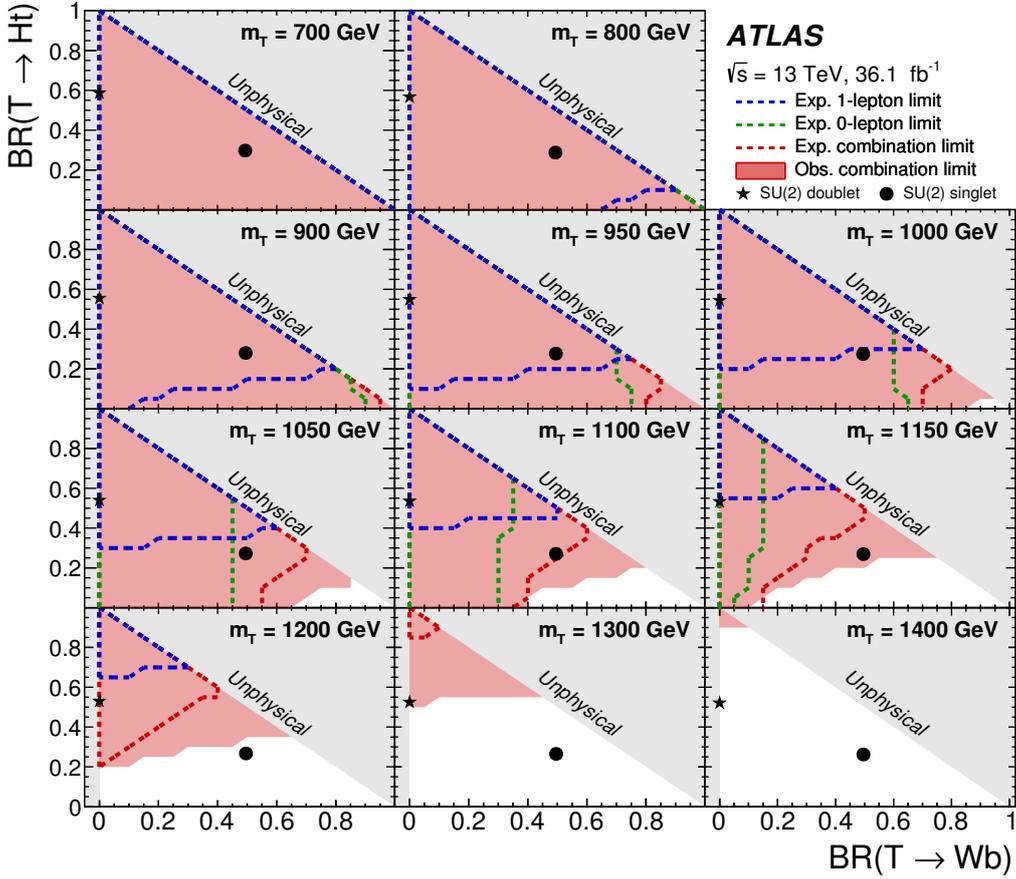
Figure 18. Observed (red filled area) and expected (red dashed line) 95% CL exclusion in the plane of $\mathcal{B}(T \to Wb)$ versus $\mathcal{B}(T \to Ht)$, for different values of the vector-like T quark mass for the combination of the 1-lepton and 0-lepton searches. In the figure, the branching ratio is denoted "BR". The background estimate used in the computation of the limits is the result obtained from the background-only fit to data. Also shown are the expected exclusions by the individual searches, which can be compared to that obtained through their combination. The grey (light shaded) area corresponds to the unphysical region where the sum of branching ratios exceeds unity, or is smaller than zero. The default branching ratio values from the PROTOS event generator for the weak-isospin singlet and doublet cases are shown as plain circle and star symbols, respectively.
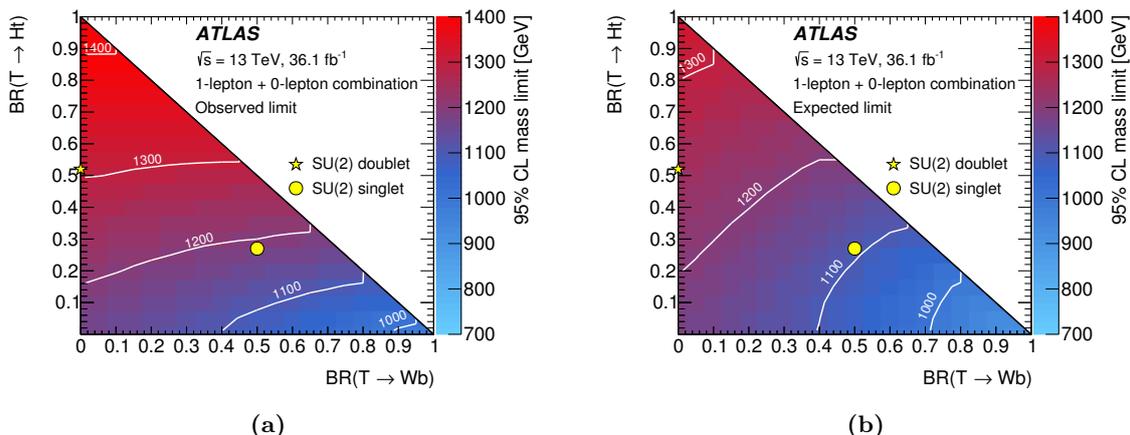
Figure 19. (a) Observed and (b) expected limit (95% CL) on the mass of the T quark in the plane of $\mathcal{B}(T \to Ht)$ versus $\mathcal{B}(T \to Wb)$ for the combination of the 1-lepton and 0-lepton searches. In the figure, the branching ratio is denoted "BR". The background estimate used in the computation of the limits is the result obtained from the background-only fit to data. Contour lines are provided to guide the eye. The yellow markers indicate the branching ratios for the SU(2) singlet and doublet scenarios with masses above ≈ 800 GeV, where they are approximately independent of the T quark mass.
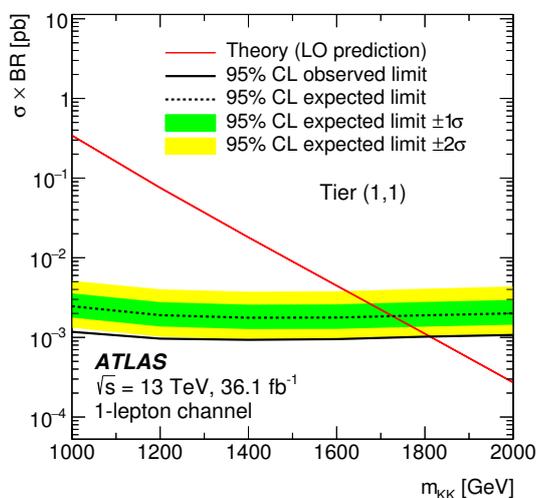

Figure 20. Observed (solid line) and expected (dashed line) 95% CL upper limits on the production cross section times branching ratio of four-top-quark events as a function of the Kaluza-Klein mass (m_{KK}) from tier (1,1) in the symmetric case ($\xi = R_4/R_5 = 1$). The background estimate used in the computation of the limits is the result obtained from the background-only fit to data. The surrounding shaded bands correspond to ± 1 and ± 2 standard deviations around the expected limit. The thin red line shows the theoretical prediction, computed at LO in QCD, for the production cross section of four-top-quark events by tier (1,1) assuming $\mathcal{B}(A^{(1,1)} \to t\bar{t}) = 1$, where the heavy photon $A^{(1,1)}$ is the lightest particle of this tier.

10 Conclusion

A search for pair production of up-type vector-like quarks (T) with significant branching ratio into a top quark and either a Standard Model Higgs boson or a Z boson is presented. The same analysis is also used to search for four-top-quark production, in several new physics scenarios. The search is based on pp collisions at $\sqrt{s} = 13$ TeV recorded in 2015 and 2016 with the ATLAS detector at the CERN Large Hadron Collider and corresponds to an integrated luminosity of $36.1\,\text{fb}^{-1}$. Data are analysed in the lepton+jets final state, characterised by an isolated electron or muon with high transverse momentum, large missing transverse momentum and multiple jets, as well as the jets+E_T^miss final state, characterised by multiple jets and large missing transverse momentum. The search exploits the high multiplicity of b-jets, the high scalar sum of transverse momenta of all final-state objects, and the presence of boosted, hadronically decaying top quarks and Higgs bosons reconstructed as large-radius jets, characteristic of signal events.

No significant excess of events above the Standard Model expectation is observed, and 95% CL lower limits are placed on the mass of the vector-like T quark under several branching ratio hypotheses assuming contributions only from $T \to Wb$, Zt, Ht. The 95% CL observed lower limits on the T quark mass lie between 0.99 TeV and 1.43 TeV depending on the values of the branching ratios into the three decay modes. Assuming $\mathcal{B}(T \to Ht) = 1$ and $\mathcal{B}(T \to Zt) = 1$, observed (expected) 95% CL limits of $m_T > 1.43$ TeV (1.34 TeV) TeV and $m_T > 1.17\,(1.18)$ TeV, respectively, are obtained. The observed (expected) 95% CL limits for a weak-isospin doublet and singlet are $m_T > 1.31\,(1.26)$ TeV and $m_T > 1.19\,(1.11)$ TeV, respectively. Additionally, upper limits on the four-top-quark production cross section are set in several new physics scenarios. In the case of $t\bar{t}t\bar{t}$ production from a contact interaction in an EFT model, the observed (expected) 95% CL upper limit on the production cross section is 16 fb ($31^{+12}_{-9}\,\text{fb}$). In the context of a 2UED/RPP model, 95% CL observed (expected) lower limits on m_{KK} of 1.8 TeV (1.7 TeV) are derived.

References

[1] ATLAS collaboration, *Observation of a new particle in the search for the Standard Model Higgs boson with the ATLAS detector at the LHC*, *Phys. Lett.* **B 716** (2012) 1 [arXiv:1207.7214] [INSPIRE].

[2] CMS collaboration, *Observation of a new boson at a mass of* 125 *GeV with the CMS experiment at the LHC*, *Phys. Lett.* **B 716** (2012) 30 [arXiv:1207.7235] [INSPIRE].

[3] L. Susskind, *Dynamics of spontaneous symmetry breaking in the Weinberg-Salam theory*, *Phys. Rev.* **D 20** (1979) 2619 [INSPIRE].

[4] C.T. Hill and E.H. Simmons, *Strong dynamics and electroweak symmetry breaking*, *Phys. Rept.* **381** (2003) 235 [*Erratum ibid.* **390** (2004) 553] [hep-ph/0203079] [INSPIRE].

[5] D.B. Kaplan, H. Georgi and S. Dimopoulos, *Composite Higgs scalars*, *Phys. Lett.* **B 136** (1984) 187 [INSPIRE].

[6] K. Agashe, R. Contino and A. Pomarol, *The minimal composite Higgs model*, *Nucl. Phys.* **B 719** (2005) 165 [hep-ph/0412089] [INSPIRE].

[7] F. del Aguila and M.J. Bowick, *The possibility of new fermions with* $\Delta I = 0$ *mass*, *Nucl. Phys.* **B 224** (1983) 107 [INSPIRE].

[8] J.A. Aguilar-Saavedra, *Identifying top partners at LHC*, *JHEP* **11** (2009) 030 [arXiv:0907.3155] [INSPIRE].

[9] J.A. Aguilar-Saavedra, *Mixing with vector-like quarks: constraints and expectations*, *EPJ Web Conf.* **60** (2013) 16012 [arXiv:1306.4432] [INSPIRE].

[10] J.A. Aguilar-Saavedra, R. Benbrik, S. Heinemeyer and M. Pérez-Victoria, *Handbook of vectorlike quarks: mixing and single production*, *Phys. Rev.* **D 88** (2013) 094010 [arXiv:1306.0572] [INSPIRE].

[11] A. Pomarol and J. Serra, *Top quark compositeness: feasibility and implications*, *Phys. Rev.* **D 78** (2008) 074026 [arXiv:0806.3247] [INSPIRE].

[12] B. Lillie, J. Shu and T.M.P. Tait, *Top compositeness at the Tevatron and LHC*, *JHEP* **04** (2008) 087 [arXiv:0712.3057] [INSPIRE].

[13] K. Kumar, T.M.P. Tait and R. Vega-Morales, *Manifestations of top compositeness at colliders*, *JHEP* **05** (2009) 022 [arXiv:0901.3808] [INSPIRE].

[14] G. Cacciapaglia, H. Cai, A. Deandrea, T. Flacke, S.J. Lee and A. Parolini, *Composite scalars at the LHC: the Higgs, the sextet and the octet*, *JHEP* **11** (2015) 201 [arXiv:1507.02283] [INSPIRE].

[15] M. Guchait, F. Mahmoudi and K. Sridhar, *Associated production of a Kaluza-Klein excitation of a gluon with a $t\bar{t}$ pair at the LHC*, *Phys. Lett.* **B 666** (2008) 347 [arXiv:0710.2234] [INSPIRE].

[16] H. Georgi, L. Kaplan, D. Morin and A. Schenk, *Effects of top compositeness*, *Phys. Rev.* **D 51** (1995) 3888 [hep-ph/9410307] [INSPIRE].

[17] C. Degrande, J.-M. Gerard, C. Grojean, F. Maltoni and G. Servant, *Non-resonant new physics in top pair production at hadron colliders*, *JHEP* **03** (2011) 125 [arXiv:1010.6304] [INSPIRE].

[18] G. Cacciapaglia, A. Deandrea and J. Llodra-Perez, *A dark matter candidate from Lorentz invariance in 6D*, *JHEP* **03** (2010) 083 [arXiv:0907.4993] [INSPIRE].

[19] G. Cacciapaglia, R. Chierici, A. Deandrea, L. Panizzi, S. Perries and S. Tosi, *Four tops on the real projective plane at LHC*, *JHEP* **10** (2011) 042 [arXiv:1107.4616] [INSPIRE].

[20] ATLAS collaboration, *Search for pair production of vector-like top quarks in events with one lepton, jets and missing transverse momentum in $\sqrt{s} = 13\,TeV$ pp collisions with the ATLAS detector*, *JHEP* **08** (2017) 052 [arXiv:1705.10751] [INSPIRE].

[21] ATLAS collaboration, *Search for pair production of heavy vector-like quarks decaying to high-p_T W bosons and b quarks in the lepton-plus-jets final state in pp collisions at $\sqrt{s} = 13\,TeV$ with the ATLAS detector*, *JHEP* **10** (2017) 141 [arXiv:1707.03347] [INSPIRE].

[22] CMS collaboration, *Search for pair production of vector-like T and B quarks in single-lepton final states using boosted jet substructure in proton-proton collisions at $\sqrt{s} = 13\,TeV$*, *JHEP* **11** (2017) 085 [arXiv:1706.03408] [INSPIRE].

[23] CMS collaboration, *Search for pair production of vector-like quarks in the $bW\bar{b}W$ channel from proton-proton collisions at $\sqrt{s} = 13\,TeV$*, *Phys. Lett.* **B 779** (2018) 82 [arXiv:1710.01539] [INSPIRE].

[24] ATLAS collaboration, *Analysis of events with b-jets and a pair of leptons of the same charge in pp collisions at $\sqrt{s} = 8\,TeV$ with the ATLAS detector*, *JHEP* **10** (2015) 150 [arXiv:1504.04605] [INSPIRE].

[25] ATLAS collaboration, *Search for production of vector-like quark pairs and of four top quarks in the lepton-plus-jets final state in pp collisions at $\sqrt{s} = 8\,TeV$ with the ATLAS detector*, *JHEP* **08** (2015) 105 [arXiv:1505.04306] [INSPIRE].

[26] CMS collaboration, *Search for Standard Model production of four top quarks with same-sign and multilepton final states in proton-proton collisions at $\sqrt{s} = 13\,TeV$*, *Eur. Phys. J.* **C 78** (2018) 140 [arXiv:1710.10614] [INSPIRE].

[27] ATLAS collaboration, *The ATLAS experiment at the CERN Large Hadron Collider*, 2008 *JINST* **3** S08003 [INSPIRE].

[28] ATLAS collaboration, *ATLAS insertable B-layer technical design report*, CERN-LHCC-2010-013, CERN, Geneva, Switzerland, (2010) [ATLAS-TDR-19].

[29] ATLAS collaboration, *Performance of the ATLAS trigger system in* 2015, *Eur. Phys. J.* **C 77** (2017) 317 [arXiv:1611.09661] [INSPIRE].

[30] ATLAS collaboration, *Vertex reconstruction performance of the ATLAS detector at $\sqrt{s} = 13\,TeV$*, ATL-PHYS-PUB-2015-026, CERN, Geneva, Switzerland, (2015).

[31] ATLAS collaboration, *Electron efficiency measurements with the ATLAS detector using the* 2015 *LHC proton-proton collision data*, ATLAS-CONF-2016-024, CERN, Geneva, Switzerland, (2016).

[32] ATLAS collaboration, *Electron and photon energy calibration with the ATLAS detector using data collected in* 2015 *at $\sqrt{s} = 13\,TeV$*, ATL-PHYS-PUB-2016-015, CERN, Geneva, Switzerland, (2016).

[33] ATLAS collaboration, *Muon reconstruction performance of the ATLAS detector in proton-proton collision data at $\sqrt{s} = 13\,TeV$*, *Eur. Phys. J.* **C 76** (2016) 292 [arXiv:1603.05598] [INSPIRE].

[34] M. Cacciari, G.P. Salam and G. Soyez, *The anti-k_t jet clustering algorithm*, *JHEP* **04** (2008) 063 [arXiv:0802.1189] [INSPIRE].

[35] M. Cacciari and G.P. Salam, *Dispelling the N^3 myth for the k_t jet-finder*, *Phys. Lett.* **B 641** (2006) 57 [hep-ph/0512210] [INSPIRE].

[36] M. Cacciari, G.P. Salam and G. Soyez, *FastJet user manual*, *Eur. Phys. J.* **C 72** (2012) 1896 [arXiv:1111.6097] [INSPIRE].

[37] ATLAS collaboration, *Topological cell clustering in the ATLAS calorimeters and its performance in LHC run* 1, *Eur. Phys. J.* **C 77** (2017) 490 [arXiv:1603.02934] [INSPIRE].

[38] ATLAS collaboration, *Jet energy scale measurements and their systematic uncertainties in proton-proton collisions at $\sqrt{s} = 13\,TeV$ with the ATLAS detector*, *Phys. Rev.* **D 96** (2017) 072002 [arXiv:1703.09665] [INSPIRE].

[39] ATLAS collaboration, *Selection of jets produced in* 13 *TeV proton-proton collisions with the ATLAS detector*, ATLAS-CONF-2015-029, CERN, Geneva, Switzerland, (2015).

[40] ATLAS collaboration, *Performance of pile-up mitigation techniques for jets in pp collisions at $\sqrt{s} = 8\,TeV$ using the ATLAS detector*, *Eur. Phys. J.* **C 76** (2016) 581 [arXiv:1510.03823] [INSPIRE].

[41] ATLAS collaboration, *Performance of b-jet identification in the ATLAS experiment*, 2016 *JINST* **11** P04008 [arXiv:1512.01094] [INSPIRE].

[42] ATLAS collaboration, *Optimisation of the ATLAS b-tagging performance for the* 2016 *LHC run*, ATL-PHYS-PUB-2016-012, CERN, Geneva, Switzerland, (2016).

[43] B. Nachman, P. Nef, A. Schwartzman, M. Swiatlowski and C. Wanotayaroj, *Jets from jets: re-clustering as a tool for large radius jet reconstruction and grooming at the LHC*, *JHEP* **02** (2015) 075 [arXiv:1407.2922] [INSPIRE].

[44] D. Krohn, J. Thaler and L.-T. Wang, *Jet trimming*, *JHEP* **02** (2010) 084 [arXiv:0912.1342] [INSPIRE].

[45] ATLAS collaboration, *Performance of algorithms that reconstruct missing transverse momentum in $\sqrt{s} = 8\,TeV$ proton-proton collisions in the ATLAS detector*, *Eur. Phys. J.* **C 77** (2017) 241 [arXiv:1609.09324] [INSPIRE].

[46] ATLAS collaboration, *Performance of missing transverse momentum reconstruction for the ATLAS detector in the first proton-proton collisions at at $\sqrt{s} = 13\,TeV$*, ATL-PHYS-PUB-2015-027, CERN, Geneva, Switzerland, (2015).

[47] T. Gleisberg et al., *Event generation with SHERPA 1.1*, *JHEP* **02** (2009) 007 [arXiv:0811.4622] [INSPIRE].

[48] D.J. Lange, *The EvtGen particle decay simulation package*, *Nucl. Instrum. Meth.* **A 462** (2001) 152 [INSPIRE].

[49] T. Sjöstrand, S. Mrenna and P.Z. Skands, *A brief introduction to PYTHIA 8.1*, *Comput. Phys. Commun.* **178** (2008) 852 [arXiv:0710.3820] [INSPIRE].

[50] ATLAS collaboration, *The ATLAS simulation infrastructure*, *Eur. Phys. J.* **C 70** (2010) 823 [arXiv:1005.4568] [INSPIRE].

[51] GEANT4 collaboration, S. Agostinelli et al., *GEANT4: a simulation toolkit*, *Nucl. Instrum. Meth.* **A 506** (2003) 250 [INSPIRE].

[52] ATLAS collaboration, *The simulation principle and performance of the ATLAS fast calorimeter simulation FastCaloSim*, ATL-PHYS-PUB-2010-013, CERN, Geneva, Switzerland, (2010).

[53] J.A. Aguilar-Saavedra, *PROTOS, a PROgram for TOp Simulations*, http://jaguilar.web.cern.ch/jaguilar/protos/.

[54] R.D. Ball et al., *Parton distributions with LHC data*, *Nucl. Phys.* **B 867** (2013) 244 [arXiv:1207.1303] [INSPIRE].

[55] ATLAS collaboration, *ATLAS run 1 PYTHIA8 tunes*, ATL-PHYS-PUB-2014-021, CERN, Geneva, Switzerland, (2014).

[56] M. Czakon and A. Mitov, *Top++: a program for the calculation of the top-pair cross-section at hadron colliders*, *Comput. Phys. Commun.* **185** (2014) 2930 [arXiv:1112.5675] [INSPIRE].

[57] M. Cacciari, M. Czakon, M. Mangano, A. Mitov and P. Nason, *Top-pair production at hadron colliders with next-to-next-to-leading logarithmic soft-gluon resummation*, *Phys. Lett.* **B 710** (2012) 612 [arXiv:1111.5869] [INSPIRE].

[58] P. Bärnreuther, M. Czakon and A. Mitov, *Percent level precision physics at the Tevatron: first genuine NNLO QCD corrections to $q\bar{q} \to t\bar{t} + X$*, *Phys. Rev. Lett.* **109** (2012) 132001 [arXiv:1204.5201] [INSPIRE].

[59] M. Czakon and A. Mitov, *NNLO corrections to top-pair production at hadron colliders: the all-fermionic scattering channels*, *JHEP* **12** (2012) 054 [arXiv:1207.0236] [INSPIRE].

[60] M. Czakon and A. Mitov, *NNLO corrections to top pair production at hadron colliders: the quark-gluon reaction*, *JHEP* **01** (2013) 080 [arXiv:1210.6832] [INSPIRE].

[61] M. Czakon, P. Fiedler and A. Mitov, *Total top-quark pair-production cross section at hadron colliders through $O(\alpha_S^4)$*, *Phys. Rev. Lett.* **110** (2013) 252004 [arXiv:1303.6254] [INSPIRE].

[62] A.D. Martin, W.J. Stirling, R.S. Thorne and G. Watt, *Parton distributions for the LHC*, *Eur. Phys. J.* **C 63** (2009) 189 [arXiv:0901.0002] [INSPIRE].

[63] A.D. Martin, W.J. Stirling, R.S. Thorne and G. Watt, *Uncertainties on α_S in global PDF analyses and implications for predicted hadronic cross sections*, *Eur. Phys. J.* **C 64** (2009) 653 [arXiv:0905.3531] [INSPIRE].

[64] M. Botje et al., *The PDF4LHC working group interim recommendations*, arXiv:1101.0538 [INSPIRE].

[65] H.-L. Lai et al., *New parton distributions for collider physics*, *Phys. Rev.* **D 82** (2010) 074024 [arXiv:1007.2241] [INSPIRE].

[66] J. Gao et al., *CT10 next-to-next-to-leading order global analysis of QCD*, *Phys. Rev.* **D 89** (2014) 033009 [arXiv:1302.6246] [INSPIRE].

[67] J. Alwall et al., *The automated computation of tree-level and next-to-leading order differential cross sections and their matching to parton shower simulations*, *JHEP* **07** (2014) 079 [arXiv:1405.0301] [INSPIRE].

[68] P. Meade and M. Reece, *BRIDGE: Branching Ratio Inquiry/Decay Generated Events*, hep-ph/0703031 [INSPIRE].

[69] S. Frixione, P. Nason and G. Ridolfi, *A positive-weight next-to-leading-order Monte Carlo for heavy flavour hadroproduction*, *JHEP* **09** (2007) 126 [arXiv:0707.3088] [INSPIRE].

[70] P. Nason, *A new method for combining NLO QCD with shower Monte Carlo algorithms*, *JHEP* **11** (2004) 040 [hep-ph/0409146] [INSPIRE].

[71] S. Frixione, P. Nason and C. Oleari, *Matching NLO QCD computations with parton shower simulations: the POWHEG method*, *JHEP* **11** (2007) 070 [arXiv:0709.2092] [INSPIRE].

[72] S. Alioli, P. Nason, C. Oleari and E. Re, *A general framework for implementing NLO calculations in shower Monte Carlo programs: the POWHEG BOX*, *JHEP* **06** (2010) 043 [arXiv:1002.2581] [INSPIRE].

[73] ATLAS collaboration, *Comparison of Monte Carlo generator predictions to ATLAS measurements of top pair production at 7 TeV*, ATL-PHYS-PUB-2015-002, CERN, Geneva, Switzerland, (2015).

[74] T. Sjöstrand, S. Mrenna and P.Z. Skands, *PYTHIA 6.4 physics and manual*, *JHEP* **05** (2006) 026 [hep-ph/0603175] [INSPIRE].

[75] P.Z. Skands, *Tuning Monte Carlo generators: the Perugia tunes*, *Phys. Rev.* **D 82** (2010) 074018 [arXiv:1005.3457] [INSPIRE].

[76] ATLAS collaboration, *Search for the Standard Model Higgs boson produced in association with top quarks and decaying into $b\bar{b}$ in pp collisions at $\sqrt{s} = 8$ TeV with the ATLAS detector*, *Eur. Phys. J.* **C 75** (2015) 349 [arXiv:1503.05066] [INSPIRE].

[77] ATLAS collaboration, *Measurements of top-quark pair differential cross-sections in the lepton+jets channel in pp collisions at $\sqrt{s} = 8$ TeV using the ATLAS detector*, *Eur. Phys. J.* **C 76** (2016) 538 [arXiv:1511.04716] [INSPIRE].

[78] M. Czakon, D. Heymes and A. Mitov, *High-precision differential predictions for top-quark pairs at the LHC*, *Phys. Rev. Lett.* **116** (2016) 082003 [arXiv:1511.00549] [INSPIRE].

[79] M. Czakon, D. Heymes and A. Mitov, *Dynamical scales for multi-TeV top-pair production at the LHC*, *JHEP* **04** (2017) 071 [arXiv:1606.03350] [INSPIRE].

[80] F. Cascioli, P. Maierhöfer, N. Moretti, S. Pozzorini and F. Siegert, *NLO matching for $t\bar{t}b\bar{b}$ production with massive b-quarks*, *Phys. Lett.* **B 734** (2014) 210 [arXiv:1309.5912] [INSPIRE].

[81] F. Cascioli, P. Maierhofer and S. Pozzorini, *Scattering amplitudes with open loops*, *Phys. Rev. Lett.* **108** (2012) 111601 [arXiv:1111.5206] [INSPIRE].

[82] R. Frederix, E. Re and P. Torrielli, *Single-top t-channel hadroproduction in the four-flavour scheme with POWHEG and aMC@NLO*, *JHEP* **09** (2012) 130 [arXiv:1207.5391] [INSPIRE].

[83] S. Frixione, E. Laenen, P. Motylinski and B.R. Webber, *Single-top production in MC@NLO*, *JHEP* **03** (2006) 092 [hep-ph/0512250] [INSPIRE].

[84] N. Kidonakis, *Next-to-next-to-leading-order collinear and soft gluon corrections for t-channel single top quark production*, *Phys. Rev.* **D 83** (2011) 091503 [arXiv:1103.2792] [INSPIRE].

[85] N. Kidonakis, *Two-loop soft anomalous dimensions for single top quark associated production with a W^- or H^-*, *Phys. Rev.* **D 82** (2010) 054018 [arXiv:1005.4451] [INSPIRE].

[86] N. Kidonakis, *NNLL resummation for s-channel single top quark production*, *Phys. Rev.* **D 81** (2010) 054028 [arXiv:1001.5034] [INSPIRE].

[87] T. Gleisberg and S. Höche, *Comix, a new matrix element generator*, *JHEP* **12** (2008) 039 [arXiv:0808.3674] [INSPIRE].

[88] S. Schumann and F. Krauss, *A parton shower algorithm based on Catani-Seymour dipole factorisation*, *JHEP* **03** (2008) 038 [arXiv:0709.1027] [INSPIRE].

[89] S. Höche, F. Krauss, M. Schönherr and F. Siegert, *QCD matrix elements + parton showers: the NLO case*, *JHEP* **04** (2013) 027 [arXiv:1207.5030] [INSPIRE].

[90] NNPDF collaboration, R.D. Ball et al., *Parton distributions for the LHC run II*, *JHEP* **04** (2015) 040 [arXiv:1410.8849] [INSPIRE].

[91] C. Anastasiou, L.J. Dixon, K. Melnikov and F. Petriello, *High precision QCD at hadron colliders: electroweak gauge boson rapidity distributions at NNLO*, *Phys. Rev.* **D 69** (2004) 094008 [hep-ph/0312266] [INSPIRE].

[92] R. Raitio and W.W. Wada, *Higgs boson production at large transverse momentum in QCD*, *Phys. Rev.* **D 19** (1979) 941 [INSPIRE].

[93] W. Beenakker, S. Dittmaier, M. Krämer, B. Plumper, M. Spira and P.M. Zerwas, *NLO QCD corrections to $t\bar{t}H$ production in hadron collisions*, *Nucl. Phys.* **B 653** (2003) 151 [hep-ph/0211352] [INSPIRE].

[94] S. Dawson, C. Jackson, L.H. Orr, L. Reina and D. Wackeroth, *Associated Higgs production with top quarks at the Large Hadron Collider: NLO QCD corrections*, *Phys. Rev.* **D 68** (2003) 034022 [hep-ph/0305087] [INSPIRE].

[95] Y. Zhang, W.-G. Ma, R.-Y. Zhang, C. Chen and L. Guo, *QCD NLO and EW NLO corrections to $t\bar{t}H$ production with top quark decays at hadron collider*, *Phys. Lett.* **B 738** (2014) 1 [arXiv:1407.1110] [INSPIRE].

[96] S. Frixione, V. Hirschi, D. Pagani, H.-S. Shao and M. Zaro, *Electroweak and QCD corrections to top-pair hadroproduction in association with heavy bosons*, *JHEP* **06** (2015) 184 [arXiv:1504.03446] [INSPIRE].

[97] A. Djouadi, J. Kalinowski and M. Spira, *HDECAY: a program for Higgs boson decays in the Standard Model and its supersymmetric extension*, *Comput. Phys. Commun.* **108** (1998) 56 [hep-ph/9704448] [INSPIRE].

[98] ATLAS collaboration, *Measurement of the top quark-pair production cross section with ATLAS in pp collisions at $\sqrt{s} = 7\,TeV$*, *Eur. Phys. J.* **C 71** (2011) 1577 [arXiv:1012.1792] [INSPIRE].

[99] ATLAS collaboration, *Luminosity determination in pp collisions at $\sqrt{s} = 8\,TeV$ using the ATLAS detector at the LHC*, *Eur. Phys. J.* **C 76** (2016) 653 [arXiv:1608.03953] [INSPIRE].

[100] M. Bahr et al., *HERWIG++ physics and manual*, *Eur. Phys. J.* **C 58** (2008) 639 [arXiv:0803.0883] [INSPIRE].

[101] ATLAS collaboration, *Simulation of top quark production for the ATLAS experiment at $\sqrt{s} = 13\,TeV$*, ATL-PHYS-PUB-2016-004, CERN, Geneva, Switzerland, (2016).

[102] ATLAS collaboration, *Search for the Standard Model Higgs boson produced in association with top quarks and decaying into a $b\bar{b}$ pair in pp collisions at $\sqrt{s} = 13\,TeV$ with the ATLAS detector*, *Phys. Rev.* **D 97** (2018) 072016 [arXiv:1712.08895] [INSPIRE].

[103] LHC HIGGS CROSS SECTION WORKING GROUP collaboration, D. de Florian et al., *Handbook of LHC Higgs cross sections: 4. Deciphering the nature of the Higgs sector*, arXiv:1610.07922 [INSPIRE].

[104] S. Frixione, E. Laenen, P. Motylinski, B.R. Webber and C.D. White, *Single-top hadroproduction in association with a W boson*, *JHEP* **07** (2008) 029 [arXiv:0805.3067] [INSPIRE].

[105] ATLAS collaboration, *Evidence for the $H \to b\bar{b}$ decay with the ATLAS detector*, *JHEP* **12** (2017) 024 [arXiv:1708.03299] [INSPIRE].

[106] J.M. Campbell and R.K. Ellis, *An update on vector boson pair production at hadron colliders*, *Phys. Rev.* **D 60** (1999) 113006 [hep-ph/9905386] [INSPIRE].

[107] J. Alwall et al., *Comparative study of various algorithms for the merging of parton showers and matrix elements in hadronic collisions*, *Eur. Phys. J.* **C 53** (2008) 473 [arXiv:0706.2569] [INSPIRE].

[108] ATLAS collaboration, *Measurement of the $W^{\pm}Z$ boson pair-production cross section in pp collisions at $\sqrt{s} = 13\,TeV$ with the ATLAS Detector*, *Phys. Lett.* **B 762** (2016) 1 [arXiv:1606.04017] [INSPIRE].

[109] J.M. Campbell and R.K. Ellis, *$t\bar{t}W^{\pm}$ production and decay at NLO*, *JHEP* **07** (2012) 052 [arXiv:1204.5678] [INSPIRE].

[110] M.V. Garzelli, A. Kardos, C.G. Papadopoulos and Z. Trócsányi, *$t\bar{t}W^{\pm}$ and $t\bar{t}Z$ hadroproduction at NLO accuracy in QCD with parton shower and hadronization effects*, *JHEP* **11** (2012) 056 [arXiv:1208.2665] [INSPIRE].

[111] LHC Higgs Cross Section Working Group collaboration, S. Dittmaier et al., *Handbook of LHC Higgs cross sections: 1. Inclusive observables*, arXiv:1101.0593 [INSPIRE].

[112] W. Verkerke and D.P. Kirkby, *The RooFit toolkit for data modeling*, *eConf* **C 0303241** (2003) MOLT007 [physics/0306116] [INSPIRE].

[113] W. Verkerke and D. Kirkby, *RooFit users manual*, http://roofit.sourceforge.net/.

[114] G. Cowan, K. Cranmer, E. Gross and O. Vitells, *Asymptotic formulae for likelihood-based tests of new physics*, *Eur. Phys. J.* **C 71** (2011) 1554 [*Erratum ibid.* **C 73** (2013) 2501] [arXiv:1007.1727] [INSPIRE].

[115] T. Junk, *Confidence level computation for combining searches with small statistics*, *Nucl. Instrum. Meth.* **A 434** (1999) 435 [hep-ex/9902006] [INSPIRE].

[116] A.L. Read, *Presentation of search results: the CL_S technique*, *J. Phys.* **G 28** (2002) 2693 [INSPIRE].

[117] ATLAS collaboration, *ATLAS computing acknowledgements*, ATL-GEN-PUB-2016-002, CERN, Geneva, Switzerland, (2016).

The ATLAS collaboration

M. Aaboud[137d], G. Aad[88], B. Abbott[115], O. Abdinov[12,*], B. Abeloos[119], S.H. Abidi[161],
O.S. AbouZeid[139], N.L. Abraham[151], H. Abramowicz[155], H. Abreu[154], Y. Abulaiti[6],
B.S. Acharya[167a,167b,a], S. Adachi[157], L. Adamczyk[41a], J. Adelman[110], M. Adersberger[102],
T. Adye[133], A.A. Affolder[139], Y. Afik[154], C. Agheorghiesei[28c], J.A. Aguilar-Saavedra[128a,128f],
F. Ahmadov[68,b], G. Aielli[135a,135b], S. Akatsuka[71], T.P.A. Åkesson[84], E. Akilli[52], A.V. Akimov[98],
G.L. Alberghi[22a,22b], J. Albert[172], P. Albicocco[50], M.J. Alconada Verzini[74], S. Alderweireldt[108],
M. Aleksa[32], I.N. Aleksandrov[68], C. Alexa[28b], G. Alexander[155], T. Alexopoulos[10], M. Alhroob[115],
B. Ali[130], M. Aliev[76a,76b], G. Alimonti[94a], J. Alison[33], S.P. Alkire[140], C. Allaire[119],
B.M.M. Allbrooke[151], B.W. Allen[118], P.P. Allport[19], A. Aloisio[106a,106b], A. Alonso[39], F. Alonso[74],
C. Alpigiani[140], A.A. Alshehri[56], M.I. Alstaty[88], B. Alvarez Gonzalez[32], D. Álvarez Piqueras[170],
M.G. Alviggi[106a,106b], B.T. Amadio[16], Y. Amaral Coutinho[26a], L. Ambroz[122], C. Amelung[25],
D. Amidei[92], S.P. Amor Dos Santos[128a,128c], S. Amoroso[32], C.S. Amrouche[52], C. Anastopoulos[141],
L.S. Ancu[52], N. Andari[19], T. Andeen[11], C.F. Anders[60b], J.K. Anders[18], K.J. Anderson[33],
A. Andreazza[94a,94b], V. Andrei[60a], S. Angelidakis[37], I. Angelozzi[109], A. Angerami[38],
A.V. Anisenkov[111,c], A. Annovi[126a], C. Antel[60a], M.T. Anthony[141], M. Antonelli[50],
D.J.A. Antrim[166], F. Anulli[134a], M. Aoki[69], L. Aperio Bella[32], G. Arabidze[93], Y. Arai[69],
J.P. Araque[128a], V. Araujo Ferraz[26a], R. Araujo Pereira[26a], A.T.H. Arce[48], R.E. Ardell[80],
F.A. Arduh[74], J-F. Arguin[97], S. Argyropoulos[66], A.J. Armbruster[32], L.J. Armitage[79],
O. Arnaez[161], H. Arnold[109], M. Arratia[30], O. Arslan[23], A. Artamonov[99,*], G. Artoni[122],
S. Artz[86], S. Asai[157], N. Asbah[45], A. Ashkenazi[155], E.M. Asimakopoulou[168], L. Asquith[151],
K. Assamagan[27], R. Astalos[146a], R.J. Atkin[147a], M. Atkinson[169], N.B. Atlay[143], K. Augsten[130],
G. Avolio[32], R. Avramidou[36a], B. Axen[16], M.K. Ayoub[35a], G. Azuelos[97,d], A.E. Baas[60a],
M.J. Baca[19], H. Bachacou[138], K. Bachas[76a,76b], M. Backes[122], P. Bagnaia[134a,134b], M. Bahmani[42],
H. Bahrasemani[144], A.J. Bailey[170], J.T. Baines[133], M. Bajic[39], O.K. Baker[179], P.J. Bakker[109],
D. Bakshi Gupta[82], E.M. Baldin[111,c], P. Balek[175], F. Balli[138], W.K. Balunas[124], E. Banas[42],
A. Bandyopadhyay[23], Sw. Banerjee[176,e], A.A.E. Bannoura[177], L. Barak[155], W.M. Barbe[37],
E.L. Barberio[91], D. Barberis[53a,53b], M. Barbero[88], T. Barillari[103], M-S Barisits[32],
J.T. Barkeloo[118], T. Barklow[145], N. Barlow[30], R. Barnea[154], S.L. Barnes[36c], B.M. Barnett[133],
R.M. Barnett[16], Z. Barnovska-Blenessy[36a], A. Baroncelli[136a], G. Barone[25], A.J. Barr[122],
L. Barranco Navarro[170], F. Barreiro[85], J. Barreiro Guimarães da Costa[35a], R. Bartoldus[145],
A.E. Barton[75], P. Bartos[146a], A. Basalaev[125], A. Bassalat[119], R.L. Bates[56], S.J. Batista[161],
S. Batlamous[137e], J.R. Batley[30], M. Battaglia[139], M. Bauce[134a,134b], F. Bauer[138], K.T. Bauer[166],
H.S. Bawa[145,f], J.B. Beacham[113], M.D. Beattie[75], T. Beau[83], P.H. Beauchemin[165], P. Bechtle[23],
H.P. Beck[18,g], H.C. Beck[58], K. Becker[51], M. Becker[86], C. Becot[112], A.J. Beddall[20e],
A. Beddall[20b], V.A. Bednyakov[68], M. Bedognetti[109], C.P. Bee[150], T.A. Beermann[32],
M. Begalli[26a], M. Begel[27], A. Behera[150], J.K. Behr[45], A.S. Bell[81], G. Bella[155], L. Bellagamba[22a],
A. Bellerive[31], M. Bellomo[154], K. Belotskiy[100], N.L. Belyaev[100], O. Benary[155,*],
D. Benchekroun[137a], M. Bender[102], N. Benekos[10], Y. Benhammou[155], E. Benhar Noccioli[179],
J. Benitez[66], D.P. Benjamin[48], M. Benoit[52], J.R. Bensinger[25], S. Bentvelsen[109], L. Beresford[122],
M. Beretta[50], D. Berge[45], E. Bergeaas Kuutmann[168], N. Berger[5], L.J. Bergsten[25], J. Beringer[16],
S. Berlendis[57], N.R. Bernard[89], G. Bernardi[83], C. Bernius[145], F.U. Bernlochner[23], T. Berry[80],
P. Berta[86], C. Bertella[35a], G. Bertoli[148a,148b], I.A. Bertram[75], C. Bertsche[45], G.J. Besjes[39],
O. Bessidskaia Bylund[148a,148b], M. Bessner[45], N. Besson[138], A. Bethani[87], S. Bethke[103],
A. Betti[23], A.J. Bevan[79], J. Beyer[103], R.M. Bianchi[127], O. Biebel[102], D. Biedermann[17],
R. Bielski[87], K. Bierwagen[86], N.V. Biesuz[126a,126b], M. Biglietti[136a], T.R.V. Billoud[97], M. Bindi[58],
A. Bingul[20b], C. Bini[134a,134b], S. Biondi[22a,22b], T. Bisanz[58], C. Bittrich[47], D.M. Bjergaard[48],

J.E. Black[145], K.M. Black[24], R.E. Blair[6], T. Blazek[146a], I. Bloch[45], C. Blocker[25], A. Blue[56],
U. Blumenschein[79], Dr. Blunier[34a], G.J. Bobbink[109], V.S. Bobrovnikov[111,c], S.S. Bocchetta[84],
A. Bocci[48], C. Bock[102], D. Boerner[177], D. Bogavac[102], A.G. Bogdanchikov[111], C. Bohm[148a],
V. Boisvert[80], P. Bokan[168,h], T. Bold[41a], A.S. Boldyrev[101], A.E. Bolz[60b], M. Bomben[83],
M. Bona[79], J.S. Bonilla[118], M. Boonekamp[138], A. Borisov[132], G. Borissov[75], J. Bortfeldt[32],
D. Bortoletto[122], V. Bortolotto[135a,135b], D. Boscherini[22a], M. Bosman[13], J.D. Bossio Sola[29],
J. Boudreau[127], E.V. Bouhova-Thacker[75], D. Boumediene[37], C. Bourdarios[119], S.K. Boutle[56],
A. Boveia[113], J. Boyd[32], I.R. Boyko[68], A.J. Bozson[80], J. Bracinik[19], N. Brahimi[88], A. Brandt[8],
G. Brandt[177], O. Brandt[60a], F. Braren[45], U. Bratzler[158], B. Brau[89], J.E. Brau[118],
W.D. Breaden Madden[56], K. Brendlinger[45], A.J. Brennan[91], L. Brenner[45], R. Brenner[168],
S. Bressler[175], B. Brickwedde[86], D.L. Briglin[19], T.M. Bristow[49], D. Britton[56], D. Britzger[60b],
I. Brock[23], R. Brock[93], G. Brooijmans[38], T. Brooks[80], W.K. Brooks[34b], E. Brost[110],
J.H Broughton[19], P.A. Bruckman de Renstrom[42], D. Bruncko[146b], A. Bruni[22a], G. Bruni[22a],
L.S. Bruni[109], S. Bruno[135a,135b], B.H. Brunt[30], M. Bruschi[22a], N. Bruscino[127], P. Bryant[33],
L. Bryngemark[45], T. Buanes[15], Q. Buat[32], P. Buchholz[143], A.G. Buckley[56], I.A. Budagov[68],
F. Buehrer[51], M.K. Bugge[121], O. Bulekov[100], D. Bullock[8], T.J. Burch[110], S. Burdin[77],
C.D. Burgard[109], A.M. Burger[5], B. Burghgrave[110], K. Burka[42], S. Burke[133], I. Burmeister[46],
J.T.P. Burr[122], D. Büscher[51], V. Büscher[86], E. Buschmann[58], P. Bussey[56], J.M. Butler[24],
C.M. Buttar[56], J.M. Butterworth[81], P. Butti[32], W. Buttinger[32], A. Buzatu[153],
A.R. Buzykaev[111,c], G. Cabras[22a,22b], S. Cabrera Urbán[170], D. Caforio[130], H. Cai[169],
V.M.M. Cairo[2], O. Cakir[4a], N. Calace[52], P. Calafiura[16], A. Calandri[88], G. Calderini[83],
P. Calfayan[64], G. Callea[40a,40b], L.P. Caloba[26a], S. Calvente Lopez[85], D. Calvet[37], S. Calvet[37],
T.P. Calvet[150], M. Calvetti[126a,126b], R. Camacho Toro[33], S. Camarda[32], P. Camarri[135a,135b],
D. Cameron[121], R. Caminal Armadans[89], C. Camincher[57], S. Campana[32], M. Campanelli[81],
A. Camplani[94a,94b], A. Campoverde[143], V. Canale[106a,106b], M. Cano Bret[36c], J. Cantero[116],
T. Cao[155], Y. Cao[169], M.D.M. Capeans Garrido[32], I. Caprini[28b], M. Caprini[28b], M. Capua[40a,40b],
R.M. Carbone[38], R. Cardarelli[135a], F. Cardillo[51], I. Carli[131], T. Carli[32], G. Carlino[106a],
B.T. Carlson[127], L. Carminati[94a,94b], R.M.D. Carney[148a,148b], S. Caron[108], E. Carquin[34b],
S. Carrá[94a,94b], G.D. Carrillo-Montoya[32], D. Casadei[147b], M.P. Casado[13,i], A.F. Casha[161],
M. Casolino[13], D.W. Casper[166], R. Castelijn[109], V. Castillo Gimenez[170], N.F. Castro[128a,128e],
A. Catinaccio[32], J.R. Catmore[121], A. Cattai[32], J. Caudron[23], V. Cavaliere[27], E. Cavallaro[13],
D. Cavalli[94a], M. Cavalli-Sforza[13], V. Cavasinni[126a,126b], E. Celebi[20d], F. Ceradini[136a,136b],
L. Cerda Alberich[170], A.S. Cerqueira[26b], A. Cerri[151], L. Cerrito[135a,135b], F. Cerutti[16],
A. Cervelli[22a,22b], S.A. Cetin[20d], A. Chafaq[137a], DC Chakraborty[110], S.K. Chan[59], W.S. Chan[109],
Y.L. Chan[62a], P. Chang[169], J.D. Chapman[30], D.G. Charlton[19], C.C. Chau[31],
C.A. Chavez Barajas[151], S. Che[113], A. Chegwidden[93], S. Chekanov[6], S.V. Chekulaev[163a],
G.A. Chelkov[68,j], M.A. Chelstowska[32], C. Chen[36a], C. Chen[67], H. Chen[27], J. Chen[36a], J. Chen[38],
S. Chen[35b], S. Chen[124], X. Chen[35c,k], Y. Chen[70], Y.-H. Chen[45], H.C. Cheng[92], H.J. Cheng[35a,35d],
A. Cheplakov[68], E. Cheremushkina[132], R. Cherkaoui El Moursli[137e], E. Cheu[7], K. Cheung[63],
L. Chevalier[138], V. Chiarella[50], G. Chiarelli[126a], G. Chiodini[76a], A.S. Chisholm[32], A. Chitan[28b],
I. Chiu[157], Y.H. Chiu[172], M.V. Chizhov[68], K. Choi[64], A.R. Chomont[119], S. Chouridou[156],
Y.S. Chow[109], V. Christodoulou[81], M.C. Chu[62a], J. Chudoba[129], A.J. Chuinard[90],
J.J. Chwastowski[42], L. Chytka[117], D. Cinca[46], V. Cindro[78], I.A. Cioară[23], A. Ciocio[16],
F. Cirotto[106a,106b], Z.H. Citron[175], M. Citterio[94a], A. Clark[52], M.R. Clark[38], P.J. Clark[49],
R.N. Clarke[16], C. Clement[148a,148b], Y. Coadou[88], M. Cobal[167a,167c], A. Coccaro[53a,53b],
J. Cochran[67], A.E.C. Coimbra[175], L. Colasurdo[108], B. Cole[38], A.P. Colijn[109], J. Collot[57],
P. Conde Muiño[128a,128b], E. Coniavitis[51], S.H. Connell[147b], I.A. Connelly[87], S. Constantinescu[28b],
F. Conventi[106a,l], A.M. Cooper-Sarkar[122], F. Cormier[171], K.J.R. Cormier[161], M. Corradi[134a,134b],

E.E. Corrigan[84], F. Corriveau[90,m], A. Cortes-Gonzalez[32], M.J. Costa[170], D. Costanzo[141],
G. Cottin[30], G. Cowan[80], B.E. Cox[87], J. Crane[87], K. Cranmer[112], S.J. Crawley[56],
R.A. Creager[124], G. Cree[31], S. Crépé-Renaudin[57], F. Crescioli[83], M. Cristinziani[23], V. Croft[112],
G. Crosetti[40a,40b], A. Cueto[85], T. Cuhadar Donszelmann[141], A.R. Cukierman[145], M. Curatolo[50],
J. Cúth[86], S. Czekierda[42], P. Czodrowski[32], G. D'amen[22a,22b], S. D'Auria[56], L. D'Eramo[83],
M. D'Onofrio[77], M.J. Da Cunha Sargedas De Sousa[36b,128b], C. Da Via[87], W. Dabrowski[41a],
T. Dado[146a,h], S. Dahbi[137e], T. Dai[92], O. Dale[15], F. Dallaire[97], C. Dallapiccola[89], M. Dam[39],
J.R. Dandoy[124], M.F. Daneri[29], N.P. Dang[176,e], N.D Dann[87], M. Danninger[171], V. Dao[32],
G. Darbo[53a], S. Darmora[8], O. Dartsi[5], A. Dattagupta[118], T. Daubney[45], W. Davey[23], C. David[45],
T. Davidek[131], D.R. Davis[48], E. Dawe[91], I. Dawson[141], K. De[8], R. de Asmundis[106a],
A. De Benedetti[115], S. De Castro[22a,22b], S. De Cecco[83], N. De Groot[108], P. de Jong[109],
H. De la Torre[93], F. De Lorenzi[67], A. De Maria[58,n], D. De Pedis[134a], A. De Salvo[134a],
U. De Sanctis[135a,135b], A. De Santo[151], K. De Vasconcelos Corga[88], J.B. De Vivie De Regie[119],
C. Debenedetti[139], D.V. Dedovich[68], N. Dehghanian[3], M. Del Gaudio[40a,40b], J. Del Peso[85],
D. Delgove[119], F. Deliot[138], C.M. Delitzsch[7], A. Dell'Acqua[32], L. Dell'Asta[24],
M. Della Pietra[106a,106b], D. della Volpe[52], M. Delmastro[5], C. Delporte[119], P.A. Delsart[57],
D.A. DeMarco[161], S. Demers[179], M. Demichev[68], S.P. Denisov[132], D. Denysiuk[109],
D. Derendarz[42], J.E. Derkaoui[137d], F. Derue[83], P. Dervan[77], K. Desch[23], C. Deterre[45],
K. Dette[161], M.R. Devesa[29], P.O. Deviveiros[32], A. Dewhurst[133], S. Dhaliwal[25], F.A. Di Bello[52],
A. Di Ciaccio[135a,135b], L. Di Ciaccio[5], W.K. Di Clemente[124], C. Di Donato[106a,106b],
A. Di Girolamo[32], B. Di Micco[136a,136b], R. Di Nardo[32], K.F. Di Petrillo[59], A. Di Simone[51],
R. Di Sipio[161], D. Di Valentino[31], C. Diaconu[88], M. Diamond[161], F.A. Dias[39], T. Dias do Vale[128a],
M.A. Diaz[34a], J. Dickinson[16], E.B. Diehl[92], J. Dietrich[17], S. Díez Cornell[45], A. Dimitrievska[16],
J. Dingfelder[23], F. Dittus[32], F. Djama[88], T. Djobava[54b], J.I. Djuvsland[60a], M.A.B. do Vale[26c],
M. Dobre[28b], D. Dodsworth[25], C. Doglioni[84], J. Dolejsi[131], Z. Dolezal[131], M. Donadelli[26d],
J. Donini[37], J. Dopke[133], A. Doria[106a], M.T. Dova[74], A.T. Doyle[56], E. Drechsler[58], E. Dreyer[144],
T. Dreyer[58], M. Dris[10], Y. Du[36b], J. Duarte-Campderros[155], F. Dubinin[98], A. Dubreuil[52],
E. Duchovni[175], G. Duckeck[102], A. Ducourthial[83], O.A. Ducu[97,o], D. Duda[109], A. Dudarev[32],
A.Chr. Dudder[86], E.M. Duffield[16], L. Duflot[119], M. Dührssen[32], C. Dülsen[177], M. Dumancic[175],
A.E. Dumitriu[28b,p], A.K. Duncan[56], M. Dunford[60a], A. Duperrin[88], H. Duran Yildiz[4a],
M. Düren[55], A. Durglishvili[54b], D. Duschinger[47], B. Dutta[45], D. Duvnjak[1], M. Dyndal[45],
B.S. Dziedzic[42], C. Eckardt[45], K.M. Ecker[103], R.C. Edgar[92], T. Eifert[32], G. Eigen[15],
K. Einsweiler[16], T. Ekelof[168], M. El Kacimi[137c], R. El Kosseifi[88], V. Ellajosyula[88], M. Ellert[168],
F. Ellinghaus[177], A.A. Elliot[172], N. Ellis[32], J. Elmsheuser[27], M. Elsing[32], D. Emeliyanov[133],
Y. Enari[157], J.S. Ennis[173], M.B. Epland[48], J. Erdmann[46], A. Ereditato[18], S. Errede[169],
M. Escalier[119], C. Escobar[170], B. Esposito[50], O. Estrada Pastor[170], A.I. Etienvre[138], E. Etzion[155],
H. Evans[64], A. Ezhilov[125], M. Ezzi[137e], F. Fabbri[22a,22b], L. Fabbri[22a,22b], V. Fabiani[108],
G. Facini[81], R.M. Faisca Rodrigues Pereira[128a], R.M. Fakhrutdinov[132], S. Falciano[134a],
P.J. Falke[5], S. Falke[5], J. Faltova[131], Y. Fang[35a], M. Fanti[94a,94b], A. Farbin[8], A. Farilla[136a],
E.M. Farina[123a,123b], T. Farooque[93], S. Farrell[16], S.M. Farrington[173], P. Farthouat[32], F. Fassi[137e],
P. Fassnacht[32], D. Fassouliotis[9], M. Faucci Giannelli[49], A. Favareto[53a,53b], W.J. Fawcett[52],
L. Fayard[119], O.L. Fedin[125,q], W. Fedorko[171], M. Feickert[43], S. Feigl[121], L. Feligioni[88], C. Feng[36b],
E.J. Feng[32], M. Feng[48], M.J. Fenton[56], A.B. Fenyuk[132], L. Feremenga[8], J. Ferrando[45],
A. Ferrari[168], P. Ferrari[109], R. Ferrari[123a], D.E. Ferreira de Lima[60b], A. Ferrer[170], D. Ferrere[52],
C. Ferretti[92], F. Fiedler[86], A. Filipčič[78], F. Filthaut[108], M. Fincke-Keeler[172], K.D. Finelli[24],
M.C.N. Fiolhais[128a,128c,r], L. Fiorini[170], C. Fischer[13], J. Fischer[177], W.C. Fisher[93], N. Flaschel[45],
I. Fleck[143], P. Fleischmann[92], R.R.M. Fletcher[124], T. Flick[177], B.M. Flierl[102], L.M. Flores[124],
L.R. Flores Castillo[62a], N. Fomin[15], G.T. Forcolin[87], A. Formica[138], F.A. Förster[13], A.C. Forti[87],

A.G. Foster[19], D. Fournier[119], H. Fox[75], S. Fracchia[141], P. Francavilla[126a,126b], M. Franchini[22a,22b], S. Franchino[60a], D. Francis[32], L. Franconi[121], M. Franklin[59], M. Frate[166], M. Fraternali[123a,123b], D. Freeborn[81], S.M. Fressard-Batraneanu[32], B. Freund[97], W.S. Freund[26a], D. Froidevaux[32], J.A. Frost[122], C. Fukunaga[158], T. Fusayasu[104], J. Fuster[170], O. Gabizon[154], A. Gabrielli[22a,22b], A. Gabrielli[16], G.P. Gach[41a], S. Gadatsch[52], S. Gadomski[80], P. Gadow[103], G. Gagliardi[53a,53b], L.G. Gagnon[97], C. Galea[28b], B. Galhardo[128a,128c], E.J. Gallas[122], B.J. Gallop[133], P. Gallus[130], G. Galster[39], R. Gamboa Goni[79], K.K. Gan[113], S. Ganguly[175], Y. Gao[77], Y.S. Gao[145,f], F.M. Garay Walls[34a], C. García[170], J.E. García Navarro[170], J.A. García Pascual[35a], M. Garcia-Sciveres[16], R.W. Gardner[33], N. Garelli[145], V. Garonne[121], K. Gasnikova[45], A. Gaudiello[53a,53b], G. Gaudio[123a], I.L. Gavrilenko[98], A. Gavrilyuk[99], C. Gay[171], G. Gaycken[23], E.N. Gazis[10], C.N.P. Gee[133], J. Geisen[58], M. Geisen[86], M.P. Geisler[60a], K. Gellerstedt[148a,148b], C. Gemme[53a], M.H. Genest[57], C. Geng[92], S. Gentile[134a,134b], C. Gentsos[156], S. George[80], D. Gerbaudo[13], G. Gessner[46], S. Ghasemi[143], M. Ghneimat[23], B. Giacobbe[22a], S. Giagu[134a,134b], N. Giangiacomi[22a,22b], P. Giannetti[126a], S.M. Gibson[80], M. Gignac[139], D. Gillberg[31], G. Gilles[177], D.M. Gingrich[3,d], M.P. Giordani[167a,167c], F.M. Giorgi[22a], P.F. Giraud[138], P. Giromini[59], G. Giugliarelli[167a,167c], D. Giugni[94a], F. Giuli[122], M. Giulini[60b], S. Gkaitatzis[156], I. Gkialas[9,s], E.L. Gkougkousis[13], P. Gkountoumis[10], L.K. Gladilin[101], C. Glasman[85], J. Glatzer[13], P.C.F. Glaysher[45], A. Glazov[45], M. Goblirsch-Kolb[25], J. Godlewski[42], S. Goldfarb[91], T. Golling[52], D. Golubkov[132], A. Gomes[128a,128b,128e], R. Gonçalo[128a], R. Goncalves Gama[26b], G. Gonella[51], L. Gonella[19], A. Gongadze[68], F. Gonnella[19], J.L. Gonski[59], S. González de la Hoz[170], S. Gonzalez-Sevilla[52], L. Goossens[32], P.A. Gorbounov[99], H.A. Gordon[27], B. Gorini[32], E. Gorini[76a,76b], A. Gorišek[78], A.T. Goshaw[48], C. Gössling[46], M.I. Gostkin[68], C.A. Gottardo[23], C.R. Goudet[119], D. Goujdami[137c], A.G. Goussiou[140], N. Govender[147b,t], C. Goy[5], E. Gozani[154], I. Grabowska-Bold[41a], P.O.J. Gradin[168], E.C. Graham[77], J. Gramling[166], E. Gramstad[121], S. Grancagnolo[17], V. Gratchev[125], P.M. Gravila[28f], C. Gray[56], H.M. Gray[16], Z.D. Greenwood[82,u], C. Grefe[23], K. Gregersen[81], I.M. Gregor[45], P. Grenier[145], K. Grevtsov[45], J. Griffiths[8], A.A. Grillo[139], K. Grimm[145], S. Grinstein[13,v], Ph. Gris[37], J.-F. Grivaz[119], S. Groh[86], E. Gross[175], J. Grosse-Knetter[58], G.C. Grossi[82], Z.J. Grout[81], A. Grummer[107], L. Guan[92], W. Guan[176], J. Guenther[32], A. Guerguichon[119], F. Guescini[163a], D. Guest[166], O. Gueta[155], R. Gugel[51], B. Gui[113], T. Guillemin[5], S. Guindon[32], U. Gul[56], C. Gumpert[32], J. Guo[36c], W. Guo[92], Y. Guo[36a,w], Z. Guo[88], R. Gupta[43], S. Gurbuz[20a], G. Gustavino[115], B.J. Gutelman[154], P. Gutierrez[115], N.G. Gutierrez Ortiz[81], C. Gutschow[81], C. Guyot[138], M.P. Guzik[41a], C. Gwenlan[122], C.B. Gwilliam[77], A. Hönle[103], A. Haas[112], C. Haber[16], H.K. Hadavand[8], N. Haddad[137e], A. Hadef[88], S. Hageböck[23], M. Hagihara[164], H. Hakobyan[180,*], M. Haleem[178], J. Haley[116], G. Halladjian[93], G.D. Hallewell[88], K. Hamacher[177], P. Hamal[117], K. Hamano[172], A. Hamilton[147a], G.N. Hamity[141], K. Han[36a,x], L. Han[36a], S. Han[35a,35d], K. Hanagaki[69,y], M. Hance[139], D.M. Handl[102], B. Haney[124], R. Hankache[83], P. Hanke[60a], E. Hansen[84], J.B. Hansen[39], J.D. Hansen[39], M.C. Hansen[23], P.H. Hansen[39], K. Hara[164], A.S. Hard[176], T. Harenberg[177], S. Harkusha[95], P.F. Harrison[173], N.M. Hartmann[102], Y. Hasegawa[142], A. Hasib[49], S. Hassani[138], S. Haug[18], R. Hauser[93], L. Hauswald[47], L.B. Havener[38], M. Havranek[130], C.M. Hawkes[19], R.J. Hawkings[32], D. Hayden[93], C. Hayes[150], C.P. Hays[122], J.M. Hays[79], H.S. Hayward[77], S.J. Haywood[133], M.P. Heath[49], V. Hedberg[84], L. Heelan[8], S. Heer[23], K.K. Heidegger[51], J. Heilman[31], S. Heim[45], T. Heim[16], B. Heinemann[45,z], J.J. Heinrich[102], L. Heinrich[112], C. Heinz[55], J. Hejbal[129], L. Helary[32], A. Held[171], S. Hellesund[121], S. Hellman[148a,148b], C. Helsens[32], R.C.W. Henderson[75], Y. Heng[176], S. Henkelmann[171], A.M. Henriques Correia[32], G.H. Herbert[17], H. Herde[25], V. Herget[178], Y. Hernández Jiménez[147c], H. Herr[86], G. Herten[51], R. Hertenberger[102], L. Hervas[32], T.C. Herwig[124], G.G. Hesketh[81], N.P. Hessey[163a], J.W. Hetherly[43], S. Higashino[69], E. Higón-Rodriguez[170], K. Hildebrand[33],

E. Hill[172], J.C. Hill[30], K.H. Hiller[45], S.J. Hillier[19], M. Hils[47], I. Hinchliffe[16], M. Hirose[120],
D. Hirschbuehl[177], B. Hiti[78], O. Hladik[129], D.R. Hlaluku[147c], X. Hoad[49], J. Hobbs[150], N. Hod[163a],
M.C. Hodgkinson[141], A. Hoecker[32], M.R. Hoeferkamp[107], F. Hoenig[102], D. Hohn[23], D. Hohov[119],
T.R. Holmes[33], M. Holzbock[102], M. Homann[46], S. Honda[164], T. Honda[69], T.M. Hong[127],
B.H. Hooberman[169], W.H. Hopkins[118], Y. Horii[105], P. Horn[47], A.J. Horton[144], L.A. Horyn[33],
J-Y. Hostachy[57], A. Hostiuc[140], S. Hou[153], A. Hoummada[137a], J. Howarth[87], J. Hoya[74],
M. Hrabovsky[117], J. Hrdinka[32], I. Hristova[17], J. Hrivnac[119], T. Hryn'ova[5], A. Hrynevich[96],
P.J. Hsu[63], S.-C. Hsu[140], Q. Hu[27], S. Hu[36c], Y. Huang[35a], Z. Hubacek[130], F. Hubaut[88],
M. Huebner[23], F. Huegging[23], T.B. Huffman[122], E.W. Hughes[38], M. Huhtinen[32], R.F.H. Hunter[31],
P. Huo[150], A.M. Hupe[31], N. Huseynov[68,b], J. Huston[93], J. Huth[59], R. Hyneman[92], G. Iacobucci[52],
G. Iakovidis[27], I. Ibragimov[143], L. Iconomidou-Fayard[119], Z. Idrissi[137e], P. Iengo[32], R. Ignazzi[39],
O. Igonkina[109,aa], R. Iguchi[157], T. Iizawa[174], Y. Ikegami[69], M. Ikeno[69], D. Iliadis[156], N. Ilic[145],
F. Iltzsche[47], G. Introzzi[123a,123b], M. Iodice[136a], K. Iordanidou[38], V. Ippolito[134a,134b],
M.F. Isacson[168], N. Ishijima[120], M. Ishino[157], M. Ishitsuka[159], C. Issever[122], S. Istin[20a,ab],
F. Ito[164], J.M. Iturbe Ponce[62a], R. Iuppa[162a,162b], A. Ivina[175], H. Iwasaki[69], J.M. Izen[44],
V. Izzo[106a], S. Jabbar[3], P. Jacka[129], P. Jackson[1], R.M. Jacobs[23], V. Jain[2], G. Jäkel[177],
K.B. Jakobi[86], K. Jakobs[51], S. Jakobsen[65], T. Jakoubek[129], D.O. Jamin[116], D.K. Jana[82],
R. Jansky[52], J. Janssen[23], M. Janus[58], P.A. Janus[41a], G. Jarlskog[84], N. Javadov[68,b], T. Javůrek[51],
M. Javurkova[51], F. Jeanneau[138], L. Jeanty[16], J. Jejelava[54a,ac], A. Jelinskas[173], P. Jenni[51,ad],
J. Jeong[45], C. Jeske[173], S. Jézéquel[5], H. Ji[176], J. Jia[150], H. Jiang[67], Y. Jiang[36a], Z. Jiang[145],
S. Jiggins[51], F.A. Jimenez Morales[37], J. Jimenez Pena[170], S. Jin[35b], A. Jinaru[28b], O. Jinnouchi[159],
H. Jivan[147c], P. Johansson[141], K.A. Johns[7], C.A. Johnson[64], W.J. Johnson[140],
K. Jon-And[148a,148b], R.W.L. Jones[75], S.D. Jones[151], S. Jones[7], T.J. Jones[77], J. Jongmanns[60a],
P.M. Jorge[128a,128b], J. Jovicevic[163a], X. Ju[176], J.J. Junggeburth[103], A. Juste Rozas[13,v],
A. Kaczmarska[42], M. Kado[119], H. Kagan[113], M. Kagan[145], T. Kaji[174], E. Kajomovitz[154],
C.W. Kalderon[84], A. Kaluza[86], S. Kama[43], A. Kamenshchikov[132], L. Kanjir[78], Y. Kano[157],
V.A. Kantserov[100], J. Kanzaki[69], B. Kaplan[112], L.S. Kaplan[176], D. Kar[147c], M.J. Kareem[163b],
E. Karentzos[10], S.N. Karpov[68], Z.M. Karpova[68], V. Kartvelishvili[75], A.N. Karyukhin[132],
K. Kasahara[164], L. Kashif[176], R.D. Kass[113], A. Kastanas[149], Y. Kataoka[157], C. Kato[157],
A. Katre[52], J. Katzy[45], K. Kawade[70], K. Kawagoe[73], T. Kawamoto[157], G. Kawamura[58],
E.F. Kay[77], V.F. Kazanin[111,c], R. Keeler[172], R. Kehoe[43], J.S. Keller[31], E. Kellermann[84],
J.J. Kempster[19], J. Kendrick[19], O. Kepka[129], B.P. Kerševan[78], S. Kersten[177], R.A. Keyes[90],
M. Khader[169], F. Khalil-zada[12], A. Khanov[116], A.G. Kharlamov[111,c], T. Kharlamova[111],
A. Khodinov[160], T.J. Khoo[52], V. Khovanskiy[99,*], E. Khramov[68], J. Khubua[54b,ae], S. Kido[70],
M. Kiehn[52], C.R. Kilby[80], H.Y. Kim[8], S.H. Kim[164], Y.K. Kim[33], N. Kimura[167a,167c], O.M. Kind[17],
B.T. King[77], D. Kirchmeier[47], J. Kirk[133], A.E. Kiryunin[103], T. Kishimoto[157], D. Kisielewska[41a],
V. Kitali[45], O. Kivernyk[5], E. Kladiva[146b,*], T. Klapdor-Kleingrothaus[51], M.H. Klein[92],
M. Klein[77], U. Klein[77], K. Kleinknecht[86], P. Klimek[110], A. Klimentov[27], R. Klingenberg[46,*],
T. Klingl[23], T. Klioutchnikova[32], F.F. Klitzner[102], P. Kluit[109], S. Kluth[103], E. Kneringer[65],
E.B.F.G. Knoops[88], A. Knue[51], A. Kobayashi[157], D. Kobayashi[73], T. Kobayashi[157], M. Kobel[47],
M. Kocian[145], P. Kodys[131], T. Koffas[31], E. Koffeman[109], N.M. Köhler[103], T. Koi[145], M. Kolb[60b],
I. Koletsou[5], T. Kondo[69], N. Kondrashova[36c], K. Köneke[51], A.C. König[108], T. Kono[69,af],
R. Konoplich[112,ag], N. Konstantinidis[81], B. Konya[84], R. Kopeliansky[64], S. Koperny[41a],
K. Korcyl[42], K. Kordas[156], A. Korn[81], I. Korolkov[13], E.V. Korolkova[141], O. Kortner[103],
S. Kortner[103], T. Kosek[131], V.V. Kostyukhin[23], A. Kotwal[48], A. Koulouris[10],
A. Kourkoumeli-Charalampidi[123a,123b], C. Kourkoumelis[9], E. Kourlitis[141], V. Kouskoura[27],
A.B. Kowalewska[42], R. Kowalewski[172], T.Z. Kowalski[41a], C. Kozakai[157], W. Kozanecki[138],
A.S. Kozhin[132], V.A. Kramarenko[101], G. Kramberger[78], D. Krasnopevtsev[100], M.W. Krasny[83],

A. Krasznahorkay[32], D. Krauss[103], J.A. Kremer[41a], J. Kretzschmar[77], K. Kreutzfeldt[55],
P. Krieger[161], K. Krizka[16], K. Kroeninger[46], H. Kroha[103], J. Kroll[129], J. Kroll[124], J. Kroseberg[23],
J. Krstic[14], U. Kruchonak[68], H. Krüger[23], N. Krumnack[67], M.C. Kruse[48], T. Kubota[91],
S. Kuday[4b], J.T. Kuechler[177], S. Kuehn[32], A. Kugel[60a], F. Kuger[178], T. Kuhl[45], V. Kukhtin[68],
R. Kukla[88], Y. Kulchitsky[95], S. Kuleshov[34b], Y.P. Kulinich[169], M. Kuna[57], T. Kunigo[71],
A. Kupco[129], T. Kupfer[46], O. Kuprash[155], H. Kurashige[70], L.L. Kurchaninov[163a],
Y.A. Kurochkin[95], M.G. Kurth[35a,35d], E.S. Kuwertz[172], M. Kuze[159], J. Kvita[117], T. Kwan[172],
A. La Rosa[103], J.L. La Rosa Navarro[26d], L. La Rotonda[40a,40b], F. La Ruffa[40a,40b], C. Lacasta[170],
F. Lacava[134a,134b], J. Lacey[45], D.P.J. Lack[87], H. Lacker[17], D. Lacour[83], E. Ladygin[68], R. Lafaye[5],
B. Laforge[83], S. Lai[58], S. Lammers[64], W. Lampl[7], E. Lançon[27], U. Landgraf[51], M.P.J. Landon[79],
M.C. Lanfermann[52], V.S. Lang[45], J.C. Lange[13], R.J. Langenberg[32], A.J. Lankford[166], F. Lanni[27],
K. Lantzsch[23], A. Lanza[123a], A. Lapertosa[53a,53b], S. Laplace[83], J.F. Laporte[138], T. Lari[94a],
F. Lasagni Manghi[22a,22b], M. Lassnig[32], T.S. Lau[62a], A. Laudrain[119], A.T. Law[139], P. Laycock[77],
M. Lazzaroni[94a,94b], B. Le[91], O. Le Dortz[83], E. Le Guirriec[88], E.P. Le Quilleuc[138], M. LeBlanc[7],
T. LeCompte[6], F. Ledroit-Guillon[57], C.A. Lee[27], G.R. Lee[34a], S.C. Lee[153], L. Lee[59],
B. Lefebvre[90], M. Lefebvre[172], F. Legger[102], C. Leggett[16], G. Lehmann Miotto[32], W.A. Leight[45],
A. Leisos[156,ah], M.A.L. Leite[26d], R. Leitner[131], D. Lellouch[175], B. Lemmer[58], K.J.C. Leney[81],
T. Lenz[23], B. Lenzi[32], R. Leone[7], S. Leone[126a], C. Leonidopoulos[49], G. Lerner[151], C. Leroy[97],
R. Les[161], A.A.J. Lesage[138], C.G. Lester[30], M. Levchenko[125], J. Levêque[5], D. Levin[92],
L.J. Levinson[175], D. Lewis[79], B. Li[36a,w], C.-Q. Li[36a], H. Li[36b], L. Li[36c], Q. Li[35a,35d], Q. Li[36a],
S. Li[36c,36d], X. Li[36c], Y. Li[143], Z. Liang[35a], B. Liberti[135a], A. Liblong[161], K. Lie[62c], S. Liem[109],
A. Limosani[152], C.Y. Lin[30], K. Lin[93], S.C. Lin[182], T.H. Lin[86], R.A. Linck[64], B.E. Lindquist[150],
A.L. Lionti[52], E. Lipeles[124], A. Lipniacka[15], M. Lisovyi[60b], T.M. Liss[169,ai], A. Lister[171],
A.M. Litke[139], J.D. Little[8], B.L Liu[6], B. Liu[67], H. Liu[92], H. Liu[27], J.K.K. Liu[122], J.B. Liu[36a],
kliu Liu[83], M. Liu[36a], P. Liu[16], Y.L. Liu[36a], Y. Liu[36a], M. Livan[123a,123b], A. Lleres[57],
J. Llorente Merino[35a], S.L. Lloyd[79], C.Y. Lo[62b], F. Lo Sterzo[43], E.M. Lobodzinska[45], P. Loch[7],
F.K. Loebinger[87], A. Loesle[51], K.M. Loew[25], T. Lohse[17], K. Lohwasser[141], M. Lokajicek[129],
B.A. Long[24], J.D. Long[169], R.E. Long[75], L. Longo[76a,76b], K.A. Looper[113], J.A. Lopez[34b],
I. Lopez Paz[13], A. Lopez Solis[83], J. Lorenz[102], N. Lorenzo Martinez[5], M. Losada[21], P.J. Lösel[102],
X. Lou[35a], X. Lou[45], A. Lounis[119], J. Love[6], P.A. Love[75], J.J. Lozano Bahilo[170], H. Lu[62a],
N. Lu[92], Y.J. Lu[63], H.J. Lubatti[140], C. Luci[134a,134b], A. Lucotte[57], C. Luedtke[51], F. Luehring[64],
I. Luise[83], W. Lukas[65], L. Luminari[134a], B. Lund-Jensen[149], M.S. Lutz[89], P.M. Luzi[83], D. Lynn[27],
R. Lysak[129], E. Lytken[84], F. Lyu[35a], V. Lyubushkin[68], H. Ma[27], L.L. Ma[36b], Y. Ma[36b],
G. Maccarrone[50], A. Macchiolo[103], C.M. Macdonald[141], B. Maček[78], J. Machado Miguens[124],
D. Madaffari[170], R. Madar[37], W.F. Mader[47], A. Madsen[45], N. Madysa[47], J. Maeda[70],
S. Maeland[15], T. Maeno[27], A.S. Maevskiy[101], V. Magerl[51], C. Maidantchik[26a], T. Maier[102],
A. Maio[128a,128b,128e], O. Majersky[146a], S. Majewski[118], Y. Makida[69], N. Makovec[119],
B. Malaescu[83], Pa. Malecki[42], V.P. Maleev[125], F. Malek[57], U. Mallik[66], D. Malon[6], C. Malone[30],
S. Maltezos[10], S. Malyukov[32], J. Mamuzic[170], G. Mancini[50], I. Mandić[78], J. Maneira[128a,128b],
L. Manhaes de Andrade Filho[26b], J. Manjarres Ramos[47], K.H. Mankinen[84], A. Mann[102],
A. Manousos[65], B. Mansoulie[138], J.D. Mansour[35a], R. Mantifel[90], M. Mantoani[58],
S. Manzoni[94a,94b], G. Marceca[29], L. March[52], L. Marchese[122], G. Marchiori[83], M. Marcisovsky[129],
C.A. Marin Tobon[32], M. Marjanovic[37], D.E. Marley[92], F. Marroquim[26a], Z. Marshall[16],
M.U.F Martensson[168], S. Marti-Garcia[170], C.B. Martin[113], T.A. Martin[173], V.J. Martin[49],
B. Martin dit Latour[15], M. Martinez[13,v], V.I. Martinez Outschoorn[89], S. Martin-Haugh[133],
V.S. Martoiu[28b], A.C. Martyniuk[81], A. Marzin[32], L. Masetti[86], T. Mashimo[157], R. Mashinistov[98],
J. Masik[87], A.L. Maslennikov[111,c], L.H. Mason[91], L. Massa[135a,135b], P. Mastrandrea[5],
A. Mastroberardino[40a,40b], T. Masubuchi[157], P. Mättig[177], J. Maurer[28b], S.J. Maxfield[77],

D.A. Maximov[111,c], R. Mazini[153], I. Maznas[156], S.M. Mazza[139], N.C. Mc Fadden[107],
G. Mc Goldrick[161], S.P. Mc Kee[92], A. McCarn[92], T.G. McCarthy[103], L.I. McClymont[81],
E.F. McDonald[91], J.A. Mcfayden[32], G. Mchedlidze[58], M.A. McKay[43], K.D. McLean[172],
S.J. McMahon[133], P.C. McNamara[91], C.J. McNicol[173], R.A. McPherson[172,m], J.E. Mdhluli[147c],
Z.A. Meadows[89], S. Meehan[140], T. Megy[51], S. Mehlhase[102], A. Mehta[77], T. Meideck[57],
B. Meirose[44], D. Melini[170,aj], B.R. Mellado Garcia[147c], J.D. Mellenthin[58], M. Melo[146a],
F. Meloni[18], A. Melzer[23], S.B. Menary[87], L. Meng[77], X.T. Meng[92], A. Mengarelli[22a,22b],
S. Menke[103], E. Meoni[40a,40b], S. Mergelmeyer[17], C. Merlassino[18], P. Mermod[52],
L. Merola[106a,106b], C. Meroni[94a], F.S. Merritt[33], A. Messina[134a,134b], J. Metcalfe[6], A.S. Mete[166],
C. Meyer[124], J-P. Meyer[138], J. Meyer[154], H. Meyer Zu Theenhausen[60a], F. Miano[151],
R.P. Middleton[133], L. Mijović[49], G. Mikenberg[175], M. Mikestikova[129], M. Mikuž[78], M. Milesi[91],
A. Milic[161], D.A. Millar[79], D.W. Miller[33], A. Milov[175], D.A. Milstead[148a,148b], A.A. Minaenko[132],
I.A. Minashvili[54b], A.I. Mincer[112], B. Mindur[41a], M. Mineev[68], Y. Minegishi[157], Y. Ming[176],
L.M. Mir[13], A. Mirto[76a,76b], K.P. Mistry[124], T. Mitani[174], J. Mitrevski[102], V.A. Mitsou[170],
A. Miucci[18], P.S. Miyagawa[141], A. Mizukami[69], J.U. Mjörnmark[84], T. Mkrtchyan[180],
M. Mlynarikova[131], T. Moa[148a,148b], K. Mochizuki[97], P. Mogg[51], S. Mohapatra[38],
S. Molander[148a,148b], R. Moles-Valls[23], M.C. Mondragon[93], K. Mönig[45], J. Monk[39], E. Monnier[88],
A. Montalbano[144], J. Montejo Berlingen[32], F. Monticelli[74], S. Monzani[94a], R.W. Moore[3],
N. Morange[119], D. Moreno[21], M. Moreno Llácer[32], P. Morettini[53a], M. Morgenstern[109],
S. Morgenstern[32], D. Mori[144], T. Mori[157], M. Morii[59], M. Morinaga[174], V. Morisbak[121],
A.K. Morley[32], G. Mornacchi[32], J.D. Morris[79], L. Morvaj[150], P. Moschovakos[10], M. Mosidze[54b],
H.J. Moss[141], J. Moss[145,ak], K. Motohashi[159], R. Mount[145], E. Mountricha[27], E.J.W. Moyse[89],
S. Muanza[88], F. Mueller[103], J. Mueller[127], R.S.P. Mueller[102], D. Muenstermann[75], P. Mullen[56],
G.A. Mullier[18], F.J. Munoz Sanchez[87], P. Murin[146b], W.J. Murray[173,133], A. Murrone[94a,94b],
M. Muškinja[78], C. Mwewa[147a], A.G. Myagkov[132,al], J. Myers[118], M. Myska[130], B.P. Nachman[16],
O. Nackenhorst[46], K. Nagai[122], R. Nagai[69,af], K. Nagano[69], Y. Nagasaka[61], K. Nagata[164],
M. Nagel[51], E. Nagy[88], A.M. Nairz[32], Y. Nakahama[105], K. Nakamura[69], T. Nakamura[157],
I. Nakano[114], F. Napolitano[60a], R.F. Naranjo Garcia[45], R. Narayan[11], D.I. Narrias Villar[60a],
I. Naryshkin[125], T. Naumann[45], G. Navarro[21], R. Nayyar[7], H.A. Neal[92], P.Yu. Nechaeva[98],
T.J. Neep[138], A. Negri[123a,123b], M. Negrini[22a], S. Nektarijevic[108], C. Nellist[58], M.E. Nelson[122],
S. Nemecek[129], P. Nemethy[112], M. Nessi[32,am], M.S. Neubauer[169], M. Neumann[177],
P.R. Newman[19], T.Y. Ng[62c], Y.S. Ng[17], H.D.N. Nguyen[88], T. Nguyen Manh[97], E. Nibigira[37],
R.B. Nickerson[122], R. Nicolaidou[138], J. Nielsen[139], N. Nikiforou[11], V. Nikolaenko[132,al],
I. Nikolic-Audit[83], K. Nikolopoulos[19], P. Nilsson[27], Y. Ninomiya[69], A. Nisati[134a], N. Nishu[36c],
R. Nisius[103], I. Nitsche[46], T. Nitta[174], T. Nobe[157], Y. Noguchi[71], M. Nomachi[120], I. Nomidis[31],
M.A. Nomura[27], T. Nooney[79], M. Nordberg[32], N. Norjoharuddeen[122], T. Novak[78],
O. Novgorodova[47], R. Novotny[130], M. Nozaki[69], L. Nozka[117], K. Ntekas[166], E. Nurse[81], F. Nuti[91],
K. O'Connor[25], D.C. O'Neil[144], A.A. O'Rourke[45], V. O'Shea[56], F.G. Oakham[31,d], H. Oberlack[103],
T. Obermann[23], J. Ocariz[83], A. Ochi[70], I. Ochoa[38], J.P. Ochoa-Ricoux[34a], S. Oda[73], S. Odaka[69],
A. Oh[87], S.H. Oh[48], C.C. Ohm[149], H. Ohman[168], H. Oide[53a,53b], H. Okawa[164], Y. Okazaki[71],
Y. Okumura[157], T. Okuyama[69], A. Olariu[28b], L.F. Oleiro Seabra[128a], S.A. Olivares Pino[34a],
D. Oliveira Damazio[27], J.L. Oliver[1], M.J.R. Olsson[33], A. Olszewski[42], J. Olszowska[42],
A. Onofre[128a,128e], K. Onogi[105], P.U.E. Onyisi[11,an], H. Oppen[121], M.J. Oreglia[33], Y. Oren[155],
D. Orestano[136a,136b], E.C. Orgill[87], N. Orlando[62b], R.S. Orr[161], B. Osculati[53a,53b,*],
R. Ospanov[36a], G. Otero y Garzon[29], H. Otono[73], M. Ouchrif[137d], F. Ould-Saada[121],
A. Ouraou[138], Q. Ouyang[35a], M. Owen[56], R.E. Owen[19], V.E. Ozcan[20a], N. Ozturk[8], K. Pachal[144],
A. Pacheco Pages[13], L. Pacheco Rodriguez[138], C. Padilla Aranda[13], S. Pagan Griso[16],
M. Paganini[179], G. Palacino[64], S. Palazzo[40a,40b], S. Palestini[32], M. Palka[41b], D. Pallin[37],

I. Panagoulias[10], C.E. Pandini[52], J.G. Panduro Vazquez[80], P. Pani[32], L. Paolozzi[52],
Th.D. Papadopoulou[10], K. Papageorgiou[9,s], A. Paramonov[6], D. Paredes Hernandez[62b],
B. Parida[36c], A.J. Parker[75], M.A. Parker[30], K.A. Parker[45], F. Parodi[53a,53b], J.A. Parsons[38],
U. Parzefall[51], V.R. Pascuzzi[161], J.M.P Pasner[139], E. Pasqualucci[134a], S. Passaggio[53a],
Fr. Pastore[80], P. Pasuwan[148a,148b], S. Pataraia[86], J.R. Pater[87], A. Pathak[176,e], T. Pauly[32],
B. Pearson[103], S. Pedraza Lopez[170], R. Pedro[128a,128b], S.V. Peleganchuk[111,c], O. Penc[129],
C. Peng[35a,35d], H. Peng[36a], J. Penwell[64], B.S. Peralva[26b], M.M. Perego[138],
A.P. Pereira Peixoto[128a], D.V. Perepelitsa[27], F. Peri[17], L. Perini[94a,94b], H. Pernegger[32],
S. Perrella[106a,106b], V.D. Peshekhonov[68,*], K. Peters[45], R.F.Y. Peters[87], B.A. Petersen[32],
T.C. Petersen[39], E. Petit[57], A. Petridis[1], C. Petridou[156], P. Petroff[119], E. Petrolo[134a],
M. Petrov[122], F. Petrucci[136a,136b], N.E. Pettersson[89], A. Peyaud[138], R. Pezoa[34b], T. Pham[91],
F.H. Phillips[93], P.W. Phillips[133], G. Piacquadio[150], E. Pianori[173], A. Picazio[89], M.A. Pickering[122],
R. Piegaia[29], J.E. Pilcher[33], A.D. Pilkington[87], M. Pinamonti[135a,135b], J.L. Pinfold[3], M. Pitt[175],
M.-A. Pleier[27], V. Pleskot[131], E. Plotnikova[68], D. Pluth[67], P. Podberezko[111], R. Poettgen[84],
R. Poggi[123a,123b], L. Poggioli[119], I. Pogrebnyak[93], D. Pohl[23], I. Pokharel[58], G. Polesello[123a],
A. Poley[45], A. Policicchio[40a,40b], R. Polifka[32], A. Polini[22a], C.S. Pollard[45], V. Polychronakos[27],
D. Ponomarenko[100], L. Pontecorvo[134a], G.A. Popeneciu[28d], D.M. Portillo Quintero[83],
S. Pospisil[130], K. Potamianos[45], I.N. Potrap[68], C.J. Potter[30], H. Potti[11], T. Poulsen[84],
J. Poveda[32], M.E. Pozo Astigarraga[32], P. Pralavorio[88], S. Prell[67], D. Price[87], M. Primavera[76a],
S. Prince[90], N. Proklova[100], K. Prokofiev[62c], F. Prokoshin[34b], S. Protopopescu[27], J. Proudfoot[6],
M. Przybycien[41a], A. Puri[169], P. Puzo[119], J. Qian[92], Y. Qin[87], A. Quadt[58],
M. Queitsch-Maitland[45], A. Qureshi[1], S.K. Radhakrishnan[150], P. Rados[91], F. Ragusa[94a,94b],
G. Rahal[181], J.A. Raine[87], S. Rajagopalan[27], T. Rashid[119], S. Raspopov[5], M.G. Ratti[94a,94b],
D.M. Rauch[45], F. Rauscher[102], S. Rave[86], B. Ravina[141], I. Ravinovich[175], J.H. Rawling[87],
M. Raymond[32], A.L. Read[121], N.P. Readioff[57], M. Reale[76a,76b], D.M. Rebuzzi[123a,123b],
A. Redelbach[178], G. Redlinger[27], R. Reece[139], R.G. Reed[147c], K. Reeves[44], L. Rehnisch[17],
J. Reichert[124], A. Reiss[86], C. Rembser[32], H. Ren[35a,35d], M. Rescigno[134a], S. Resconi[94a],
E.D. Resseguie[124], S. Rettie[171], E. Reynolds[19], O.L. Rezanova[111,c], P. Reznicek[131], R. Richter[103],
S. Richter[81], E. Richter-Was[41b], O. Ricken[23], M. Ridel[83], P. Rieck[103], C.J. Riegel[177], O. Rifki[45],
M. Rijssenbeek[150], A. Rimoldi[123a,123b], M. Rimoldi[18], L. Rinaldi[22a], G. Ripellino[149], B. Ristić[32],
E. Ritsch[32], I. Riu[13], J.C. Rivera Vergara[34a], F. Rizatdinova[116], E. Rizvi[79], C. Rizzi[13],
R.T. Roberts[87], S.H. Robertson[90,m], A. Robichaud-Veronneau[90], D. Robinson[30],
J.E.M. Robinson[45], A. Robson[56], E. Rocco[86], C. Roda[126a,126b], Y. Rodina[88,ao],
S. Rodriguez Bosca[170], A. Rodriguez Perez[13], D. Rodriguez Rodriguez[170],
A.M. Rodríguez Vera[163b], S. Roe[32], C.S. Rogan[59], O. Røhne[121], R. Röhrig[103], C.P.A. Roland[64],
J. Roloff[59], A. Romaniouk[100], M. Romano[22a,22b], E. Romero Adam[170], N. Rompotis[77],
M. Ronzani[112], L. Roos[83], S. Rosati[134a], K. Rosbach[51], P. Rose[139], N.-A. Rosien[58],
E. Rossi[106a,106b], L.P. Rossi[53a], L. Rossini[94a,94b], J.H.N. Rosten[30], R. Rosten[140], M. Rotaru[28b],
J. Rothberg[140], D. Rousseau[119], D. Roy[147c], A. Rozanov[88], Y. Rozen[154], X. Ruan[147c],
F. Rubbo[145], F. Rühr[51], A. Ruiz-Martinez[31], Z. Rurikova[51], N.A. Rusakovich[68], H.L. Russell[90],
J.P. Rutherfoord[7], N. Ruthmann[32], E.M. Rüttinger[45], Y.F. Ryabov[125], M. Rybar[169],
G. Rybkin[119], S. Ryu[6], A. Ryzhov[132], G.F. Rzehorz[58], P. Sabatini[58], G. Sabato[109],
S. Sacerdoti[119], H.F-W. Sadrozinski[139], R. Sadykov[68], F. Safai Tehrani[134a], P. Saha[110],
M. Sahinsoy[60a], M. Saimpert[45], M. Saito[157], T. Saito[157], H. Sakamoto[157], A. Sakharov[112],
D. Salamani[52], G. Salamanna[136a,136b], J.E. Salazar Loyola[34b], D. Salek[109], P.H. Sales De Bruin[168],
D. Salihagic[103], A. Salnikov[145], J. Salt[170], D. Salvatore[40a,40b], F. Salvatore[151],
A. Salvucci[62a,62b,62c], A. Salzburger[32], D. Sammel[51], D. Sampsonidis[156], D. Sampsonidou[156],
J. Sánchez[170], A. Sanchez Pineda[167a,167c], H. Sandaker[121], C.O. Sander[45], M. Sandhoff[177],

C. Sandoval[21], D.P.C. Sankey[133], M. Sannino[53a,53b], Y. Sano[105], A. Sansoni[50], C. Santoni[37],
H. Santos[128a], I. Santoyo Castillo[151], A. Sapronov[68], J.G. Saraiva[128a,128e], O. Sasaki[69], K. Sato[164],
E. Sauvan[5], P. Savard[161,d], N. Savic[103], R. Sawada[157], C. Sawyer[133], L. Sawyer[82,u], C. Sbarra[22a],
A. Sbrizzi[22a,22b], T. Scanlon[81], D.A. Scannicchio[166], J. Schaarschmidt[140], P. Schacht[103],
B.M. Schachtner[102], D. Schaefer[33], L. Schaefer[124], J. Schaeffer[86], S. Schaepe[32], U. Schäfer[86],
A.C. Schaffer[119], D. Schaile[102], R.D. Schamberger[150], N. Scharmberg[87], V.A. Schegelsky[125],
D. Scheirich[131], F. Schenck[17], M. Schernau[166], C. Schiavi[53a,53b], S. Schier[139], L.K. Schildgen[23],
Z.M. Schillaci[25], E.J. Schioppa[32], M. Schioppa[40a,40b], K.E. Schleicher[51], S. Schlenker[32],
K.R. Schmidt-Sommerfeld[103], K. Schmieden[32], C. Schmitt[86], S. Schmitt[45], S. Schmitz[86],
U. Schnoor[51], L. Schoeffel[138], A. Schoening[60b], E. Schopf[23], M. Schott[86], J.F.P. Schouwenberg[108],
J. Schovancova[32], S. Schramm[52], N. Schuh[86], A. Schulte[86], H.-C. Schultz-Coulon[60a],
M. Schumacher[51], B.A. Schumm[139], Ph. Schune[138], A. Schwartzman[145], T.A. Schwarz[92],
H. Schweiger[87], Ph. Schwemling[138], R. Schwienhorst[93], A. Sciandra[23], G. Sciolla[25],
M. Scornajenghi[40a,40b], F. Scuri[126a], F. Scutti[91], L.M. Scyboz[103], J. Searcy[92],
C.D. Sebastiani[134a,134b], P. Seema[23], S.C. Seidel[107], A. Seiden[139], J.M. Seixas[26a],
G. Sekhniaidze[106a], K. Sekhon[92], S.J. Sekula[43], N. Semprini-Cesari[22a,22b], S. Senkin[37],
C. Serfon[121], L. Serin[119], L. Serkin[167a,167b], M. Sessa[136a,136b], H. Severini[115], T. Šfiligoj[78],
F. Sforza[165], A. Sfyrla[52], E. Shabalina[58], J.D. Shahinian[139], N.W. Shaikh[148a,148b], L.Y. Shan[35a],
R. Shang[169], J.T. Shank[24], M. Shapiro[16], A. Sharma[122], A.S. Sharma[1], P.B. Shatalov[99],
K. Shaw[167a,167b], S.M. Shaw[87], A. Shcherbakova[125], C.Y. Shehu[151], Y. Shen[115], N. Sherafati[31],
A.D. Sherman[24], P. Sherwood[81], L. Shi[153,ap], S. Shimizu[70], C.O. Shimmin[179], M. Shimojima[104],
I.P.J. Shipsey[122], S. Shirabe[73], M. Shiyakova[68,aq], J. Shlomi[175], A. Shmeleva[98],
D. Shoaleh Saadi[97], M.J. Shochet[33], S. Shojaii[91], D.R. Shope[115], S. Shrestha[113], E. Shulga[100],
P. Sicho[129], A.M. Sickles[169], P.E. Sidebo[149], E. Sideras Haddad[147c], O. Sidiropoulou[178],
A. Sidoti[22a,22b], F. Siegert[47], Dj. Sijacki[14], J. Silva[128a,128e], M. Silva Jr.[176], S.B. Silverstein[148a],
L. Simic[68], S. Simion[119], E. Simioni[86], B. Simmons[81], M. Simon[86], P. Sinervo[161], N.B. Sinev[118],
M. Sioli[22a,22b], G. Siragusa[178], I. Siral[92], S.Yu. Sivoklokov[101], J. Sjölin[148a,148b], M.B. Skinner[75],
P. Skubic[115], M. Slater[19], T. Slavicek[130], M. Slawinska[42], K. Sliwa[165], R. Slovak[131],
V. Smakhtin[175], B.H. Smart[5], J. Smiesko[146a], N. Smirnov[100], S.Yu. Smirnov[100], Y. Smirnov[100],
L.N. Smirnova[101,ar], O. Smirnova[84], J.W. Smith[58], M.N.K. Smith[38], R.W. Smith[38],
M. Smizanska[75], K. Smolek[130], A.A. Snesarev[98], I.M. Snyder[118], S. Snyder[27], R. Sobie[172,m],
F. Socher[47], A.M. Soffa[166], A. Soffer[155], A. Søgaard[49], D.A. Soh[153], G. Sokhrannyi[78],
C.A. Solans Sanchez[32], M. Solar[130], E.Yu. Soldatov[100], U. Soldevila[170], A.A. Solodkov[132],
A. Soloshenko[68], O.V. Solovyanov[132], V. Solovyev[125], P. Sommer[141], H. Son[165], W. Song[133],
A. Sopczak[130], F. Sopkova[146b], D. Sosa[60b], C.L. Sotiropoulou[126a,126b], S. Sottocornola[123a,123b],
R. Soualah[167a,167c], A.M. Soukharev[111,c], D. South[45], B.C. Sowden[80], S. Spagnolo[76a,76b],
M. Spalla[103], M. Spangenberg[173], F. Spanò[80], D. Sperlich[17], F. Spettel[103], T.M. Spieker[60a],
R. Spighi[22a], G. Spigo[32], L.A. Spiller[91], M. Spousta[131], A. Stabile[94a,94b], R. Stamen[60a],
S. Stamm[17], E. Stanecka[42], R.W. Stanek[6], C. Stanescu[136a], M.M. Stanitzki[45], B.S. Stapf[109],
S. Stapnes[121], E.A. Starchenko[132], G.H. Stark[33], J. Stark[57], S.H Stark[39], P. Staroba[129],
P. Starovoitov[60a], S. Stärz[32], R. Staszewski[42], M. Stegler[45], P. Steinberg[27], B. Stelzer[144],
H.J. Stelzer[32], O. Stelzer-Chilton[163a], H. Stenzel[55], T.J. Stevenson[79], G.A. Stewart[32],
M.C. Stockton[118], G. Stoicea[28b], P. Stolte[58], S. Stonjek[103], A. Straessner[47], J. Strandberg[149],
S. Strandberg[148a,148b], M. Strauss[115], P. Strizenec[146b], R. Ströhmer[178], D.M. Strom[118],
R. Stroynowski[43], A. Strubig[49], S.A. Stucci[27], B. Stugu[15], J. Stupak[115], N.A. Styles[45], D. Su[145],
J. Su[127], S. Suchek[60a], Y. Sugaya[120], M. Suk[130], V.V. Sulin[98], D.M.S. Sultan[52], S. Sultansoy[4c],
T. Sumida[71], S. Sun[92], X. Sun[3], K. Suruliz[151], C.J.E. Suster[152], M.R. Sutton[151], S. Suzuki[69],
M. Svatos[129], M. Swiatlowski[33], S.P. Swift[2], A. Sydorenko[86], I. Sykora[146a], T. Sykora[131], D. Ta[86],

K. Tackmann[45], J. Taenzer[155], A. Taffard[166], R. Tafirout[163a], E. Tahirovic[79], N. Taiblum[155],
H. Takai[27], R. Takashima[72], E.H. Takasugi[103], K. Takeda[70], T. Takeshita[142], Y. Takubo[69],
M. Talby[88], A.A. Talyshev[111,c], J. Tanaka[157], M. Tanaka[159], R. Tanaka[119], R. Tanioka[70],
B.B. Tannenwald[113], S. Tapia Araya[34b], S. Tapprogge[86], A. Tarek Abouelfadl Mohamed[83],
S. Tarem[154], G. Tarna[28b,p], G.F. Tartarelli[94a], P. Tas[131], M. Tasevsky[129], T. Tashiro[71],
E. Tassi[40a,40b], A. Tavares Delgado[128a,128b], Y. Tayalati[137e], A.C. Taylor[107], A.J. Taylor[49],
G.N. Taylor[91], P.T.E. Taylor[91], W. Taylor[163b], A.S. Tee[75], P. Teixeira-Dias[80], D. Temple[144],
H. Ten Kate[32], P.K. Teng[153], J.J. Teoh[120], F. Tepel[177], S. Terada[69], K. Terashi[157], J. Terron[85],
S. Terzo[13], M. Testa[50], R.J. Teuscher[161,m], S.J. Thais[179], T. Theveneaux-Pelzer[45], F. Thiele[39],
J.P. Thomas[19], P.D. Thompson[19], A.S. Thompson[56], L.A. Thomsen[179], E. Thomson[124],
Y. Tian[38], R.E. Ticse Torres[58], V.O. Tikhomirov[98,as], Yu.A. Tikhonov[111,c], S. Timoshenko[100],
P. Tipton[179], S. Tisserant[88], K. Todome[159], S. Todorova-Nova[5], S. Todt[47], J. Tojo[73],
S. Tokár[146a], K. Tokushuku[69], E. Tolley[113], M. Tomoto[105], L. Tompkins[145,at], K. Toms[107],
B. Tong[59], P. Tornambe[51], E. Torrence[118], H. Torres[47], E. Torró Pastor[140], C. Tosciri[122],
J. Toth[88,au], F. Touchard[88], D.R. Tovey[141], C.J. Treado[112], T. Trefzger[178], F. Tresoldi[151],
A. Tricoli[27], I.M. Trigger[163a], S. Trincaz-Duvoid[83], M.F. Tripiana[13], W. Trischuk[161], B. Trocmé[57],
A. Trofymov[45], C. Troncon[94a], M. Trovatelli[172], F. Trovato[151], L. Truong[147b], M. Trzebinski[42],
A. Trzupek[42], F. Tsai[45], K.W. Tsang[62a], J.C-L. Tseng[122], P.V. Tsiareshka[95], N. Tsirintanis[9],
S. Tsiskaridze[13], V. Tsiskaridze[150], E.G. Tskhadadze[54a], I.I. Tsukerman[99], V. Tsulaia[16],
S. Tsuno[69], D. Tsybychev[150], Y. Tu[62b], A. Tudorache[28b], V. Tudorache[28b], T.T. Tulbure[28a],
A.N. Tuna[59], S. Turchikhin[68], D. Turgeman[175], I. Turk Cakir[4b,av], R. Turra[94a], P.M. Tuts[38],
G. Ucchielli[22a,22b], I. Ueda[69], M. Ughetto[148a,148b], F. Ukegawa[164], G. Unal[32], A. Undrus[27],
G. Unel[166], F.C. Ungaro[91], Y. Unno[69], K. Uno[157], J. Urban[146b], P. Urquijo[91], P. Urrejola[86],
G. Usai[8], J. Usui[69], L. Vacavant[88], V. Vacek[130], B. Vachon[90], K.O.H. Vadla[121], A. Vaidya[81],
C. Valderanis[102], E. Valdes Santurio[148a,148b], M. Valente[52], S. Valentinetti[22a,22b], A. Valero[170],
L. Valéry[45], R.A. Vallance[19], A. Vallier[5], J.A. Valls Ferrer[170], T.R. Van Daalen[13],
W. Van Den Wollenberg[109], H. van der Graaf[109], P. van Gemmeren[6], J. Van Nieuwkoop[144],
I. van Vulpen[109], M.C. van Woerden[109], M. Vanadia[135a,135b], W. Vandelli[32], A. Vaniachine[160],
P. Vankov[109], R. Vari[134a], E.W. Varnes[7], C. Varni[53a,53b], T. Varol[43], D. Varouchas[119],
A. Vartapetian[8], K.E. Varvell[152], J.G. Vasquez[179], G.A. Vasquez[34b], F. Vazeille[37],
D. Vazquez Furelos[13], T. Vazquez Schroeder[90], J. Veatch[58], V. Vecchio[136a,136b], L.M. Veloce[161],
F. Veloso[128a,128c], S. Veneziano[134a], A. Ventura[76a,76b], M. Venturi[172], N. Venturi[32], V. Vercesi[123a],
M. Verducci[136a,136b], W. Verkerke[109], A.T. Vermeulen[109], J.C. Vermeulen[109], M.C. Vetterli[144,d],
N. Viaux Maira[34b], O. Viazlo[84], I. Vichou[169,*], T. Vickey[141], O.E. Vickey Boeriu[141],
G.H.A. Viehhauser[122], S. Viel[16], L. Vigani[122], M. Villa[22a,22b], M. Villaplana Perez[94a,94b],
E. Vilucchi[50], M.G. Vincter[31], V.B. Vinogradov[68], A. Vishwakarma[45], C. Vittori[22a,22b],
I. Vivarelli[151], S. Vlachos[10], M. Vogel[177], P. Vokac[130], G. Volpi[13], S.E. von Buddenbrock[147c],
E. von Toerne[23], V. Vorobel[131], K. Vorobev[100], M. Vos[170], J.H. Vossebeld[77], N. Vranjes[14],
M. Vranjes Milosavljevic[14], V. Vrba[130], M. Vreeswijk[109], R. Vuillermet[32], I. Vukotic[33],
P. Wagner[23], W. Wagner[177], J. Wagner-Kuhr[102], H. Wahlberg[74], S. Wahrmund[47], K. Wakamiya[70],
J. Walder[75], R. Walker[102], W. Walkowiak[143], V. Wallangen[148a,148b], A.M. Wang[59], C. Wang[36b,p],
F. Wang[176], H. Wang[16], H. Wang[3], J. Wang[60b], J. Wang[152], P. Wang[43], Q. Wang[115],
R.-J. Wang[83], R. Wang[36a], R. Wang[6], S.M. Wang[153], T. Wang[38], W. Wang[153,aw], W. Wang[36a,ax],
Y. Wang[36a], Z. Wang[36c], C. Wanotayaroj[45], A. Warburton[90], C.P. Ward[30], D.R. Wardrope[81],
A. Washbrook[49], P.M. Watkins[19], A.T. Watson[19], M.F. Watson[19], G. Watts[140], S. Watts[87],
B.M. Waugh[81], A.F. Webb[11], S. Webb[86], C. Weber[179], M.S. Weber[18], S.M. Weber[60a],
S.A. Weber[31], J.S. Webster[6], A.R. Weidberg[122], B. Weinert[64], J. Weingarten[58], M. Weirich[86],
C. Weiser[51], P.S. Wells[32], T. Wenaus[27], T. Wengler[32], S. Wenig[32], N. Wermes[23], M.D. Werner[67],

P. Werner[32], M. Wessels[60a], T.D. Weston[18], K. Whalen[118], N.L. Whallon[140], A.M. Wharton[75], A.S. White[92], A. White[8], M.J. White[1], R. White[34b], D. Whiteson[166], B.W. Whitmore[75], F.J. Wickens[133], W. Wiedenmann[176], M. Wielers[133], C. Wiglesworth[39], L.A.M. Wiik-Fuchs[51], A. Wildauer[103], F. Wilk[87], H.G. Wilkens[32], H.H. Williams[124], S. Williams[30], C. Willis[93], S. Willocq[89], J.A. Wilson[19], I. Wingerter-Seez[5], E. Winkels[151], F. Winklmeier[118], O.J. Winston[151], B.T. Winter[23], M. Wittgen[145], M. Wobisch[82,u], A. Wolf[86], T.M.H. Wolf[109], R. Wolff[88], M.W. Wolter[42], H. Wolters[128a,128c], V.W.S. Wong[171], N.L. Woods[139], S.D. Worm[19], B.K. Wosiek[42], K.W. Woźniak[42], K. Wraight[56], M. Wu[33], S.L. Wu[176], X. Wu[52], Y. Wu[36a], T.R. Wyatt[87], B.M. Wynne[49], S. Xella[39], Z. Xi[92], L. Xia[35c], D. Xu[35a], H. Xu[36a], L. Xu[27], T. Xu[138], W. Xu[92], B. Yabsley[152], S. Yacoob[147a], K. Yajima[120], D.P. Yallup[81], D. Yamaguchi[159], Y. Yamaguchi[159], A. Yamamoto[69], T. Yamanaka[157], F. Yamane[70], M. Yamatani[157], T. Yamazaki[157], Y. Yamazaki[70], Z. Yan[24], H. Yang[36c,36d], H. Yang[16], S. Yang[66], Y. Yang[153], Y. Yang[157], Z. Yang[15], W-M. Yao[16], Y.C. Yap[45], Y. Yasu[69], E. Yatsenko[5], K.H. Yau Wong[23], J. Ye[43], S. Ye[27], I. Yeletskikh[68], E. Yigitbasi[24], E. Yildirim[86], K. Yorita[174], K. Yoshihara[124], C. Young[145], C.J.S. Young[32], J. Yu[8], J. Yu[67], X. Yue[60a], S.P.Y. Yuen[23], I. Yusuff[30,ay], B. Zabinski[42], G. Zacharis[10], R. Zaidan[13], A.M. Zaitsev[132,al], N. Zakharchuk[45], J. Zalieckas[15], S. Zambito[59], D. Zanzi[32], C. Zeitnitz[177], G. Zemaityte[122], J.C. Zeng[169], Q. Zeng[145], O. Zenin[132], T. Ženiš[146a], D. Zerwas[119], M. Zgubič[122], D. Zhang[36b], D. Zhang[92], F. Zhang[176], G. Zhang[36a,ax], H. Zhang[35b], J. Zhang[6], L. Zhang[51], L. Zhang[36a], M. Zhang[169], P. Zhang[35b], R. Zhang[23], R. Zhang[36a,p], X. Zhang[36b], Y. Zhang[35a,35d], Z. Zhang[119], X. Zhao[43], Y. Zhao[36b,x], Z. Zhao[36a], A. Zhemchugov[68], B. Zhou[92], C. Zhou[176], L. Zhou[43], M. Zhou[35a,35d], M. Zhou[150], N. Zhou[36c], Y. Zhou[7], C.G. Zhu[36b], H. Zhu[36a], H. Zhu[35a], J. Zhu[92], Y. Zhu[36a], X. Zhuang[35a], K. Zhukov[98], V. Zhulanov[111,az], A. Zibell[178], D. Zieminska[64], N.I. Zimine[68], S. Zimmermann[51], Z. Zinonos[103], M. Zinser[86], M. Ziolkowski[143], L. Živković[14], G. Zobernig[176], A. Zoccoli[22a,22b], K. Zoch[58], T.G. Zorbas[141], R. Zou[33], M. zur Nedden[17] and L. Zwalinski[32]

1   Department of Physics, University of Adelaide, Adelaide, Australia
2   Physics Department, SUNY Albany, Albany NY, United States of America
3   Department of Physics, University of Alberta, Edmonton AB, Canada
4   (a) Department of Physics, Ankara University, Ankara; (b) Istanbul Aydin University, Istanbul; (c) Division of Physics, TOBB University of Economics and Technology, Ankara, Turkey
5   LAPP, Univ. Grenoble Alpes, Univ. Savoie Mont Blanc, CNRS/IN2P3, Annecy, France
6   High Energy Physics Division, Argonne National Laboratory, Argonne IL, United States of America
7   Department of Physics, University of Arizona, Tucson AZ, United States of America
8   Department of Physics, The University of Texas at Arlington, Arlington TX, United States of America
9   Physics Department, National and Kapodistrian University of Athens, Athens, Greece
10 Physics Department, National Technical University of Athens, Zografou, Greece
11 Department of Physics, The University of Texas at Austin, Austin TX, United States of America
12 Institute of Physics, Azerbaijan Academy of Sciences, Baku, Azerbaijan
13 Institut de Física d'Altes Energies (IFAE), The Barcelona Institute of Science and Technology, Barcelona, Spain
14 Institute of Physics, University of Belgrade, Belgrade, Serbia
15 Department for Physics and Technology, University of Bergen, Bergen, Norway
16 Physics Division, Lawrence Berkeley National Laboratory and University of California, Berkeley CA, United States of America
17 Department of Physics, Humboldt University, Berlin, Germany
18 Albert Einstein Center for Fundamental Physics and Laboratory for High Energy Physics, University of Bern, Bern, Switzerland
19 School of Physics and Astronomy, University of Birmingham, Birmingham, United Kingdom

20 [a] *Department of Physics, Bogazici University, Istanbul;* [b] *Department of Physics Engineering, Gaziantep University, Gaziantep;* [d] *Istanbul Bilgi University, Faculty of Engineering and Natural Sciences, Istanbul;* [e] *Bahcesehir University, Faculty of Engineering and Natural Sciences, Istanbul, Turkey*

21 *Centro de Investigaciones, Universidad Antonio Narino, Bogota, Colombia*

22 [a] *INFN Sezione di Bologna;* [b] *Dipartimento di Fisica e Astronomia, Università di Bologna, Bologna, Italy*

23 *Physikalisches Institut, University of Bonn, Bonn, Germany*

24 *Department of Physics, Boston University, Boston MA, United States of America*

25 *Department of Physics, Brandeis University, Waltham MA, United States of America*

26 [a] *Universidade Federal do Rio De Janeiro COPPE/EE/IF, Rio de Janeiro;* [b] *Electrical Circuits Department, Federal University of Juiz de Fora (UFJF), Juiz de Fora;* [c] *Federal University of Sao Joao del Rei (UFSJ), Sao Joao del Rei;* [d] *Instituto de Fisica, Universidade de Sao Paulo, Sao Paulo, Brazil*

27 *Physics Department, Brookhaven National Laboratory, Upton NY, United States of America*

28 [a] *Transilvania University of Brasov, Brasov;* [b] *Horia Hulubei National Institute of Physics and Nuclear Engineering;* [c] *Department of Physics, Alexandru Ioan Cuza University of Iasi, Iasi;* [d] *National Institute for Research and Development of Isotopic and Molecular Technologies, Physics Department, Cluj Napoca;* [e] *University Politehnica Bucharest, Bucharest;* [f] *West University in Timisoara, Timisoara, Romania*

29 *Departamento de Física, Universidad de Buenos Aires, Buenos Aires, Argentina*

30 *Cavendish Laboratory, University of Cambridge, Cambridge, United Kingdom*

31 *Department of Physics, Carleton University, Ottawa ON, Canada*

32 *CERN, Geneva, Switzerland*

33 *Enrico Fermi Institute, University of Chicago, Chicago IL, United States of America*

34 [a] *Departamento de Física, Pontificia Universidad Católica de Chile, Santiago;* [b] *Departamento de Física, Universidad Técnica Federico Santa María, Valparaíso, Chile*

35 [a] *Institute of High Energy Physics, Chinese Academy of Sciences, Beijing;* [b] *Department of Physics, Nanjing University, Jiangsu;* [c] *Physics Department, Tsinghua University, Beijing;* [d] *University of Chinese Academy of Science (UCAS), Beijing, China*

36 [a] *Department of Modern Physics and State Key Laboratory of Particle Detection and Electronics, University of Science and Technology of China, Anhui;* [b] *School of Physics, Shandong University, Shandong;* [c] *School of Physics and Astronomy, Key Laboratory for Particle Physics, Astrophysics and Cosmology, Ministry of Education; Shanghai Key Laboratory for Particle Physics and Cosmology, Shanghai Jiao Tong University;* [d] *Tsung-Dao Lee Institute, Shanghai, China*

37 *Université Clermont Auvergne, CNRS/IN2P3, LPC, Clermont-Ferrand, France*

38 *Nevis Laboratory, Columbia University, Irvington NY, United States of America*

39 *Niels Bohr Institute, University of Copenhagen, Kobenhavn, Denmark*

40 [a] *INFN Gruppo Collegato di Cosenza, Laboratori Nazionali di Frascati;* [b] *Dipartimento di Fisica, Università della Calabria, Rende, Italy*

41 [a] *AGH University of Science and Technology, Faculty of Physics and Applied Computer Science, Krakow;* [b] *Marian Smoluchowski Institute of Physics, Jagiellonian University, Krakow, Poland*

42 *Institute of Nuclear Physics Polish Academy of Sciences, Krakow, Poland*

43 *Physics Department, Southern Methodist University, Dallas TX, United States of America*

44 *Physics Department, University of Texas at Dallas, Richardson TX, United States of America*

45 *DESY, Hamburg and Zeuthen, Germany*

46 *Lehrstuhl für Experimentelle Physik IV, Technische Universität Dortmund, Dortmund, Germany*

47 *Institut für Kern- und Teilchenphysik, Technische Universität Dresden, Dresden, Germany*

48 *Department of Physics, Duke University, Durham NC, United States of America*

49 *SUPA - School of Physics and Astronomy, University of Edinburgh, Edinburgh, United Kingdom*

50 *INFN e Laboratori Nazionali di Frascati, Frascati, Italy*

51 *Fakultät für Mathematik und Physik, Albert-Ludwigs-Universität, Freiburg, Germany*

[52] *Departement de Physique Nucleaire et Corpusculaire, Université de Genève, Geneva, Switzerland*

[53] *(a) INFN Sezione di Genova; (b) Dipartimento di Fisica, Università di Genova, Genova, Italy*

[54] *(a) E. Andronikashvili Institute of Physics, Iv. Javakhishvili Tbilisi State University, Tbilisi; (b) High Energy Physics Institute, Tbilisi State University, Tbilisi, Georgia*

[55] *II. Physikalisches Institut, Justus-Liebig-Universität, Germany*

[56] *SUPA - School of Physics and Astronomy, University of Glasgow, Glasgow, United Kingdom*

[57] *LPSC, Université Grenoble Alpes, CNRS-IN2P3, Grenoble INP, Grenoble, France*

[58] *II Physikalisches Institut, Georg-August-Universität, Göttingen, Germany*

[59] *Laboratory for Particle Physics and Cosmology, Harvard University, Cambridge MA, United States of America*

[60] *(a) Kirchhoff-Institut für Physik, Ruprecht-Karls-Universität Heidelberg, Heidelberg; (b) Physikalisches Institut, Ruprecht-Karls-Universität Heidelberg, Heidelberg, Germany*

[61] *Faculty of Applied Information Science, Hiroshima Institute of Technology, Hiroshima, Japan*

[62] *(a) Department of Physics, The Chinese University of Hong Kong, Shatin, N.T., Hong Kong; (b) Department of Physics, The University of Hong Kong, Hong Kong; (c) Department of Physics and Institute for Advanced Study, The Hong Kong University of Science and Technology, Clear Water Bay, Kowloon, Hong Kong, China*

[63] *Department of Physics, National Tsing Hua University, Hsinchu, Taiwan*

[64] *Department of Physics, Indiana University, Bloomington IN, United States of America*

[65] *Institut für Astro- und Teilchenphysik, Leopold-Franzens-Universität, Innsbruck, Austria*

[66] *University of Iowa, Iowa City IA, United States of America*

[67] *Department of Physics and Astronomy, Iowa State University, Ames IA, United States of America*

[68] *Joint Institute for Nuclear Research, JINR Dubna, Dubna, Russia*

[69] *KEK, High Energy Accelerator Research Organization, Tsukuba, Japan*

[70] *Graduate School of Science, Kobe University, Kobe, Japan*

[71] *Faculty of Science, Kyoto University, Kyoto, Japan*

[72] *Kyoto University of Education, Kyoto, Japan*

[73] *Research Center for Advanced Particle Physics and Department of Physics, Kyushu University, Fukuoka, Japan*

[74] *Instituto de Física La Plata, Universidad Nacional de La Plata and CONICET, La Plata, Argentina*

[75] *Physics Department, Lancaster University, Lancaster, United Kingdom*

[76] *(a) INFN Sezione di Lecce; (b) Dipartimento di Matematica e Fisica, Università del Salento, Lecce, Italy*

[77] *Oliver Lodge Laboratory, University of Liverpool, Liverpool, United Kingdom*

[78] *Department of Experimental Particle Physics, Jožef Stefan Institute and Department of Physics, University of Ljubljana, Ljubljana, Slovenia*

[79] *School of Physics and Astronomy, Queen Mary University of London, London, United Kingdom*

[80] *Department of Physics, Royal Holloway University of London, Surrey, United Kingdom*

[81] *Department of Physics and Astronomy, University College London, London, United Kingdom*

[82] *Louisiana Tech University, Ruston LA, United States of America*

[83] *Laboratoire de Physique Nucléaire et de Hautes Energies, UPMC and Université Paris-Diderot and CNRS/IN2P3, Paris, France*

[84] *Fysiska institutionen, Lunds universitet, Lund, Sweden*

[85] *Departamento de Fisica Teorica C-15 and CIAFF, Universidad Autonoma de Madrid, Madrid, Spain*

[86] *Institut für Physik, Universität Mainz, Mainz, Germany*

[87] *School of Physics and Astronomy, University of Manchester, Manchester, United Kingdom*

[88] *CPPM, Aix-Marseille Université and CNRS/IN2P3, Marseille, France*

[89] *Department of Physics, University of Massachusetts, Amherst MA, United States of America*

[90] *Department of Physics, McGill University, Montreal QC, Canada*

[91] *School of Physics, University of Melbourne, Victoria, Australia*

[92] *Department of Physics, The University of Michigan, Ann Arbor MI, United States of America*

93 *Department of Physics and Astronomy, Michigan State University, East Lansing MI, United States of America*

94 (a) *INFN Sezione di Milano;* (b) *Dipartimento di Fisica, Università di Milano, Milano, Italy*

95 *B.I. Stepanov Institute of Physics, National Academy of Sciences of Belarus, Minsk, Republic of Belarus*

96 *Research Institute for Nuclear Problems of Byelorussian State University, Minsk, Republic of Belarus*

97 *Group of Particle Physics, University of Montreal, Montreal QC, Canada*

98 *P.N. Lebedev Physical Institute of the Russian Academy of Sciences, Moscow, Russia*

99 *Institute for Theoretical and Experimental Physics (ITEP), Moscow, Russia*

100 *National Research Nuclear University MEPhI, Moscow, Russia*

101 *D.V. Skobeltsyn Institute of Nuclear Physics, M.V. Lomonosov Moscow State University, Moscow, Russia*

102 *Fakultät für Physik, Ludwig-Maximilians-Universität München, München, Germany*

103 *Max-Planck-Institut für Physik (Werner-Heisenberg-Institut), München, Germany*

104 *Nagasaki Institute of Applied Science, Nagasaki, Japan*

105 *Graduate School of Science and Kobayashi-Maskawa Institute, Nagoya University, Nagoya, Japan*

106 (a) *INFN Sezione di Napoli;* (b) *Dipartimento di Fisica, Università di Napoli, Napoli, Italy*

107 *Department of Physics and Astronomy, University of New Mexico, Albuquerque NM, United States of America*

108 *Institute for Mathematics, Astrophysics and Particle Physics, Radboud University Nijmegen/Nikhef, Nijmegen, Netherlands*

109 *Nikhef National Institute for Subatomic Physics and University of Amsterdam, Amsterdam, Netherlands*

110 *Department of Physics, Northern Illinois University, DeKalb IL, United States of America*

111 *Budker Institute of Nuclear Physics, SB RAS, Novosibirsk, Russia*

112 *Department of Physics, New York University, New York NY, United States of America*

113 *Ohio State University, Columbus OH, United States of America*

114 *Faculty of Science, Okayama University, Okayama, Japan*

115 *Homer L. Dodge Department of Physics and Astronomy, University of Oklahoma, Norman OK, United States of America*

116 *Department of Physics, Oklahoma State University, Stillwater OK, United States of America*

117 *Palacký University, RCPTM, Olomouc, Czech Republic*

118 *Center for High Energy Physics, University of Oregon, Eugene OR, United States of America*

119 *LAL, Univ. Paris-Sud, CNRS/IN2P3, Université Paris-Saclay, Orsay, France*

120 *Graduate School of Science, Osaka University, Osaka, Japan*

121 *Department of Physics, University of Oslo, Oslo, Norway*

122 *Department of Physics, Oxford University, Oxford, United Kingdom*

123 (a) *INFN Sezione di Pavia;* (b) *Dipartimento di Fisica, Università di Pavia, Pavia, Italy*

124 *Department of Physics, University of Pennsylvania, Philadelphia PA, United States of America*

125 *National Research Centre "Kurchatov Institute" B.P.Konstantinov Petersburg Nuclear Physics Institute, St. Petersburg, Russia*

126 (a) *INFN Sezione di Pisa;* (b) *Dipartimento di Fisica E. Fermi, Università di Pisa, Pisa, Italy*

127 *Department of Physics and Astronomy, University of Pittsburgh, Pittsburgh PA, United States of America*

128 (a) *Laboratório de Instrumentação e Física Experimental de Partículas - LIP, Lisboa;* (b) *Faculdade de Ciências, Universidade de Lisboa, Lisboa;* (c) *Department of Physics, University of Coimbra, Coimbra;* (e) *Departamento de Fisica, Universidade do Minho, Braga, Portugal;* (f) *Departamento de Fisica Teorica y del Cosmos, Universidad de Granada, Granada (Spain), Spain;* (g) *Dep Fisica and CEFITEC of Faculdade de Ciencias e Tecnologia, Universidade Nova de Lisboa, Caparica, Portugal*

129 *Institute of Physics, Academy of Sciences of the Czech Republic, Praha, Czech Republic*

[130] *Czech Technical University in Prague, Praha, Czech Republic*

[131] *Charles University, Faculty of Mathematics and Physics, Prague, Czech Republic*

[132] *State Research Center Institute for High Energy Physics (Protvino), NRC KI, Russia*

[133] *Particle Physics Department, Rutherford Appleton Laboratory, Didcot, United Kingdom*

[134] [a] *INFN Sezione di Roma;* [b] *Dipartimento di Fisica, Sapienza Università di Roma, Roma, Italy*

[135] [a] *INFN Sezione di Roma Tor Vergata;* [b] *Dipartimento di Fisica, Università di Roma Tor Vergata, Roma, Italy*

[136] [a] *INFN Sezione di Roma Tre;* [b] *Dipartimento di Matematica e Fisica, Università Roma Tre, Roma, Italy*

[137] [a] *Faculté des Sciences Ain Chock, Réseau Universitaire de Physique des Hautes Energies - Université Hassan II, Casablanca;* [b] *Centre National de l'Energie des Sciences Techniques Nucleaires, Rabat;* [c] *Faculté des Sciences Semlalia, Université Cadi Ayyad, LPHEA-Marrakech;* [d] *Faculté des Sciences, Université Mohamed Premier and LPTPM, Oujda;* [e] *Faculté des sciences, Université Mohammed V, Rabat, Morocco*

[138] *Institut de Recherches sur les Lois Fondamentales de l'Univers, DSM/IRFU, CEA Saclay, Gif-sur-Yvette, France*

[139] *Santa Cruz Institute for Particle Physics, University of California Santa Cruz, Santa Cruz CA, United States of America*

[140] *Department of Physics, University of Washington, Seattle WA, United States of America*

[141] *Department of Physics and Astronomy, University of Sheffield, Sheffield, United Kingdom*

[142] *Department of Physics, Shinshu University, Nagano, Japan*

[143] *Department Physik, Universität Siegen, Siegen, Germany*

[144] *Department of Physics, Simon Fraser University, Burnaby BC, Canada*

[145] *SLAC National Accelerator Laboratory, Stanford CA, United States of America*

[146] [a] *Faculty of Mathematics, Physics and Informatics, Comenius University, Bratislava;* [b] *Department of Subnuclear Physics, Institute of Experimental Physics of the Slovak Academy of Sciences, Kosice, Slovak Republic*

[147] [a] *Department of Physics, University of Cape Town, Cape Town;* [b] *Department of Mechanical Engineering Science, University of Johannesburg, Johannesburg;* [c] *School of Physics, University of the Witwatersrand, Johannesburg, South Africa*

[148] [a] *Department of Physics, Stockholm University;* [b] *The Oskar Klein Centre, Stockholm, Sweden*

[149] *Physics Department, Royal Institute of Technology, Stockholm, Sweden*

[150] *Departments of Physics and Astronomy, Stony Brook University, Stony Brook NY, United States of America*

[151] *Department of Physics and Astronomy, University of Sussex, Brighton, United Kingdom*

[152] *School of Physics, University of Sydney, Sydney, Australia*

[153] *Institute of Physics, Academia Sinica, Taipei, Taiwan*

[154] *Department of Physics, Technion: Israel Institute of Technology, Haifa, Israel*

[155] *Raymond and Beverly Sackler School of Physics and Astronomy, Tel Aviv University, Tel Aviv, Israel*

[156] *Department of Physics, Aristotle University of Thessaloniki, Thessaloniki, Greece*

[157] *International Center for Elementary Particle Physics and Department of Physics, The University of Tokyo, Tokyo, Japan*

[158] *Graduate School of Science and Technology, Tokyo Metropolitan University, Tokyo, Japan*

[159] *Department of Physics, Tokyo Institute of Technology, Tokyo, Japan*

[160] *Tomsk State University, Tomsk, Russia*

[161] *Department of Physics, University of Toronto, Toronto ON, Canada*

[162] [a] *INFN-TIFPA;* [b] *University of Trento, Trento, Italy*

[163] [a] *TRIUMF, Vancouver BC;* [b] *Department of Physics and Astronomy, York University, Toronto ON, Canada*

[164] *Division of Physics and Tomonaga Center for the History of the Universe, Faculty of Pure and Applied Sciences, University of Tsukuba, Tsukuba, Japan*

[165] *Department of Physics and Astronomy, Tufts University, Medford MA, United States of America*

[166] *Department of Physics and Astronomy, University of California Irvine, Irvine CA, United States of America*

[167] [(a)] *INFN Gruppo Collegato di Udine, Sezione di Trieste, Udine;* [(b)] *ICTP, Trieste;* [(c)] *Dipartimento di Chimica, Fisica e Ambiente, Università di Udine, Udine, Italy*

[168] *Department of Physics and Astronomy, University of Uppsala, Uppsala, Sweden*

[169] *Department of Physics, University of Illinois, Urbana IL, United States of America*

[170] *Instituto de Fisica Corpuscular (IFIC), Centro Mixto Universidad de Valencia - CSIC, Spain*

[171] *Department of Physics, University of British Columbia, Vancouver BC, Canada*

[172] *Department of Physics and Astronomy, University of Victoria, Victoria BC, Canada*

[173] *Department of Physics, University of Warwick, Coventry, United Kingdom*

[174] *Waseda University, Tokyo, Japan*

[175] *Department of Particle Physics, The Weizmann Institute of Science, Rehovot, Israel*

[176] *Department of Physics, University of Wisconsin, Madison WI, United States of America*

[177] *Fakultät für Mathematik und Naturwissenschaften, Fachgruppe Physik, Bergische Universität Wuppertal, Wuppertal, Germany*

[178] *Fakultät für Physik und Astronomie, Julius-Maximilians-Universität, Würzburg, Germany*

[179] *Department of Physics, Yale University, New Haven CT, United States of America*

[180] *Yerevan Physics Institute, Yerevan, Armenia*

[181] *Centre de Calcul de l'Institut National de Physique Nucléaire et de Physique des Particules (IN2P3), Villeurbanne, France*

[182] *Academia Sinica Grid Computing, Institute of Physics, Academia Sinica, Taipei, Taiwan*

[a] *Also at Department of Physics, King's College London, London, United Kingdom*

[b] *Also at Institute of Physics, Azerbaijan Academy of Sciences, Baku, Azerbaijan*

[c] *Also at Novosibirsk State University, Novosibirsk, Russia*

[d] *Also at TRIUMF, Vancouver BC, Canada*

[e] *Also at Department of Physics and Astronomy, University of Louisville, Louisville, KY, United States of America*

[f] *Also at Department of Physics, California State University, Fresno CA, United States of America*

[g] *Also at Department of Physics, University of Fribourg, Fribourg, Switzerland*

[h] *Also at II Physikalisches Institut, Georg-August-Universität, Göttingen, Germany*

[i] *Also at Departament de Fisica de la Universitat Autonoma de Barcelona, Barcelona, Spain*

[j] *Also at Tomsk State University, Tomsk, and Moscow Institute of Physics and Technology State University, Dolgoprudny, Russia*

[k] *Also at The Collaborative Innovation Center of Quantum Matter (CICQM), Beijing, China*

[l] *Also at Universita di Napoli Parthenope, Napoli, Italy*

[m] *Also at Institute of Particle Physics (IPP), Canada*

[n] *Also at Dipartimento di Fisica E. Fermi, Università di Pisa, Pisa, Italy*

[o] *Also at Horia Hulubei National Institute of Physics and Nuclear Engineering, Romania*

[p] *Also at CPPM, Aix-Marseille Université and CNRS/IN2P3, Marseille, France*

[q] *Also at Department of Physics, St. Petersburg State Polytechnical University, St. Petersburg, Russia*

[r] *Also at Borough of Manhattan Community College, City University of New York, New York City, United States of America*

[s] *Also at Department of Financial and Management Engineering, University of the Aegean, Chios, Greece*

[t] *Also at Centre for High Performance Computing, CSIR Campus, Rosebank, Cape Town, South Africa*

[u] *Also at Louisiana Tech University, Ruston LA, United States of America*

[v] *Also at Institucio Catalana de Recerca i Estudis Avancats, ICREA, Barcelona, Spain*

[w] *Also at Department of Physics, The University of Michigan, Ann Arbor MI, United States of*

     America

[x] *Also at LAL, Univ. Paris-Sud, CNRS/IN2P3, Université Paris-Saclay, Orsay, France*

[y] *Also at Graduate School of Science, Osaka University, Osaka, Japan*

[z] *Also at Fakultät für Mathematik und Physik, Albert-Ludwigs-Universität, Freiburg, Germany*

[aa] *Also at Institute for Mathematics, Astrophysics and Particle Physics, Radboud University Nijmegen/Nikhef, Nijmegen, Netherlands*

[ab] *Also at Near East University, Nicosia, North Cyprus, Mersin 10, Turkey*

[ac] *Also at Institute of Theoretical Physics, Ilia State University, Tbilisi, Georgia*

[ad] *Also at CERN, Geneva, Switzerland*

[ae] *Also at Georgian Technical University (GTU),Tbilisi, Georgia*

[af] *Also at Ochadai Academic Production, Ochanomizu University, Tokyo, Japan*

[ag] *Also at Manhattan College, New York NY, United States of America*

[ah] *Also at Hellenic Open University, Patras, Greece*

[ai] *Also at The City College of New York, New York NY, United States of America*

[aj] *Also at Departamento de Fisica Teorica y del Cosmos, Universidad de Granada, Granada (Spain), Spain*

[ak] *Also at Department of Physics, California State University, Sacramento CA, United States of America*

[al] *Also at Moscow Institute of Physics and Technology State University, Dolgoprudny, Russia*

[am] *Also at Departement de Physique Nucleaire et Corpusculaire, Université de Genève, Geneva, Switzerland*

[an] *Also at Department of Physics, The University of Texas at Austin, Austin TX, United States of America*

[ao] *Also at Institut de Física d'Altes Energies (IFAE), The Barcelona Institute of Science and Technology, Barcelona, Spain*

[ap] *Also at School of Physics, Sun Yat-sen University, Guangzhou, China*

[aq] *Also at Institute for Nuclear Research and Nuclear Energy (INRNE) of the Bulgarian Academy of Sciences, Sofia, Bulgaria*

[ar] *Also at Faculty of Physics, M.V.Lomonosov Moscow State University, Moscow, Russia*

[as] *Also at National Research Nuclear University MEPhI, Moscow, Russia*

[at] *Also at Department of Physics, Stanford University, Stanford CA, United States of America*

[au] *Also at Institute for Particle and Nuclear Physics, Wigner Research Centre for Physics, Budapest, Hungary*

[av] *Also at Giresun University, Faculty of Engineering, Turkey*

[aw] *Also at Department of Physics, Nanjing University, Jiangsu, China*

[ax] *Also at Institute of Physics, Academia Sinica, Taipei, Taiwan*

[ay] *Also at University of Malaya, Department of Physics, Kuala Lumpur, Malaysia*

[az] *Also at Budker Institute of Nuclear Physics, SB RAS, Novosibirsk, Russia*

[*] *Deceased*